NUMERICAL SOLUTION OF POTENTIAL FLOW ABOUT ARBITRARY TWO-DIMENSIONAL MULTIPLE BODIES

eirs
ENGINEERING & INDUSTRIAL RESEARCH STATION
Aerospace Engineering

Joe F. Thompson

and

Frank C. Thames

Mississippi State University
Mississippi State, Miss. 39762

MSSU-EIRS-ASE-82-2

Numerical Solution of Potential Flow About Arbitrary Two-Dimensional Multiple Bodies*

Joe F. Thompson and Frank C. Thames+

Department of Aerospace Engineering
Mississippi State University
Mississippi State, Mississippi 39762

*Research sponsored by NASA-Langley Research Center, Grant NGR 25-001-055

+NASA Langley Research Center

Table of Contents

		Page
Abstract		3
I.	INTRODUCTION	4
II.	BOUNDARY-FITTED CURVILINEAR COORDINATE SYSTEM	7
	A. Mathematical Construction	7
	B. Numerical Implementation	10
III.	POTENTIAL FLOW SOLUTION	13
	A. Laplace Equation	13
	B. Velocity	14
	C. Kutta Condition	15
	D. Superposition of Solutions	16
	E. Surface Pressure and Force Coefficients	18
	F. Multiple Airfoils	18
IV.	EFFECT OF NUMERICAL PARAMETERS	21
	A. Effect of Point Distribution on Airfoil Contour	22
	B. Effect of Number of Lines Surrounding the Body	25
	C. Effect of Location of Outer Boundary	25
	D. Effect of Order of Extrapolation Used in Kutta Condition	26
	E. Effect of Order of Velocity Difference Expression Used in Kutta Condition	26
	F. Effect of Order of Velocity Difference Expression Used in Pressure Calculation	26
	G. Effect of Order of Pressure Integration	27
	H. Recommended Values	27
V.	MULTIPLE-BODY SOLUTIONS	29
VI.	CONCLUSION	33
APPENDIX--DERIVATIVES AND VECTORS IN THE TRANSFORMED PLANE		34
REFERENCES		37

Abstract

A procedure for the finite-difference numerical solution of the lifting potential flow about any number of arbitrarily shaped bodies is given. The solution is based on a technique of automatic numerical generation of a curvilinear coordinate system having coordinate lines coincident with the contours of all bodies in the field, regardless of their shapes and number. The effects of all numerical parameters involved are analyzed and appropriate values are recommended. Comparisons with analytic solutions for single Karman-Trefftz airfoils and a circular cylinder pair show excellent agreement. The paper serves also to illustrate the technique of application of the boundary-fitted coordinate systems to the numerical solution of partial differential equations.

I. INTRODUCTION

Numerical incompressible potential flow solutions for bodies of arbitrary shape have generally fallen into three categories:

(1) Integral equation methods, whereby various singular solutions of Laplace's equation are superposed to construct a solution satisfying the boundary conditions of the particular problem of interest. This type of approach is represented by the work in references 1-8. In these methods singular solutions of Laplace's equation are distributed on the body surface, and perhaps also in its interior, with the body surface represented by quadralateral or triangular panels. The strengths of the singularities are then determined such that the superposition of the onset velocity field and that induced by the totality of the singularities satisfies the condition of vanishing normal velocity at the body surface at certain points.

This approach has been carried to a high degree of refinement and is presently capable of treating the flow about multiple bodies of arbitrary shape. This procedure obviates calculation in the entire flow field and involves instead the solution of a matrix equation of order equal to the number of points of application of the boundary condition on the bodies. The primary output is the surface pressure distribution on the bodies and the resulting aerodynamic coefficients. The velocity field can also be obtained, but this requires the evaluation of the velocity at each point in the field from a summation over all the singularities involved--a time consuming process. The determination of streamlines, or equivalently the stream function, from the velocity field is still another numerical problem itself.

(2) Finite element methods, as represented by references 9-11. Here the calculation is carried out in the entire flow field, the field being divided into finite elements. The flow solution is obtained by applying an integral variational principle, or other integral relations, over the aggregate of elements, which leads to a matrix solution of order equal to the total number of elements in the field. The solution is thus obtained in the entire flow field. However, not all derivatives can be made continuous across the boundaries between the various elements.

(3) Conformal transformation, whereby the field is transformed to one of simple geometry on which the solution is known (two-dimensional flow only). The classic Theodorsen method [12] is one of this type. A comparative discussion of earlier applications of this and other procedures is given in [1]. Recently Ives [13] has extended this approach to multiple bodies.

Finite difference solutions have been severely hindered in the past by the problem of fitting curved boundaries into the computational grid. The use of interpolation between grid points to represent boundary conditions on a curved boundary passing through a rectangular grid may lead to poor application of the boundary conditions. Since finite difference solutions depend on continuity of derivatives, the distribution of points at will in the field leads to difference expressions involving large numbers of points, loss of repeat patterns over the field, and hence unreasonably complex computer codes.

However, if a curvilinear coordinate system with coordinate lines coincident with the field boundaries can be found, these problems vanish, and the finite difference approach can give very smooth solutions that do

not lack continuity of derivatives. The potential flow solution reported herein is based on just such an approach.

The present finite-difference potential flow solution utilizes a method of automatic numerical generation of a general boundary-fitted curvilinear coordinate system having coordinate lines coincident with all boundaries of a general multi-connected region containing any number of arbitrarily shaped bodies, which has been reported earlier (Ref. 14-16). The curvilinear coordinates are generated as the solutions of an elliptic partial differential system with Dirichlet boundary conditions, one coordinate being specified to be constant on each of the boundaries, and a distribution of the other being specified along the boundaries. No restrictions are placed on the shape of the boundaries, which may even be time-dependent, and the method is not restricted to single bodies or, in principle, to two dimensions. Coordinate lines may be concentrated as desired along the boundaries. Procedures have also been developed to control the coordinate line spacing in the field by varying the generating elliptic system.

Regardless of the number or shapes of the bodies and regardless of the spacing of the curvilinear coordinate lines, all numerical computations, both to generate the coordinate system and to subsequently solve the Laplace equation for the stream function are done on a rectangular grid with a square mesh, i.e., in the transformed plane. Although not necessary in the present application, it is also possible to cause the boundary-fitted coordinate system to change in time however desired and still have all computation done on the fixed rectangular grid with square mesh [17]. This allows the curvilinear coordinate system in the physical plane to

deform with a deforming body, free surface, or any other boundary, keeping a coordinate line always coincident with the boundary at all times. The physical coordinate system has been, in effect, eliminated from the problem, at the expense of adding two elliptic equations to the original system.

Since the curvilinear coordinate system has coordinate lines coincident with the surface contours of all bodies present, all boundary conditions may be expressed at grid points, and normal derivatives on the bodies may be represented using only finite differences between grid points on coordinate lines, without need of any interpolation, even though the coordinate system is not orthogonal at the boundary. With this method of boundary-fitted coordinate system generation, the treatment of fields with complex boundaries and any number of bodies is not inherently more difficult than problems with simple geometry.

This use of numerically-generated boundary-fitted coordinate systems is not peculiar to the present application to potential flow, but rather is applicable to the numerical solution of any partial differential system. Other applications presently under consideration include viscous incompressible and compressible flow, free surface flows, turbulent flows, and solid mechanics problems. Some examples of such applications are given in Ref. 17-20. Documentation of the coordinate system generation procedure and computer program are given in Ref. 18 and 19. The procedure is briefly summarized in the next section. The present paper serves also to illustrate the technique of application of the boundary-fitted coordinate systems in the numerical solution of partial differential equations.

II. BOUNDARY-FITTED CURVILINEAR COORDINATE SYSTEM

A. Mathematical Construction

Let it be desired to transform the two-dimensional, doubly-connected region, D, bounded by two closed contours of arbitrary shape into a rectangular region, D*, as shown in Fig. 1. The general transformation from

the physical plane (x,y) to the transformed plane (ξ,η) is given by $\xi = \xi(x,y)$, $\eta = \eta(x,y)$. Since the basic idea of the transformation is to generate transformation functions such that all boundaries are coincident with coordinate lines, the curvilinear coordinates (ξ,η) are taken as solutions of some suitable elliptic boundary value problem with one of these coordinates constant on the boundaries. The choice of a suitable elliptic system is restricted somewhat by the need for certain maximum principles as discussed in Ref. 18. The system given below allows considerable control to be exercized over the spacing of the curvilinear coordinate lines in the field:

$$\xi_{xx} + \xi_{yy} = P(\xi,\eta) \tag{1a}$$

$$\eta_{xx} + \eta_{yy} = Q(\xi,\eta) \tag{1b}$$

with Dirichlet boundary conditions, η = constant = η_1 on Γ_1, η = constant = η_2 on Γ_2; $\xi(x,y)$ a multiple valued solution with a branch of $\xi(x,y)$ specified (but not constant) on Γ_1 and Γ_2. The curve Γ_1 on the physical plane transforms to the lower boundary, Γ_1^*, of the transformed plane. Similarly, Γ_2 transforms to Γ_2^*, etc. The right and left boundaries of the rectangular transformed plane, Γ_3^* and Γ_4^*, are coincident in the physical plane. The curve which transforms to these boundaries connects Γ_1 and Γ_2 and determines a branch cut for the multiple valued function $\xi(x,y)$. Thus the functions and all derivatives are continuous across this cut. The inhomogeneous functions $P(\xi,\eta)$ and $Q(\xi,\eta)$ are sums of decaying exponentials that allow coordinate lines to be attracted to specified lines and/or points in the field or on the boundaries as discussed in more detail in Ref. 17-19. These functions, along with the derivative transformation relations are given in the appendix.

Now since it is desired to do all numerical computation in the rectangular transformed plane, it is necessary to interchange the dependent and independent variables in (1). Thus using the relations from the appendix,

$$\alpha x_{\xi\xi} - 2\beta x_{\xi\eta} + \gamma x_{\eta\eta} = - J^2[x_\xi P(\xi,\eta) + x_\eta Q(\xi,\eta)] \quad (2a)$$

$$\alpha y_{\xi\xi} - 2\beta y_{\xi\eta} + \gamma y_{\eta\eta} = - J^2[y_\xi P(\xi,\eta) + y_\eta Q(\xi,\eta)] \quad (2b)$$

where

$$\alpha = x_\eta^2 + y_\eta^2 \qquad \gamma = x_\xi^2 + y_\xi^2$$

$$\beta = x_\xi x_\eta + y_\xi y_\eta \qquad J = x_\xi y_\eta - x_\eta y_\xi$$

with the transformed boundary conditions, $x = f_1(\xi,\eta_1)$ on Γ_1^*, $y = g_1(\xi,\eta_1)$ on Γ_1^*, $x = f_2(\xi,\eta_2)$ on Γ_2^*, $y = g_2(\xi,\eta_2)$ on Γ_2^*. (In the present application, x and y are nondimensionalized with respect to the airfoil chord.)

The curvilinear coordinate system so generated has a constant η-line coincident with each boundary in the physical plane. The ξ-lines may be spaced in any manner desired around the boundaries by specification of the ξ boundary conditions, or equivalently by specification of (x,y) at the equi-spaced ξ-points on the η_1 and η_2 lines of the transformed plane. Control of the spacing of the η-lines may be exercised by varying the attraction parameters in the functions $P(\xi,\eta)$ and $Q(\xi,\eta)$ of Eq. (2) as discussed in Ref. 18 and 19.

The same procedure for boundary-fitted coordinate generation may be applied to regions that are more than doubly connected, i.e., have more than two closed boundaries or, equivalently, more than one body or hole within a single outer boundary. One possible transformation to the rectangular field for any number of bodies is illustrated in Fig. 2. Here the η-coordinate is required to be equal to the same constant on all the interior boundaries, i.e., on all bodies in the field. Let all the bodies be connected by arbitrary cuts and, similarly, one body be connected to the outer boundary by an arbitrary cut. Since the η-coordinate is equal

to the same constant on all the bodies, it is, of course, equal to that constant on the cuts between the bodies also. By contrast, the ξ-coordinate is taken constant on the cut between one body and the outer boundary. Since the locations of these cuts are not specified, the specification of η or ξ as constant on a cut does not overspecify the elliptic problem.

Note that all bodies except one are split into two segments. Each cut appears twice on the transformed field boundary of course, the two segments corresponding to the two "sides" of the cut in the physical plane and thus being re-entrant boundaries with the functions of all derivatives continuous thereon. Thus, x and y are specified on the portions of the lower boundary of the transformed field that corresponds to the bodies, and also on the entire upper boundary, corresponding to the outer boundary in the physical field. The remaining portions of the lower boundary and the entire side boundaries are re-entrant boundaries, and thus neither require nor allow specification of (x,y) thereon. Other arrangements are also possible as discussed in detail in Ref. 18 and 19, two of which are used below.

Again the elliptic Dirichlet problem (2) is solved to generate the boundary-fitted coordinates (ξ,η). All computation, both to generate the coordinates and subsequently to solve the partial differential system of interest, are again done on the rectangular field with square mesh in the transformed plane.

B. Numerical Implementation

The transformed field for a single airfoil is illustrated in Fig. 3a. The physical coordinates of I points describing the body surface, (x,y), provide the boundary conditions along the $j = 1$ line, and those of I points on the physical remote boundary, usually a circle of radius ten or

more chords, supply the boundary conditions along the j = J line of the transformed field. Since the side boundaries of the transformed field are re-entrant, corresponding to the cut in the physical plane, we have $f_{I,j} = f_{1,j}$ and $f_{I+1,j} = f_{2,j}$ for all j. Note that the values of x and y are not specified on these side boundaries. All derivatives in (2) are approximated by second-order central difference expressions ($\Delta\xi$ and $\Delta\eta$ are both unity by construction, the actual values of ξ and η being immaterial since cancellation occurs after substitution in the transformed equations.):

$$(f_\xi)_{ij} \triangleq \frac{1}{2}(f_{i+1,j} - f_{i-1,j}) \tag{3a}$$

$$(f_\eta)_{ij} \triangleq \frac{1}{2}(f_{i,j+1} - f_{i,j-1}) \tag{3b}$$

$$(f_{\xi\xi})_{ij} \triangleq f_{i+1,j} - 2f_{ij} + f_{i-1,j} \tag{3c}$$

$$(f_{\eta\eta})_{ij} \triangleq f_{i,j+1} - 2f_{ij} + f_{i,j-1} \tag{3d}$$

$$(f_{\xi\eta})_{ij} \triangleq \frac{1}{4}(f_{i+1,j+1} - f_{i+1,j-1} - f_{i-1,j+1} + f_{i-1,j-1}) \tag{3e}$$

The resulting set of 2I(J-1) nonlinear difference equations, two for each point (i,j) for i = 1, 2, --, I-1 and J = 2, 3, --, J-1, are solved by accelerated Gauss-Seidel (SOR) iteration using overrelaxation. The iteration is considered to have converged when the maximum absolute change on the field between iterates is less than a specified value. A range of acceleration parameters was examined, and a value of 1.85 was nearly optimum for the airfoils considered. After convergence of the solution of (2), the values of the coefficients α, β, γ, J, at each point of the field are stored for use in the solution of the stream function equation.

The transformed field for two airfoils is illustrated in Fig. 3b. The physical coordinates of body #2 at points i = 1---I1, those of body #1 at points i = I2---I3, and finally the remaining points i = I4---I on body

#2 are input as boundary conditions on the j = 1 line in the transformed plane. The remaining points, i = (I1 + 1)---(I2 - 1) and i = (I3 + 1)---(I4 - 1), on the j = 1 line are re-entrant points corresponding to the cut between the bodies in the physical plane. Therefore values at these points are not specified, but rather the relations $f_{I1 + k,1} = f_{I4 - k,1}$ and $f_{I1 + k,0} = f_{I4 - k,2}$ for k = 1---(I2 - I1 - 1) hold. The rest of the procedure is unchanged from the case of a single airfoil, except that two difference equations at each of the points (i,1) for i = (I1 + 1)---(I2 - 1) are added to the system, so that the total number of equations is now 2I(J-1) + 2(I2 - I1 - 1).

III. POTENTIAL FLOW SOLUTION

A. Laplace Equation

The two-dimensional irrotational flow about any number of bodies may be described by the Laplace equation for the stream function, ψ:

$$\psi_{xx} + \psi_{yy} = 0 \tag{4}$$

with boundary conditions

$$\psi(x,y) = \text{constant on each body} \tag{5a}$$

$$\psi(x,y) = y\cos\theta - x\sin\theta \text{ at infinity} \tag{5b}$$

where θ is the angle of attack of the free stream relative to the positive x-axis. Here the stream function is nondimensionalized relative to the airfoil chord and the free stream velocity. When transformed to the curvilinear coordinate system this equation becomes (see appendix)

$$\alpha\psi_{\xi\xi} - 2\beta\psi_{\xi\eta} + \gamma\psi_{\eta\eta} + J^2[Q(\xi,\eta)\psi_{\eta} + P(\xi,\eta)\psi_{\xi}] = 0 \tag{6}$$

where α, β, γ, and J are given above, and the transformed boundary conditions are, for a single body,

$$\psi(\xi,\eta) = \psi_o \text{ on } \eta = \eta_1 \text{ (i.e., on } \Gamma_1^*) \tag{7a}$$

$$\psi(\xi,\eta) = y(\xi,\eta_2)\cos\theta - x(\xi,\eta_2)\sin\theta \text{ on } \eta = \eta_2 \text{ (i.e., on } \Gamma_2^*) \tag{7b}$$

The uniqueness is implied by requiring that the solution be periodic in $-\infty < \xi < \infty$, $\eta_1 \leq \eta \leq \eta_2$. α, β, γ, and J are calculated during the generation of the coordinate system. Equation (6) is approximated using second-order, central differences for all derivatives, and the resulting difference equation is solved by accelerated Gauss-Seidel (SOR) iteration on the rectangular transformed field.

The solution of (6) on the transformed field is constructed in the same manner that has been previously described for the solut n of (2). The single equation (6) replaces the two equations (2a) and (2b), and the boundary conditions are given by (7). The total number of difference equations thus is I(J-1) for a single airfoil and I(J-1) + (I2 - I1 - 1) for two airfoils.

B. Velocity

The velocity components are calculated from the equations $u = \psi_y$, $v = -\psi_x$, which in the transformed plane become, from the appendix,

$$u = (x_\xi \psi_\eta - x_\eta \psi_\xi)/J \tag{8a}$$

$$v = (y_\xi \psi_\eta - y_\eta \psi_\xi)/J \tag{8b}$$

Velocities in the interior of the field may be obtained from these relations using second-order, central difference expressions for all derivatives as given by Eq. (3).

On the body surface, $\psi_\xi = 0$, so that these expressions reduce to $u = x_\xi \psi_\eta / J$ and $v = y_\xi \psi_\eta / J$. Also, the unit tangent vector the the body surface is given by (see appendix)

$$\underset{\sim}{\tau} = (\underset{\sim}{i} x_\xi + \underset{\sim}{j} y_\xi)/\sqrt{\gamma} \tag{9}$$

Then the velocity component tangential to the surface is given by

$$v_t = \underset{\sim}{v} \cdot \underset{\sim}{\tau} = (u x_\xi + v y_\xi)/\sqrt{\gamma} = \frac{\sqrt{\gamma}}{J} \psi_\eta \tag{10}$$

On the surface, the ξ-derivatives are approximated by the second-order, central difference expressions of Eq. (3a), as in the interior of the field, at all points except those on the cut, i = 1 and i = I, where second order, one-sided expressions are used. Thus

$$(f_\xi)_{1,1} = \frac{1}{2}(-f_{3,1} + 4f_{2,1} - 3f_{1,1}) \tag{11a}$$

$$(f_\xi)_{I,1} = \frac{1}{2}(f_{I-2,1} - 4f_{I-1,1} + 3f_{I,1}) \tag{11b}$$

The η-derivatives on the surface are approximated at all points by one-sided expressions. First, second, and third order expressions as follows were evaluated as discussed in the next section:

$$(f_\eta)_{i,1} = f_{i,2} - f_{i,1} \quad \text{(first order)} \tag{12a}$$

$$(f_\eta)_{i,1} = \frac{1}{2}(-f_{i,3} + 4f_{i,2} - 3f_{i,1}) \quad \text{(second order)} \tag{12b}$$

$$(f_\eta)_{i,1} = \frac{1}{6}(2f_{i,4} - 9f_{i,3} + 18f_{i,2} - 11f_{i,1}) \quad \text{(third order)} \tag{12c}$$

C. Kutta Condition

The value of the boundary value of ψ on the body, ψ_o, is determined by imposing the Kutta condition that the flow leave the sharp trailing edge of an airfoil smoothly. For a cusped trailing edge (zero included angle) this condition requires only that the velocity approach the same value at the trailing edge on the upper and lower surfaces of the airfoil. For a trailing edge with finite included angle it is required that the trailing edge be a stagnation point. It was found, however, that the requirement that the same limit be approached at the trailing edge on the upper and lower surfaces was superior numerically with both types of trailing edges. This limit condition was also applied by Giesing [1] as the Kutta condition with a finite trailing edge in the potential flow solution using superposition of singularities.

In the present solution the Kutta condition thus was applied by requiring that the value of the velocity component tangential to the body surface extrapolated at the trailing edge from neighboring points on the

upper surface be equal to that extrapolated from neighboring points on the lower surface. One, two, and three point extrapolations were evaluated, as well as the simple requirement that the velocity vanish at the trailing edge. These applications of the Kutta condition are as follows (Here superscript o refers to the trailing edge, and the other superscripts to successively distant neighboring points on the body surface as illustrated in Fig. 4. These points are, of course, equi-spaced in the transformed plane.):

$$v_t^{(1+)} = v_t^{(o)} = v_t^{(1-)} \qquad \text{(first order)} \quad (13a)$$

$$2v_t^{(1+)} - v_t^{(2+)} = v_t^{(o)} = 2v_t^{(1-)} - v_t^{(2-)} \qquad \text{(second order)} \quad (13b)$$

$$3v_t^{(1+)} - 3v_t^{(2+)} + v_t^{(3+)} = v_t^{(o)} = 3v_t^{(1-)} - 3v_t^{(2-)} + v_t^{(3-)} \qquad \text{(third order)} \quad (13c)$$

D. Superposition of Solutions

Since the system to be solved is linear in ψ, the solution for a single airfoil at any angle of attack may be obtained by superposing three component solutions: (1) a solution at 0° angle of attack with no circulation, (2) a solution at 90° angle of attack with no circulation, and (3) a solution with circulation but zero free stream velocity as done by Giesing [1]. These three component solutions, written $\psi^{(i)}(\xi,\eta)$, $i = 1, 2, 3$, each satisfy Eq. (6), with the respective boundary conditions

$$\psi_{i,1}^{(1)} = 0 \ , i = 1\text{---}I \qquad (14a)$$

$$\psi_{i,J}^{(1)} = y_{i,J} \ , \ i = 1\text{---}I \qquad (14b)$$

$$\psi_{i,1}^{(2)} = 0 \ , \ i = 1\text{---}I \qquad (15a)$$

$$\psi^{(2)}_{i,J} = -x_{i,J}\ ,\ i = 1\text{---}I \tag{15b}$$

$$\psi^{(3)}_{i,1} = 1\ ,\ i = 1\text{---}I \tag{16a}$$

$$\psi^{(3)}_{i,J} = 0\ ,\ i = 1\text{---}I \tag{16b}$$

The complete solution with arbitrary circulation then is

$$\psi(\xi,\eta;\lambda) = \psi^{(1)}(\xi,\eta)\ \cos\theta + \psi^{(2)}(\xi,\eta)\ \sin\theta - \lambda\psi^{(3)}(\xi,\eta) \tag{17}$$

The Kutta condition is then satisfied by choosing the coefficient λ such that the one of Eq. (13a) - (13c) being applied is satisfied, the tangential velocities being given by Eq. (10) with ψ from Eq. (17), using a one-sided difference expression analogous to Eq. (11) for the η-derivative.

Thus it is only necessary to solve the system of difference equations three times for a given airfoil. The solution at any angle of attack may then be obtained without re-solving the difference system.

E. Surface Pressure and Force Coefficients

The pressure coefficient at any point in the field may be obtained from the velocities via the Bernoulli equation, which in the present non-dimensional variables is

$$C_p = 1 - |\underset{\sim}{v}|^2 \tag{18}$$

On the body surface this becomes, from (10),

$$C_p = 1 - \frac{\gamma}{J^2}\,\psi_\eta^{\,2} \tag{19}$$

with the derivative evaluated by one of the difference expressions of (12).

The nondimensional force on the body is given by

$$\underset{\sim}{F} = -\oint C_p\ \underset{\sim}{n}\ ds \tag{20}$$

where $\underset{\sim}{n}$ is the unit outward normal to the surface, and ds is an increment of arc length along the surface. Since $\underset{\sim}{n}ds = \underset{\sim}{k} \times d\underset{\sim}{r}$, where $\underset{\sim}{r}$ is the position vector of points on the surface and $\underset{\sim}{k}$ is the unit normal to the two-dimensional plane, this becomes (see appendix)

$$\underset{\sim}{F} = -\oint C_p \left(\underset{\sim}{k} \times \frac{d\underset{\sim}{r}}{d\xi}\right)d\xi = -\oint C_p \left(\underset{\sim}{j}x_\xi - \underset{\sim}{i}y_\xi\right)d\xi$$

The unit vector in the direction of the free stream is $\underset{\sim}{a} = \underset{\sim}{i}\cos\theta + \underset{\sim}{j}\sin\theta$, and that normal to the free stream is $\underset{\sim}{k} \times \underset{\sim}{a} = \underset{\sim}{j}\cos\theta - \underset{\sim}{i}\sin\theta$, so that the lift and drag coefficients are

$$C_L = \underset{\sim}{a} \cdot \underset{\sim}{F} = \oint C_p \left(-x_\xi \cos\theta - y_\xi \sin\theta\right)d\xi \qquad (21a)$$

$$C_D = \left(\underset{\sim}{k} \times \underset{\sim}{a}\right) \cdot \underset{\sim}{F} = \oint C_p \left(y_\xi \cos\theta - x_\xi \sin\theta\right)d\xi \qquad (21b)$$

These integrals can be evaluated by numerical quadrature using either the trapezoidal rule or Simpson's rule, both of which were evaluated during the course of the investigation. For the former we have

$$\oint f\, d\xi = \frac{1}{2}\left(f_{1,1} + f_{I,1}\right) + \sum_{i=2}^{I-1} f_{i,1} \qquad \text{(first order)} \qquad (22a)$$

while for the latter, with I odd,

$$\oint f\, d\xi = \frac{1}{3}\left(f_{1,1} + f_{I,1}\right) + \frac{4}{3}\left(f_{2,1} + f_{I-1,1}\right) + \frac{2}{3}\sum_{i=3}^{I-2} f_{i,1} \qquad \text{(second order)} \qquad (22b)$$

F. Multiple Airfoils

With two airfoils, the boundary condition of Eq. (5a) becomes

$$\psi(x,y) = \psi_1 \quad \text{on the surface of body \#1} \qquad (23a)$$

$$\psi(x,y) = \psi_2 \quad \text{on the surface of body \#2} \qquad (23b)$$

With reference to Fig. 3b and the discussion in the previous section on

the coordinate system solution, these boundary conditions become, ir the transformed field,

$$\psi_{i,1} = \psi_1 \qquad i = I2---I3 \tag{24a}$$

$$\psi_{i,1} = \psi_2 \qquad i = 1---I1 \text{ and } i = I4---I \tag{24b}$$

As in the case of the coordinate system solution, the remaining portions of the j = 1 line are re-entrant boundaries, so that points thereon are treated as field points rather than boundary points. The ξ-derivatives at the surface points, I1, I2, I3, and I4, on the cuts between the bodies are also evaluated using the one-sided expressions of Eq. (11) in the calculation of the velocity on the surface.

The Kutta condition must be applied on each body. Therefore, a fourth component solution is added, and the four component solutions each satisfy Eq. (6), with the respective boundary conditions

$$\psi^{(1)}_{i,1} = 0 \qquad i = 1---I1,\ I2---I3,\ I4---I \tag{25a}$$

$$\psi^{(1)}_{i,J} = y_{i,J} \qquad i = 1---I \tag{25b}$$

$$\psi^{(2)}_{i,1} = 0 \qquad i = 1---I1,\ I2---I3,\ I4---I \tag{26a}$$

$$\psi^{(2)}_{i,J} = -x_{i,J} \qquad i = 1---I \tag{26b}$$

$$\psi^{(3)}_{i,1} = 0 \qquad i = 1---I1,\ I4---I \tag{27a}$$

$$\psi^{(3)}_{i,1} = 1 \qquad i = I2---I3 \tag{27b}$$

$$\psi^{(3)}_{i,J} = 0 \qquad i = 1\text{---}I \tag{27c}$$

$$\psi^{(4)}_{i,1} = 1 \qquad i = 1\text{---}I1,\ I4\text{---}I \tag{28a}$$

$$\psi^{(4)}_{i,1} = 0 \qquad i = I2\text{---}I3 \tag{28b}$$

$$\psi^{(4)}_{i,J} = 0 \qquad i = 1\text{---}I \tag{28c}$$

The complete solution with arbitrary circulation about each body is

$$\psi(\xi,\eta;\lambda_1,\lambda_2) = \psi^{(1)}(\xi,\eta)\cos\theta + \psi^{(2)}(\xi,\eta)\sin\theta + \lambda_1\psi^{(3)}(\xi,\eta) + \lambda_2\psi^{(4)}(\xi,\eta) \tag{29}$$

The Kutta condition is then satisfied by choosing the coefficients λ_1 and λ_2 such that the one of Eq. (13a) - (13c) being applied is satisfied on each body. This requires only the simultaneous solution of two linear algebraic equations. Generalizing to N bodies, it is necessary to solve the difference equation system N + 2 times for a given multiple airfoil system. The solution at any orientation of the free stream may then be obtained without re-solving the difference system.

IV. EFFECT OF NUMERICAL PARAMETERS

An extensive study was made to determine the effects of the various parameters involved on the accuracy of the numerical solution. Numerical results for the lift and drag coefficients, the surface pressure distribution, and the stream function contours for two Karman-Trefftz airfoils were compared with the analytic solutions (Ref. 21) using several values for each of the parameters that must be chosen in the numerical solution.

The numerical parameters involved in the solution are the following:

Coordinate System Parameters

I - number of points on the airfoil (number of ξ-lines).

J - number of lines surrounding the airfoil (number of η-lines).

r_∞ - radius of outer boundary.

ε_{CS} - convergence criterion for iteration error norms. (Iteration is terminated when the maximum absolute change in x and y over the field between iterations becomes less than ε_{CS})

Potential Flow Solution Parameters

ε_{PF} - convergence criterion for iteration error norms. (See note with ε_{CS} above)

Q_E - order of extrapolation used in satisfaction of Kutta condition. (See Eq. 13)

Q_{VK} - order of approximation in calculation of surface velocity used in satisfaction of Kutta condition. (See Eq. 12)

Q_{VP} - order of approximation in calculation of surface velocity used in surface pressure calculation. (See Eq. 12)

Q_I - order of approximation of pressure integration used in calculation of force coefficients. (See Eq. 22)

The comparison of the numerical results with the analytic solutions is presented in terms of the following quantities:

ΔC_L - lift coefficient error (numerical minus analytic).

ΔC_D - drag coefficient error (analytic is zero).

N_∞ - maximum norm of stream function error (maximum absolute difference between numerical and analytic values over entire field).

N_2 - Euclidean norm of relative stream function error (root-mean-square over entire field of difference between numerical and analytic values relative to analytic value).

Finally, results for these two airfoils at the zero-lift angle and a few other angles are also compared with the analytic solutions.

The parameter comparison cases and the values of the numerical parameters used therein are listed in Table 1, while the comparison of results is given in Tables 2 and 3. The number of iterations and the computer time required (UNIVAC 1106) are given correspondingly in Tables 4 and 5. The zero-lift angle results and results at other angles are given in Tables 6 and 7. The airfoil contours are shown in Figs. 5 and 6, and the points on the contours and the Karman-Trefftz parameters are given in Tables 8-10. Typical coordinate systems are shown in Fig. 7. Only a portion of the field is shown in each instance.) In addition, selected plots of the surface pressure distribution and the stream function contours in comparison with the analytic solution are presented in Figs. 8-17. In each figure the line is the analytic solution and the symbols are the numerical results. Finally, the numerical results for a Liebeck laminar airfoil are given in Figs. 18-21, in comparison with experimental data (Ref. 22).

A. Effect of Point Distribution on Airfoil Contour

As expected, the results generally improve as the number of points on the airfoil contour is increased. There are, however, some exceptions,

and the point distribution is important as well. The cases cited below with a number of points ending in '7' have points spaced at equal angles on the circle in the complex plane from which the airfoil was generated, with three additional points at half, quarter, and eighth spacing added above and below the trailing edge.

The pressure distribution for Airfoil #1 with 37 points on the contour agrees fairly well with the analytic solution but with some small deviation near the slope break on the upper surface (Fig. 8a). With 67 points the agreement is excellent (Fig. 8b). An increase to 127 points gives no real improvement and, in fact, a single low point appears at the slope break. The streamlines also show some slight deviation from the analytic curves with 37 points on the airfoil, particularly below the airfoil, but near perfect agreement is obtained with 67 points (Fig. 9). The lift and drag coefficient errors both decrease progressively as the number of points on the airfoil increases from 37 to 67 to 127 points for Airfoil #1 (Table 2). However, the Euclidean error norm of the stream function increases slightly for 127 points after decreasing for 67 points. These trends are the same with Airfoil #2, except that the case of 127 points is not quite as good as that with 67 points in any respect except C_D (Table 3).

The accuracy deteriorated significantly for both airfoils when the above-mentioned additional points near the trailing edge were removed. Thus the case of 61 points, having only equi-angular spaced points (in the complex plane), does not give as good agreement in the pressure distribution, the streamlines, or the force coefficients (Table 2) as does the case with the additional points (67 points). In fact, the force coefficients show an order of magnitude improvement for Airfoil #1 with the addition of these points near the trailing edge.

A similar addition of points between the equi-angular points near the leading edge, however, does not necessarily improve the solution. Fig. 8a and 10 show that for Airfoil #1 the pressure distribution with 43 points has a pressure dip near the leading edge that does not occur with 37 points or in the analytical curve. This effect becomes even more pronounced as more points near the leading edge are added (47 points). The streamlines also show some deviation from the analytical solution in the vicinity of the leading edge. The leading edge pressure peak is, however, better represented with the additional points, as is the small pressure dip that occurs at the slope break on the upper surface. The overall agreement for the pressure distribution is somewhat better with the addition of the six leading edge points to 37 point contour, and this is reflected in an improvement in the force coefficients (order-of-magnitude improvement in drag). The second addition of points (43 to 47) was deleterious in all respects. The addition of points near the leading edge of a contour with 67 points (total of 73 points), however, did not improve the force coefficients, and the pressure coefficient agreement deteriorated somewhat on the upper surface near the leading edge and near the slope break (Fig. 8b & c).

With Airfoil #2, the addition of the points between the equi-angular points near the leading edge (73 points total) deepened the low pressure spike near the leading edge beyond the analytical curve by a large amount, with a resultant adverse effect on the force coefficients (Fig. 15b & c). Although the lift did improve somewhat in one case (increase from 43 to 47), it appears that a more regular spacing of points is appropriate on the smooth portions of the contour. If the spacing is to be decreased near the leading edge, the variation should be smooth and gradual, especially with leading edges having large curvature placed at large angles of attack. More closely

spaced points should be added near the trailing edge, however. It should be noted that the equi-angular spacing in the complex plane gives an automatic concentration of points near the leading edge, but this concentration is smooth and gradual.

B. Effect of Number of Lines Surrounding the Body

Both the force coefficients improved somewhat with both airfoils as the number of lines surrounding the airfoil (n-lines) was increased, the trend being more marked with the thicker profile of Airfoil #1. However, the pressure dip at the slope break on the upper surface of Airfoil #1 was deepened beyond the analytical, and more of a dip appeared at the trailing edge (Fig. 11b & c). With Airfoil #2 there was little noticeable effect of the decreased number of lines on the pressure distribution or the streamlines. Thirty lines is clearly adequate for 1% accuracy in lift with the outer boundary located at 10 chords.

C. Effect of Location of Outer Boundary

Since the boundary conditions applied on the outer boundary are those appropriate at infinity, the outer boundary must be sufficiently distant from the body for accuracy. This effect was analyzed by changing both the outer boundary radius and the number of lines surrounding the body, so that the average mesh spacing would be unchanged. As expected, the force coefficients do improve as the outer boundary recedes. However, 10 chords was adequate for 1% accuracy in lift. A decrease in the outer boundary radius to 5 chords produced deterioration in both force coefficients. The use of a more distant outer boundary definitely requires an increase in the number of lines surrounding the body.

The effect of an increase in the outer boundary radius from 10 to 20 chords was not discernable in the pressure distribution and streamlines

for Airfoil #2. The effects with Airfoil #1 (Fig. 11) were similar to those of an increase in the number of lines surrounding the body. This results from the natural tendency of the coordinate system to expand outward from the body, so that a simultaneous increase in the outer boundary radius and the number of lines surrounding the body results in a closer line spacing near the body, even though the average spacing is unchanged.

D. Effect of Order of Extrapolation Used in Kutta Condition

The use of two or one point extrapolation of the velocity to the trailing edge in application of the Kutta condition resulted in a progressively deeper low pressure spike at the trailing edge with Airfoil #1 (cf Fig. 8c & 13b). This spike is removed with three-point extrapolation. This effect was less pronounced with Airfoil #2 since the trailing edge was less sharp. The use of the requirement that the trailing edge be a stagnation point gave about as good results as the use of the extrapolation to the trailing edge with the less sharp trailing edge of Airfoil #2 (cf Fig. 8c & 13a). Three-point extrapolation is the most appropriate condition, as is indicated by the ΔC_L values for Airfoil #1 in Table 2.

E. Effect of Order of Velocity Difference Expression Used in Kutta Condition

A first-order expression for the velocity is not sufficiently accurate and produced a low pressure spike at the trailing edge with Airfoil #1. This spike was removed by the use of a second-order expression (Fig. 8c). Further increase in order gave no improvement (Fig. 13d). Again these effects are less evident with the less sharp trailing edge of Airfoil #2.

F. Effect of Order of Velocity Difference Expression Used in Pressure Calculation Calculation

Here again a first-order expression does not give an accurate pressure distribution with Airfoil #1 (Fig. 14a). A second-order expression, however,

is quite accurate, (Fig. 8c) and little further improvement occured with an increase to third-order (Fig. 14b).

G. Effect of Order of Pressure Integration

Perhaps surprisingly, Simpson's rule (second-order) did not give as accurate a pressure integration as did the first-order trapezoidal rule. This probably is a result of the fact that although the points on the contour are equally spaced in the transformed plane, so that Simpson's rule can be applied, they are not equally spaced in the physical plane. Therefore, the truncation error term of the Simpson integration will be dependent on the rate-of-change of the physical coordinate spacing, so that, although the order is second, the coefficient may be high with a resultant loss in overall accuracy in regions of rapidly varying spacing.

H. Recommended Values

In view of the present results, 1% accuracy in lift can be achieved with the following values for the numerical parameters:

(a) 37 points on the airfoil contour, spaced with smooth and gradual concentration near the leading edge and with a few more closely spaced points added near the trailing edge.

(b) 30 lines surrounding the airfoil.

(c) Outer boundary at 10 chords.

(d) Coordinate system convergence criteria of 10^{-4}.

(e) Stream function convergence criteria of 10^{-4}.

(f) Three-point extrapolation to trailing edge in satisfaction of Kutta condition.

(g) Second-order difference expression for velocity.

(h) Trapezoidal pressure integration.

These values are the minimum considered adequate for 1% accuracy in lift. The changes in force coefficients encountered with more stringent values are summarized in Table 11 for Airfoil #1.

Items (f) - (h) are adequate for even higher accuracy. However, items (a) - (c) must be increased, and items (d) - (e) decreased for higher accuracy. A change of the convergence criteria to 10^{-5} is relatively inexpensive in computer time. However, computer time varies approximately linearly with the number of points on the airfoil and quadratically with the number of lines surrounding the airfoil. More points on the contour will obviously be required with more irregularly shaped bodies. The computer time is not significantly affected by the shape with the same number of points.

V. MULTIPLE-BODY SOLUTIONS

In the present study, the numerical results for potential flow about two circular cylinders, aligned such that a line connecting the circle centers is normal to the uniform free stream velocity, are compared with the analytic solution for the pressure distribution on the cylinder surfaces (Ref. 23). The cylinder axes were separated by three radii in all cases. The outer boundary was located at 20 cylinder diameters from the mid-point between the cylinders in all cases, and there were 40 η-lines surrounding the bodies, except as noted.

As noted above, there are a number of different possible arrangements in which the boundaries in a multiple-body field may be distributed around the rectangular boundary of the transformed field. Many of these arrangements are illustrated in Ref. 18-19. Three such arrangements were considered in the present study (Fig. 22).

If the generating partial differential system for the curvilinear coordinates is simply the pair of Laplace equations ($P = Q = 0$ in (2)), then the coordinate lines have a tendency to be attracted, as it were, to convex portions of the boundary and repelled from concave portions. This presents a problem with the two-body segment arrangement shown in Fig. 22a, for, with the η-coordinate having the same value on both bodies, the cut connecting the bodies must also be a line of the same η-value. Consequently, a concave region develops at the intersections of this cut with the bodies. The resulting coordinate system is shown in Fig. 23a, and the results for the surface pressure distribution in Fig. 23b are grossly in error because of the large truncation error that occurs with the widely spaced coordinate lines in the regions of the cut intersections.

However, coordinate system control, as discussed above, can be used to attract the coordinate lines into these concave regions. As noted above, it is possible to attract the coordinate lines to specified lines and/or points on the boundary and in the field. Various different combinations of line and point attractions were considered and representative results are shown in Figs. 24 and 25.

In Fig. 24a-e, the coordinate systems and pressure distributions are shown for five amplitudes of point attraction of the η-lines (surrounding the bodies) to the cut intersections. The attraction decay factor (see appendix) was 0.5 in all cases given. Too large a decay factor is ineffective, while too small a factor extends the attraction beyond the local region of interest. The pressure distribution changes drastically from that from that obtained without attraction (Fig. 23) as the attraction amplitude is initially increased. The changes become progressively smaller as the amplitude increases farther, with very little change from an amplitude of 500 to one of 2000. (Although the best fit to the analytic solution occurs with an amplitude of 250, this is only a fortuitous circumstance, since the results are still changing with attraction amplitude at that point.) This progressively diminishing effect of increasing attraction amplitude is also evident in the force coefficiencs normal to the free stream given in Table 12 .

Comparison of Figs. 24d and 24f shows the effect of decreasing the number of ξ-lines passing between the bodies. The solution is not greatly affected by the decrease in the number of lines except in the region of the cut intersections, where the angle between the ξ-line emanating from the cut intersection and the η-line between the bodies is smaller. Too small an angle between coordinate lines increases the local truncation

error, so that it is necessary to avoid having the ξ-line emanating from the cut intersection deviate greatly from 45°. This means that the point spacing on the cut between the bodies should be nearly the same as that on the body contours in the neighborhood of the cut intersections. Table 12 shows that an addition of four lines between the bodies, by contrast, had little effect.

This need for relatively equal point spacing on the body contours and the cut between is further illustrated in Figs. 25b and 25d, where, with fewer points on the bodies, the smaller number of lines between the bodies gives better results. The force coefficients results in Table 12 show a further deterioration as still more lines are added between the bodies. This figure also shows that, with this smaller number of points on the bodies, the increasing attraction produces little change from an amplitude of 500 to one of 1000, but a larger change then occurs at a larger amplitude. Comparison of the force coefficients in Table 12 also shows that 31 points on each body is not enough for accuracy.

That the addition of more points on the body contour in the neighborhood of the cut intersection is inferior to uniformly spaced points is illustrated in Figure 26a. Here the additional closely spaced points on the contour have caused the ξ-line angles on the contour near the cut intersections to become too small. Some control over these angles can be exercised by attracting the ξ-lines, as well as the η-line to the cut intersections, the results of which are illustrated in Figure 26b. However, the curvature of the ξ-lines in the field near the cut is now quite large, and truncation error results therefrom. Other combinations of attractions were also considered, and some results therefor are given in Table 12.

Table 12 also gives the force coefficients for some cases with closer and more distant outer boundaries and cases with fewer η-lines surrounding the bodies. These results show only small differences with 61 points on the bodies.

Two other coordinate system configurations are shown in Figs. 27 and 28. That of Fig. 28 is similar to a bi-polar coordinate system and produces a near-perfect comparison with the analytic results on one cylinder with 61 points on each body. With 31 points, however, the accuracy is not quite as good. Since this configuration has different coordinate values on the two bodies, cut intersections of the type discussed above do not occur, and the coordinate system is much more regular near the bodies. However, in contrast to the previous configuration, the results on the other cylinder are not quite identical. This appeared to be a bi-stable situation, with excellent comparison occuring on the other cylinder in some cases, a result, perhaps, of the SOR iteration sweeping the field in one direction. The force coefficient of the previously considered configuration #1 with 61 points on the contour (0.6534) is within 3% of the essentially exact value (0.6331) obtained from Fig. 28b. The results of the configuration of Fig. 27 could be improved by coordinate system control as used above.

Finally, Figs. 29 and 30 show the coordinate system and potential solution for a multiple airfoil consisting of two Karman-Trefftz airfoils, one being positioned as a separated flap. Coordinate system control has been used to attract the coordinate lines to the airfoils and to the cut between.

VI. CONCLUSION

The use of body-fitted curvilinear coordinate systems allows numerical potential flow solutions for fields containing any number of bodies of arbitrary shape to be produced by finite-difference methods essentially as easily as that about single simple bodies. The computer code is not dependent on either the number or the shapes of the bodies, so that different bodies can be treated by simple changes in the input. Further investigation of the control of the coordinate system is presently in progress with the purpose of improving the coordinate configuration in concave regions created by cut intersections with members of multiple-body combinations. Multiple-body viscous solutions are also under development.

APPENDIX

DERIVATIVES AND VECTORS IN THE TRANSFORMED PLANE

Derivative Transformations

$$f_x = \left(\frac{\partial f}{\partial x}\right)_{y,t} = (y_\eta f_\xi - y_\xi f_\eta)/J \tag{A.1}$$

$$f_y = \left(\frac{\partial f}{\partial y}\right)_{x,t} = (x_\xi f_\eta - x_\eta f_\xi)/J \tag{A.2}$$

$$f_t = \left(\frac{\partial f}{\partial t}\right)_{x,y} = \left(\frac{\partial f}{\partial t}\right)_{\xi,\eta} - \frac{1}{J}(y_\eta f_\xi - y_\xi f_\eta)\left(\frac{\partial x}{\partial t}\right)_{\xi,\eta} - \frac{1}{J}(x_\xi f_\eta - x_\eta f_\xi)\left(\frac{\partial y}{\partial t}\right)_{\xi,\eta} \tag{A.3}$$

$$\nabla^2 f = \frac{\partial^2 f}{\partial x^2} + \frac{\partial^2 f}{\partial y^2} = (\alpha f_{\xi\xi} - 2\beta f_{\xi\eta} + \gamma f_{\eta\eta})/J^2 + Qf_\eta + Pf_\xi \tag{A.4}$$

Unit Vectors in the Transformed Plane

Let $\underset{\sim}{n}_\eta$ be the unit vector normal to a line of constant η and $\underset{\sim}{\tau}_\eta$ be the unit vector tangent to an η-line. Utilizing similar definitions for unit normals and tangents to ξ=constant lines, there results

$$\underset{\sim}{n}_\eta = \frac{\nabla\eta}{|\nabla\eta|} = (-y_\xi \underset{\sim}{i} + x_\xi \underset{\sim}{j})/\sqrt{\gamma} \tag{A.5}$$

$$\underset{\sim}{n}_\xi \quad \frac{\nabla\xi}{|\nabla\xi|} = (y_\eta \underset{\sim}{i} - x_\eta \underset{\sim}{j})/\sqrt{\alpha} \tag{A.6}$$

$$\underset{\sim}{\tau}_\eta \equiv \underset{\sim}{n}_\eta \times \underset{\sim}{k} = (x_\xi \underset{\sim}{i} + y_\xi \underset{\sim}{j})/\sqrt{\gamma} \tag{A.7}$$

$$\underset{\sim}{\tau}_\xi \equiv \underset{\sim}{n}_\xi \times \underset{\sim}{k} = -(x_\eta \underset{\sim}{i} + y_\eta \underset{\sim}{j})/\sqrt{\alpha} \tag{A.8}$$

where $\underset{\sim}{i}$, $\underset{\sim}{j}$, and $\underset{\sim}{k}$ are the unit vectors parallel to the conventional cartesian coordinates x, y, and z, respectively. Vector components along the tangents and normals to lines of constant ξ and η are obtained by dotting the desired vector with one of the above. For example, if $\underset{\sim}{F} = F_1 \underset{\sim}{i} + F_2 \underset{\sim}{j}$, then the component tangent to an η-line, $F_{\underset{\sim}{\tau}_\eta}$, is given by

$$F_{\underset{\sim}{\tau}_\eta} = \underset{\sim}{F} \cdot \underset{\sim}{\tau}_\eta = (x_\xi F_1 + y_\xi F_2)/\sqrt{\gamma} \tag{A.9}$$

Similarly, directional derivatives of a scalar function f in the above directions can be obtained from the inner product of the gradient of f, ∇f, and the appropriate unit vector. For example, the directional derivative normal to an η-line is

$$\frac{\partial f}{\partial n_\eta} = \underset{\sim}{n}_\eta \cdot \nabla f = (\gamma f_\eta - \beta f_\xi)/J\sqrt{\gamma} \tag{A.10}$$

Integral Transformation

Let S be the closed cylindrical surface of unit depth whose perimeter is specified by the contour Γ_1 in the physical plane (Fig. 1), and whose outward unit normal at any point is $\underset{\sim}{n}(x,y)$. (Note that this is the unit normal to the η-line coincident with Γ_1.). Then,

$$\underset{\sim}{I} \equiv \int_S f(x,y)\underset{\sim}{n}(x,y)dS = \int_{\xi_{min}}^{\xi_{max}} f[x(\xi,\eta_1),y(\xi,\eta_1)](x_\xi \underset{\sim}{j} - y_\xi \underset{\sim}{i})d\xi \tag{A.11}$$

where η_1 is the value of η on Γ_1, ξ_{min} and ξ_{max} are the minimum and maximum values of ξ, and x_ξ and y_ξ are evaluated along η_1.

Coordinate System Control

The effect of changing the functions $P(\xi,\eta)$ and $Q(\xi,\eta)$ on the coordinate system is discussed in some detail in Ref. 18 and 19. One particularly effective procedure is to choose P and Q as exponential terms, so that the coordinates are generated as the solutions of

$$\xi_{xx} + \xi_{yy} = -\sum_{i=1}^{n} a_i \, \mathrm{sgn}(\xi - \xi_i)\exp(-c_i|\xi - \xi_i|)$$

$$-\sum_{j=1}^{m} b_j \, \mathrm{sgn}(\xi - \xi_j)\exp\left(-d_j\sqrt{(\xi - \xi_j)^2 + (\eta - \eta_j)^2}\right)$$

$$\equiv P(\xi,\eta) \qquad \text{(A.12)}$$

$$\eta_{xx} + \eta_{yy} = -\sum_{i=1}^{n} a_i \, \mathrm{sgn}(\eta - \eta_i)\exp(-c_i|\eta - \eta_i|)$$

$$-\sum_{j=1}^{m} b_j \, \mathrm{sgn}(\eta - \eta_j)\exp\left(-d_j\sqrt{(\xi - \xi_j)^2 + (\eta - \eta_j)^2}\right)$$

$$\equiv Q(\xi,\eta) \qquad \text{(A.13)}$$

where the positive amplitudes and decay factors are not necessarily the same in the two equations. Here the first terms have the effect of attracting ξ-lines to the $\xi = \xi_i$ lines in Eq. (A.12), and attracting η-lines to the $\eta = \eta_i$ lines in (A.13). The second terms cause ξ-lines to be attracted to the points (ξ_j,η_j) in (A.12), and η-lines to be attracted to the points (ξ_j,η_j) in (A.13). Several examples of the use of coordinate system control are given in Ref. 18 and 19.

REFERENCES

1. J. P. Giesing, "Potential Flow About Two-Dimensional Airfoils," Rept. LB 31946, Douglas Aircraft Co. (1965).

2. J. L. Hess and A. M. O. Smith, "Calculation of Potential Flow About Arbitrary Bodies," Progress in Aeronautical Sciences, 8, 1, Pergammon Press, Oxford (1966).

3. J. P. Giesing, "Unsteady Two-Dimensional Potential Flow for Two Bodies with Lift," Rept. DAC-33552, Douglas Aircraft Co., (1967).

4. J. P. Giesing, "Nonlinear Two-Dimensional Unsteady Potential Flow with Lift," Journal of Aircraft, 5, 135 (1968).

5. J. L. Hess, "Calculation of Potential Flow About Arbitrary Three-Dimensional Lifting Bodies," Rept. MDC J5679-01, McDonnel Douglas Corp. (1972).

6. R. H. Djojodihardjo and S. E. Widnall, "A Numerical Method for the Calculation of Nonlinear, Unsteady Lifting Potential Flow Problems," AIAA Journal, 7, 2001 (1969).

7. E. Grodtkjaer, "A Direct Integral Equation Method for the Potential Flow About Arbitrary Bodies," Int. Jour. for Numerical Methods in Engineering, 6, 253 (1973).

8. W. C. Webster, "The Flow About Arbitrary, Three-Dimensional Smooth Bodies," Journal of Ship Research, 19, 206 (1975).

9. L. J. Doctors, "An Application of the Finite Element Technique to Boundary Value Problems of Potential Flow, Int. Jour. for Numerical Methods in Engineering, 2, 243 (1970).

10. J. H. Argyris and G. Maruzek, "Potential Flow Analysis by Finite Elements," Ingenieur-Archiv, 41, 1 (1972).

11. U. Meissner, "A Mixed Finite Element Model for Use in Potential Flow Problems," Int. Jour. for Numerical Methods in Engineering, 6, 467 (1973).

12. T. Theodorsen and I. E. Garrick, "General Potential Theory of Arbitrary Wing Sections," NACA TR 452 (1933).

13. D. C. Ives, "A Modern Look at Conformal Mapping, Including Doubly Connected Regions," AIAA Paper 75-842, AIAA 8th Fluid and Plasma Dynamics Conference, Hartford (1975).

14. J. F. Thompson, F. C. Thames, and C. W. Mastin, "Automatic Numerical Generation of Body-Fitted Curvilinear Coordinate System for Field Containing Any Number of Arbitrary Two-Dimensional Bodies," Journal of Computational Physics, 15, 299 (1974).

15. F. C. Thames, J. F. Thompson, and C. W. Mastin, "Numerical Solution of the Navier-Stokes Equations for Arbitrary Two-Dimensional Airfoils," Proceedings of NASA Conference on Aerodynamic Analyses Requiring Advanced Computers, Langley Research Center, NASA SP-347, (1975).

16. F. C. Thames, "Numerical Solution of the Incompressible Navier-Stokes Equations about Arbitrary Two-Dimensional Bodies," Ph.D. Dissertation, Mississippi State University (1975).

17. J. F. Thompson, F. C. Thames, and S. P. Shanks, "Use of Numerically Generated Body-Fitted Coordinate Systems for Solution of the Navier-Stokes Equations," Proceedings of AIAA 2nd Computational Fluid Dynamics Conference, Hartford, Connecticut, (1975).

18. J. F. Thompson, F. C. Thames, and C. W. Mastin, "Boundary-Fitted Curvilinear Coordinate Systems for Solution of Partial Differential Equations on Fields Containing Any Number of Arbitrary Two-Dimensional Bodies," NASA CR, Mississippi State University, to be published 1976.

19. J. F. Thompson, F. C. Thames, and C. W. Mastin, "Bodyfit-A Code for Coordinate Systems on Fields Containing any Number of Arbitrary Two-Dimensional Bodies," Journal of Computational Physics, submitted 1976.

20. J. F. Thompson, F. C. Thames, C. W. Mastin, and R. L. Walker, "Numerical Solution of the Time-Dependent Navier-Stokes Equations About Arbitrary Two-Dimensional Bodies," Journal of Computational Physics, submitted 1976.

21. K. Karamacheti, Principles of Ideal-Fluid Aerodynamics, John Wiley & Sons, Inc., (1966).

22. R. H. Liebeck, Wind Tunnel Tests of Two Airfoils Designed for High Lift Without Separation in Incompressible Flow, McDonnel Douglas Corporation, Report No. MDC-J5667/01, (1972).

23. P. M. K. Morse and H. Feshbach, Method of Theoretical Physics, Vol. II, McGraw-Hill, (1953).

TABLE 1

Parameter Comparison Cases - Airfoils #1 and #2

Case	Airfoil	I	J	r_∞	$\log_{10} \epsilon_{CS}$	α	$\log_{10} \epsilon_{PF}$	Q_E	Q_{VK}	Q_{VP}	Q_I
1	1, 2	127	30	10	-5	See Note #1	-5	3	2	2	1
2	↓	43	↓	↓	↓	↓	↓	↓	↓	↓	↓
3	↓	47	↓	↓	↓	↓	↓	↓	↓	↓	↓
4	2	53	↓	↓	↓	↓	↓	↓	↓	↓	↓
5	1, 2	73	↓	↓	↓	↓	↓	↓	↓	↓	↓
6	↓	61	↓	↓	↓	↓	↓	↓	↓	↓	↓
7	↓	67	60	↓	-4	↓	-4	↓	↓	↓	↓
8	↓	↓	↓	20	↓	↓	↓	↓	↓	↓	↓
9	↓	↓	↓	40	↓	↓	↓	↓	↓	↓	↓
10	↓	↓	↓	80	↓	↓	↓	↓	↓	↓	↓
11	↓	↓	30	5	↓	↓	↓	↓	↓	↓	↓
12	↓	↓	↓	20	↓	↓	↓	↓	↓	↓	↓
13	1	37	↓	10	-2	↓	-5	↓	↓	↓	↓
14	↓	↓	↓	↓	-3	↓	↓	↓	↓	↓	↓
15	↓	↓	↓	↓	-4	↓	↓	↓	↓	↓	↓
16	↓	↓	↓	↓	-5	↓	↓	↓	↓	↓	↓
17	1, 2	↓	↓	↓	↓	↓	↓	↓	↓	↓	↓
18	↓	↓	↓	↓	↓	↓	↓	↓	↓	↓	↓
19	↓	67	↓	↓	-4	↓	↓	↓	↓	↓	↓
20	↓	↓	↓	↓	-5	↓	↓	↓	↓	↓	↓
21	↓	↓	↓	↓	↓	↓	-2	↓	↓	↓	↓
22	↓	↓	↓	↓	↓	↓	-3	↓	↓	↓	↓
23	↓	↓	↓	↓	↓	↓	-4	↓	↓	↓	↓
24	↓	73	↓	↓	↓	↓	-5	1	↓	↓	↓
25	↓	↓	↓	↓	↓	↓	↓	2	↓	↓	↓
26	↓	↓	↓	↓	↓	↓	↓	SP	↓	↓	↓
27	↓	↓	↓	↓	↓	↓	↓	3	1	↓	↓
28	↓	↓	↓	↓	↓	↓	↓	↓	3	↓	↓
29	↓	↓	↓	↓	↓	↓	↓	↓	2	1	↓
30	↓	↓	↓	↓	↓	↓	↓	↓	2	3	↓

TABLE 1 (CONTINUED)

Case	Airfoil	I	J	r_∞	$\log_{10} \epsilon_{CS}$	α	$\log_{10} \epsilon_{PF}$	Q_E	Q_{VK}	Q_{VP}	Q_I
31	1, 2	73	30	10	-5	See Note #1	-5	3	2	2	2
32	1, 2	67	30	10	-4		-4	3	2	2	1
33	1	127	30	10	-5	-20.8596	-5	3	2	2	1
34	2	127	↓	↓	↓	- 1.6746	↓	↓	↓	↓	↓
35	2	73				- 1.65					
36	2	73				- 2.66					

Note #1: Airfoil #1 was at 0° angle of attack, and airfoil #2 was at 30°, except as noted.

Note #2: The SOR acceleration parameter for the coordinate system was 1.86 in all cases except Cases 13-18 and 32 where 1.83 was used. For the potential flow solution, 1.85 was used in all cases except Cases 18-23 where 1.87 was used. These changes do not reflect changes in the optimum value but rather are due to runs being made at different times.

Legend: Coordinate System Parameters

- I - number of points on the airfoil (number of ξ-lines)
- J - number of points from airfoil to outer boundary (number of η-lines)
- r_∞ - radius of outer boundary
- ϵ_{CS} - convergence criterion for iteration error norms (Iteration is terminated when the maximum absolute change in x and y over the field between iterations becomes less than ϵ_{CS}.)

Potential Flow Solution Parameters

- α - angle of attack
- ϵ_{PF} - convergence criterion for iteration error norms (see note with ϵ_{CS} above)
- Q_E - order of extrapolation used in satisfaction of Kutta condition (see Eq. 13).
- Q_{VK} - order of approximation in calculation of surface velocity used in satisfaction of Kutta condition (see. Eq. 12).

TABLE 1 (CONCLUDED)

Legend Continued:

Q_{VP} - order of approximation in calculation of surface velocity used in surface pressure calculation (see Eq. 12).

Q_I - order of approximation of pressure integration used in calculation of force coefficients (see Eq. 22).

TABLE 2

Comparison with Analytic Solution - Airfoil #1

Case	ΔC_L	ΔC_D	N_∞	N_2
Points on Body				
37 16	-0.0087	0.0102	3.35-01	2.06-03
43 2	0.0059	-0.0008	3.29-01	3.98-03
47 3	0.0120	-0.0212	3.29-01	4.31-03
61 6	-0.0577	-0.0325	3.28-01	4.44-03
67 20	-0.0019	0.0040	3.37-01	1.31-03
73 5	0.0019	-0.0046	3.29-01	2.07-03
127 1	0.0006	0.0017	3.40-01	9.96-03
Points to ∞, ∽ at 10				
30 32	-0.0080	0.0038	3.37-01	1.21-03
60 7	0.0032	-0.0026	3.78-01	1.38-03
Points to ∞, ∞ at 20				
30 12	-0.0169	0.0078	3.65-01	5.65-03
60 8	-0.0057	0.0010	3.64-01	7.89-04
Location of ∞, Step Size 10/60 avg.				
5 11	0.0296	-0.0067	3.08-01	2.10-03
10 7	0.0032	-0.0026	3.78-01	1.38-03
Location of ∞, Step Size 20/60 avg.				
10 32	-0.0080	0.0038	3.37-01	1.21-03
20 8	-0.0057	0.0010	3.64-01	7.89-04
Location of ∞, Step Size 40/60 avg.				
20 12	-0.0169	0.0078	3.65-01	5.65-03
40 9	-0.0100	0.0028	3.86-01	4.85-04
Location of ∞, 30 Points to ∞				
5 11	0.0300	-0.0067	3.08-01	2.10-03
10 32	-0.0080	0.0038	3.37-01	1.21-03
20 12	-0.0169	0.0078	3.65-01	5.65-03

TABLE 2 (CONTINUED)

	Case	ΔC_L	ΔC_D	N_∞	N_2
Location of ∞, 60 Points to ∞					
10	7	0.0032	-0.0026	3.78-01	1.38-03
20	8	-0.0057	0.0010	3.64-01	7.89-04
40	9	-0.0100	0.0028	3.86-01	4.85-04
80	10	-0.0120	0.0041	3.56-01	1.11-03
Coordinate System Convergence Criteria, 37 Points on Body					
10-2	13	-0.1691	0.0049	3.42-01	3.80-03
10-3	14	-0.0118	0.0108	3.36-01	3.14-03
10-4	15	-0.0108	0.0103	3.35-01	2.09-03
10-5	16	-0.0087	0.0103	3.35-01	2.06-03
Coordinate System Convergence Criteria, 67 Points on Body					
10-3	18	-0.0345	0.0035	3.38-01	1.28-03
10-4	19	-0.0051	0.0040	3.37-01	1.24-03
10-5	20	-0.0019	0.0040	3.37-01	1.31-03
Stream Function Convergence Criteria					
10-2	21	-0.0687	-0.1066	3.32-01	2.14-02
10-3	22	0.0548	-0.0084	3.37-01	1.22-03
10-4	23	-0.0096	0.0047	3.37-01	1.26-03
10-5	20	-0.0019	0.0040	3.37-01	1.31-03
Order of Extrapolation for Kutta Condition					
1	24	-0.0044	-0.0046	3.29-01	1.16-02
2	25	0.0027	-0.0046	3.29-01	1.93-03
3	5	0.0019	-0.0046	3.29-01	2.07-03
Stagnation Point	26	0.0581	-0.0050	3.30-01	1.18-02
Order of Velocity for Kutta Condition					
1	27	-0.0814	-0.0041	3.28-01	6.61-03
2	5	0.0019	-0.0046	3.29-01	2.07-03
3	28	0.0083	-0.0047	3.29-01	3.08-03
Order of Velocity for Pressure Calculation					
1	29	0.0722	0.0109	3.29-01	2.07-03
2	5	0.0019	-0.0046	3.29-01	2.07-03
3	30	0.0084	-0.0015	3.29-01	2.07-03
Order of Pressure Integration					
1	5	0.0019	-0.0046	3.29-01	2.07-03
2	31	0.0040	-0.0087	3.29-01	2.07-03

TABLE 2 (CONCLUDED)

Note: Case numbers correspond to those of Table 1.

Legend:

The comparison of the numerical results with the analytic solutions is presented in terms of the following quantities:

ΔC_L - lift coefficient error (numerical minus analytic)

ΔC_D - drag coefficient error (analytic is zero)

N_∞ - maximum norm of stream function error (maximum absolute difference between numerical and analytic values over entire field)

N_2 - Euclidean norm of relative stream function error (root-mean-square over entire field of difference between numerical and analytic values relative to analytic value)

TABLE 3

Comparison with Analytic Solution - Airfoil #2

	Case	ΔC_L	ΔC_D	N_∞	N_2
Points on Body					
43	2	-0.0633	0.2135	1.11-01	2.96-02
47	3	0.0023	0.2487	1.10-01	2.31-02
53	4	0.0086	0.2580	1.09-01	7.21-03
61	6	-0.0741	-0.0211	1.57-01	6.68-03
67	20	0.0475	-0.0250	3.13-02	1.04-03
73	5	0.0890	0.0990	1.11-01	2.05-02
127	1	0.0973	-0.0197	1.11-01	1.71-02
Points to ∞, ∞ at 10					
30	32	0.0433	-0.0253	3.93-02	2.63-03
60	7	0.0307	-0.0217	4.11-02	2.02-03
Points to ∞, ∞ at 20					
30	12	0.0412	-0.0280	4.67-02	1.48-03
60	8	0.0171	-0.0159	4.47-02	2.25-03
Location of ∞, Step Size 10/60 Avg.					
5	11	0.0929	-0.0423	4.68-02	6.86-03
10	7	0.0307	-0.0217	4.11-02	2.02-03
Location of ∞, Step Size 20/60 Avg.					
10	32	0.0433	-0.0253	3.93-02	2.63-03
20	8	0.0171	-0.0159	4.47-02	2.25-03
Location of ∞, Step Size 40/60 Avg.					
20	12	0.0412	-0.0280	4.67-02	1.48-03
40	9	0.0156	-0.0146	5.45-02	2.23-03
Location of ∞, 30 Points to ∞					
5	11	0.0929	-0.0423	4.68-02	6.86-03
10	32	0.0433	-0.0253	3.93-02	2.63-03
20	12	0.0412	-0.0280	4.67-02	1.48-03
Location of ∞, 60 Points to ∞					
10	7	0.0307	-0.0217	4.11-02	2.02-03
20	8	0.0171	-0.0159	4.47-02	2.25-03
40	9	0.0156	-0.0146	5.45-02	2.23-03
80	10	0.0176	-0.0151	6.86-02	5.22-03

TABLE 3 (CONTINUED)

	Case	ΔC_L	ΔC_D	N_∞	N_2
Coordinate System Convergence Criteria					
10-2	17	-0.4180	-0.0204	4.81-02	6.40-03
10-3	18	-0.0619	-0.0245	3.09-02	1.37-03
10-4	19	0.0430	-0.0249	3.13-02	8.89-04
10-5	20	0.0475	-0.0250	3.13-02	1.04-03
Stream Function Convergence Criteria					
10-2	21	0.6407	-0.2199	4.01-01	3.62-02
10-3	22	0.1192	-0.0620	9.32-02	4.18-03
10-4	23	0.0487	-0.0255	3.92-02	2.20-03
10-5	20	0.0475	-0.0250	3.13-02	1.04-03
Order of Extrapolation for Kutta Condition					
1	24	0.0857	0.0989	1.11-01	2.05-02
2	25	0.0902	0.0991	1.11-01	2.05-02
3	5	0.0890	0.0990	1.11-01	2.05-02
Stagnation Point	26	0.0881	0.0990	1.11-01	2.05-02
Order of Velocity for Kutta Condition					
1	27	0.1150	0.0997	1.18-01	3.62-03
2	5	0.0890	0.0990	1.11-01	2.05-02
3	28	0.1057	0.0995	1.15-01	3.11-03
Order of Velocity for Pressure Calculation					
1	29	0.02401	0.1397	1.11-01	2.05-02
2	5	0.0890	0.0990	1.11-01	2.05-02
3	30	0.0744	0.0917	1.11-01	2.05-02
Order of Pressure Integration					
1	5	0.0890	0.0990	1.11-01	2.05-02
2	31	-0.2298	0.0879	1.11-01	2.05-02

Note: Case numbers correspond to those of Table 1.

Legend:

The comparison of the numerical results with the analytic solutions is presented in terms of the following quantities:

TABLE 3 (CONCLUDED)

ΔC_L - lift coefficient error (numerical minus analytic)

ΔC_D - drag coefficient error (analytic is zero)

N_∞ - maximum norm of stream function (maximum absolute difference between numerical and analytic values over entire field)

N_2 - Euclidean norm of relative stream function error (root-mean-square over entire field of difference between numerical and analytic values relative to analytic value)

TABLE 4

Iterations and Computer Time - Airfoil #1

	Case	IT_{CS}	IT_{0}	IT_{90}	IT_{CIR}	CT_{CS}	CT_{PSI}
Points on Body							
37	16	95	60	77	78	0:57	0:56
43	2	105	62	81	84	1:14	1:09
47	3	106	65	83	92	1:19	1:11
61	6	132	79	95	124	2:04	1:52
67	20	151	83	114	121	2:28	1:59
73	5	172	96	100	156	3:10	2:35
127	1	401	197	195	348	11:57	7:46
Points at ∞, ∞ at 10							
30	32	116	53	73	101	1:58	1:39
60	7	227	73	79	188	7:21	4:06
Points to ∞, ∞ at 20							
30	12	165	58	80	125	2:44	1:49
60	8	290	74	82	208	10:13	5:44
Location of ∞, Step Size 10/60 avg.							
5	11	123	47	69	79	2:06	1:27
10	7	227	73	79	188	7:21	4:06
Location of ∞, Step Size 20/60 avg.							
10	32	116	53	73	101	1:58	1:39
20	8	290	74	82	208	10:13	5:44
Location of ∞, Step Size 40/60 avg.							
20	12	165	58	80	125	2:44	1:49
40	9	360	75	86	232	11:34	5:54
Location of ∞, 30 Points to ∞							
5	11	123	47	69	79	2:06	1:27
10	32	116	53	73	101	1:58	1:39
20	12	165	58	80	125	2:44	1:49

TABLE 4 (CONCLUDED)

Case	IT_{CS}	IT_0	IT_{90}	IT_{CIR}	CT_{CS}	CT_{PSI}
Location of ∞, 60 Points to ∞						
10	7	227	73	79	188	7:21	4:06
20	8	290	74	82	208	10:31	5:44
40	9	360	75	86	232	11:34	5:54
80	10	446	78	91	258	14:13	5:01
Coordinate System Convergence Criteria, 37 Points on Body						
10-2	13	38	59	78	78	0:30	0:57
10-3	14	54	60	77	78	0:39	0:57
10-4	15	75	60	77	78	0:49	1:16
10-5	16	95	60	77	78	0:57	0:56
Coordinate System Convergence Criteria, 67 Points on Body						
10-3	18		83	114	121		1:59
10-4	19	116	83	114	121	1:58	1:59
10-5	20	151	83	114	121	2:28	1:59
Stream Function Convergence Criteria						
10-2	21	151	6	25	30	2:28	0:40
10-3	22	151	21	54	60	2:28	1:02
10-4	23	151	51	87	90	2:28	1:30
10-5	20	151	83	114	121	2:28	1:59

Note #1: Case numbers correspond to those of Table 1.

Note #2: CPU time is given in MINUTES:SECONDS. These times are subject to some variation depending on the operating conditions at the time of the run.

Legend:

IT_{CS} - Iterations for coordinate system

IT_0 - Iterations for 0° potential flow solution

IT_{90} - Iterations for 90° potential flow solution

IT_{CIR} - Iterations for circulation potential flow solution

CT_{CS} - CPU time for coordinate system

CT_{PSI} - CPU time for complete potential flow solution

TABLE 5

Iterations and Computer Time - Airfoil #2

	Case	IT_{CS}	IT_0	IT_{90}	IT_{CIR}	CT_{CS}	CT_{PSI}
Points on Body							
43	2	95	53	72	82	1:27	1:10
37	3	104	57	77	92	1:17	1:09
53	4	118	59	81	106	1:38	1:21
61	6	144	65	88	124	2:84	2:09
67	20	162	68	92	141	2:40	2:11
73	5	182	75	100	157	3:25	2:28
127	1	419	131	170	350	12:56	1:01
Points to ∞, ∞ at 10							
30	32	125	36	61	101	2:11	2:01
60	7	239	42	75	188	7:54	3:45
Points to ∞, ∞ at 20							
30	12	225	37	64	125	4:01	2:04
60	8	299	39	71	208	9:58	3:54
Location of ∞, Step Size 10/60 Avg.							
5	11	86	34	57	79	1:33	1:19
10	7	239	42	75	188	7:54	3:45
Location of ∞, Step Size 20/60 Avg.							
10	32	125	36	61	101	2:11	2:01
20	8	299	39	71	208	9:58	3:54
Location of ∞, Step Size 40/60 Avg.							
20	12	225	37	64	125	4:01	2:04
40	9	374	37	69	231	11:60	3:57
Location of ∞, 30 Points to ∞							
5	11	86	34	57	79	1:33	1:19
10	32	125	36	61	101	2:11	2:01
20	12	225	37	64	125	4:01	2:04

TABLE 5 (CONCLUDED)

	Case	IT_{CS}	IT_0	IT_{90}	IT_{CIR}	CT_{CS}	CT_{PSI}
Location of ∞, 60 Points to ∞							
10	7	239	42	75	188	7:54	3:45
20	8	299	39	71	208	9:58	3:54
40	9	374	37	69	231	11:60	3:57
80	10	463	36	68	257	15:34	4:14
Coordinate System Convergence Criteria							
	17	52	85	97	140	1:02	2:04
10-3	18	88	71	92	141	1:32	1:55
10-4	19	125	69	92	141	2:11	1:54
10-5	20	162	68	92	141	2:40	2:11
Stream Function Convergence Criteria							
10-2	21	162	3	12	22	2:40	0:35
10-3	22	162	10	31	61	2:40	0:53
10-4	23	162	35	61	101	2:40	1:31
10-5	20	162	68	92	141	2:40	2:11

Note #1: Case numbers correspond to those of Table 1.

Note #2: CPU time is given in MINUTES:SECONDS. These times are subject to some variation depending on the operating conditions at the time of the run.

Legend:

IT_{CS} - Iterations for coordinate system

IT_0 - Iterations for 0° potential flow solution

IT_{90} - Iterations for 90° potential flow solution

IT_{CIR} - Iterations for circulation potential flow solution

CT_{CS} - CPU time for coordinate system

CT_{PSI} - CPU time for complete potential flow solution

TABLE 6

Comparison with Analytic Solution - Zero Lift and Other Angles

	Case	ΔC_L	ΔC_D	N_∞	N_2
α = -20.8596 (zero lift)	33	-0.0440	-0.0234	2.01-01	8.89-03
α = - 1.6746 (zero lift)	34	0.0000	0.0020	6.38-03	5.98-04
α = - 1.65	35	0.0000	-0.0037	6.12-03	2.98-03
α = 2.66	36	0.0128	-0.0358	1.09-02	6.87-04

Legend: See Table 2 or 3. Case 33 is Airfoil #1, and the others are Airfoil #2.

TABLE 7

Iterations and Computer Time - Zero Lift and Other Angles

	Case	IT_{CS}	IT_0	IT_{90}	IT_{CIR}	CT_{CS}	CT_{PSI}
α = -20.8596 (zero lift)	33	401	197	195	348	11:57	7:36
α = - 1.6746 (zero lift)	34	419	131	170	350	12:56	6:43
α = - 1.65	35	377	237	172	332	11:10	7:38
α = 2.66	36	377	237	172	332	11:10	7:38

Legend: See Table 4 or 5. Case 33 is Airfoil #1, and the others are Airfoil #2.

Table 8

Points on Contour - Airfoil #1

ORIGINAL PAGE IS
OF POOR QUALITY

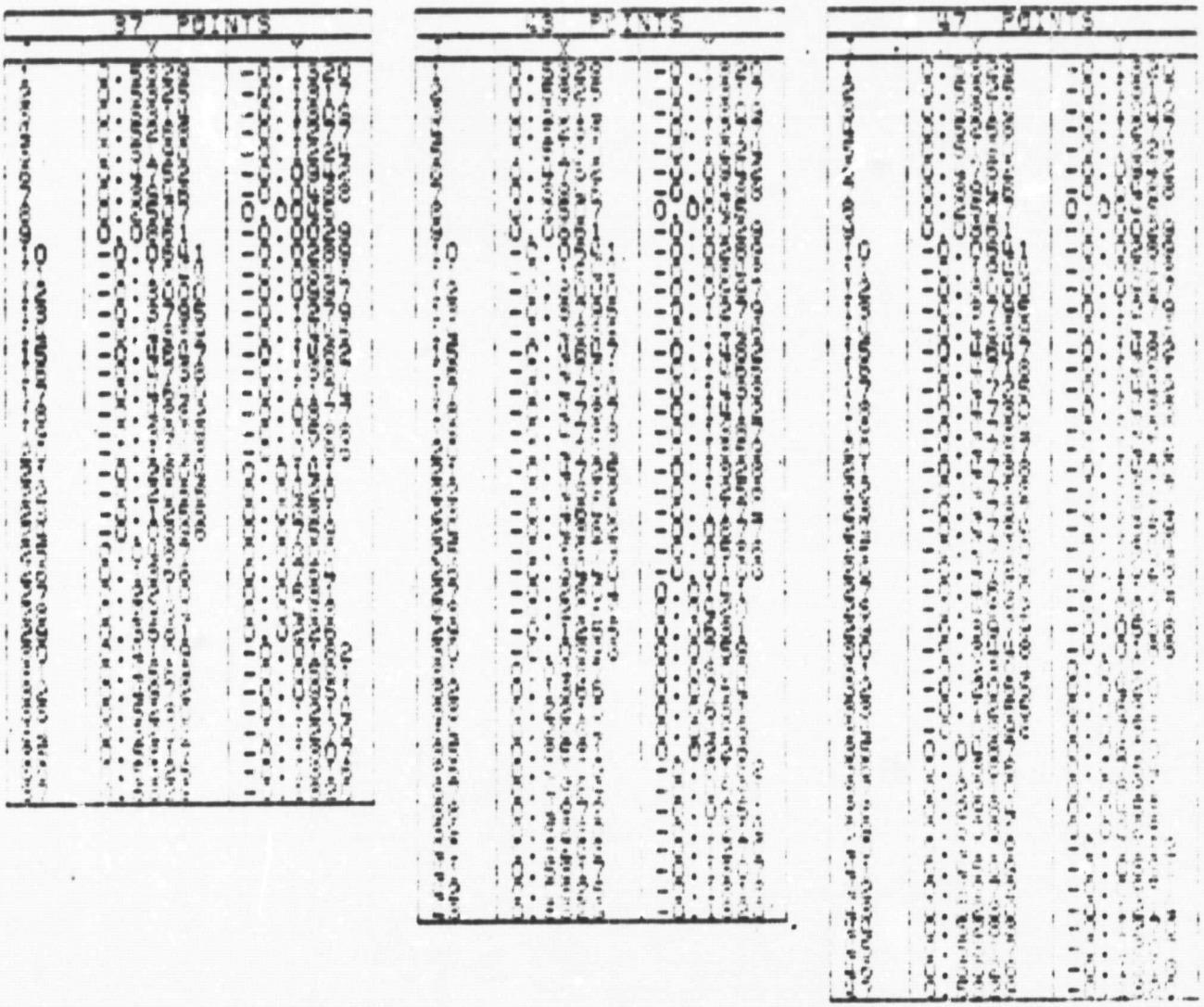

Table 8 (CONTINUED)

Table 8 (CONCLUDED)

Table 9

Points on Contour - Airfoil #2

43 POINTS

X	Y
1.000000	0.000000
0.997500	0.000000
0.990000	0.000000
0.977500	0.000000
0.960000	0.000000
0.937500	0.000000
0.910000	0.000000
0.877500	0.000000
0.840000	0.000000
0.797500	0.000000
0.750000	0.000000
0.697500	0.000000
0.640000	0.000000
0.577500	0.000000
0.510000	0.000000
0.437500	0.000000
0.360000	0.000000
0.277500	0.000000
0.190000	0.000000
0.097500	0.000000
0.000000	0.000000
0.097500	-0.000000
0.190000	-0.000000
0.277500	-0.000000
0.360000	-0.000000
0.437500	-0.000000
0.510000	-0.000000
0.577500	-0.000000
0.640000	-0.000000
0.697500	-0.000000
0.750000	-0.000000
0.797500	-0.000000
0.840000	-0.000000
0.877500	-0.000000
0.910000	-0.000000
0.937500	-0.000000
0.960000	-0.000000
0.977500	-0.000000
0.990000	-0.000000
0.997500	-0.000000
1.000000	-0.000000

47 POINTS

X	Y
1.000000	0.000000
0.997500	0.000000
0.990000	0.000000
0.977500	0.000000
0.960000	0.000000
0.937500	0.000000
0.910000	0.000000
0.877500	0.000000
0.840000	0.000000
0.797500	0.000000
0.750000	0.000000
0.697500	0.000000
0.640000	0.000000
0.577500	0.000000
0.510000	0.000000
0.437500	0.000000
0.360000	0.000000
0.277500	0.000000
0.190000	0.000000
0.097500	0.000000
0.000000	0.000000
0.097500	-0.000000
0.190000	-0.000000
0.277500	-0.000000
0.360000	-0.000000
0.437500	-0.000000
0.510000	-0.000000
0.577500	-0.000000
0.640000	-0.000000
0.697500	-0.000000
0.750000	-0.000000
0.797500	-0.000000
0.840000	-0.000000
0.877500	-0.000000
0.910000	-0.000000
0.937500	-0.000000
0.960000	-0.000000
0.977500	-0.000000
0.990000	-0.000000
0.997500	-0.000000
1.000000	-0.000000

53 POINTS

X	Y
1.000000	0.000000
0.997500	0.000000
0.990000	0.000000
0.977500	0.000000
0.960000	0.000000
0.937500	0.000000
0.910000	0.000000
0.877500	0.000000
0.840000	0.000000
0.797500	0.000000
0.750000	0.000000
0.697500	0.000000
0.640000	0.000000
0.577500	0.000000
0.510000	0.000000
0.437500	0.000000
0.360000	0.000000
0.277500	0.000000
0.190000	0.000000
0.097500	0.000000
0.000000	0.000000
0.097500	-0.000000
0.190000	-0.000000
0.277500	-0.000000
0.360000	-0.000000
0.437500	-0.000000
0.510000	-0.000000
0.577500	-0.000000
0.640000	-0.000000
0.697500	-0.000000
0.750000	-0.000000
0.797500	-0.000000
0.840000	-0.000000
0.877500	-0.000000
0.910000	-0.000000
0.937500	-0.000000
0.960000	-0.000000
0.977500	-0.000000
0.990000	-0.000000
0.997500	-0.000000
1.000000	-0.000000

TABLE 9 (CONTINUED)

Table 9 (CONCLUDED)

TABLE 10

Karman-Trefftz Transformation Parameters (Ref. 1)

Transformation: $$\frac{Z_k - m_k R_k}{Z_k - m_k L_k} = \left(\frac{Z_{k-1} - R_k}{Z_{k-1} - L_k} \right)^{m_k}, \quad k = 1, 2, --, N$$

$$m_k = 2 - \frac{\zeta_k}{\pi}$$

This transforms a circle in the Z_o plane into the airfoil in the Z_N plane through N successive transformations.

Airfoil #1

N = 3

$R_1 = 0.737277 + i0.6755902$

$L_1 = 0 + i0$

$\zeta_1 = 160°$

$R_2 = 0.39875 - i0.91706$

$L_2 = 0 + i0$

$\zeta_2 = 200°$

$R_3 = 0.93667 - i0.35021$

$L_3 = -0.843 - i0.315866$

$\zeta_3 = 12°$

Circle center = 0 + i0

Circle radius = 1.0

Airfoil Chord = 3.4647

Airfoil #2

N = 1

$R_1 = 1.0 + i0$

$L_1 = -1.0 + i0$

$\zeta_1 = 9°$

Circle Center: -0.04405 + i0.03

Circle Radius: 1.04448

Airfoil Chord: 3.9081497

TABLE 11

Changes in Force Coefficients with Increase from Adequate Parameter Values - Airfoil #1

Parameter	Change	C_L	C_D
Number of Points on Airfoil	37 to 67	0.009 to 0.002	0.01 to 0.004
Number of Lines Around Airfoil	30 to 60	0.008 to 0.003	0.004 to 0.003
Radius of Outer Boundary	10 to 20	0.008 to 0.006	0.004 to 0.001
Coordinate Convergence Criteria	10^{-4} to 10^{-5}	0.005 to 0.002	no change
Stream function Convergence Criteria	10^{-4} to 10^{-5}	0.01 to 0.002	0.005 to 0.004
Kutta Extrapolation Order	2 to 3	0.003 to 0.002	no change
Kutta Velocity Order	2 to 3	worse	worse
Velocity Order	2 to 3	worse	0.005 to 0.002
Pressure Integration Order	1 to 2	worse	worse

TABLE 12

Force Coefficient Normal to Free Stream - Two Circles

Configuration.	Amplitude of ξ-line Attraction to Cut Intersections	Amplitude of η-line Attraction to Cut Intersections	Number of Points on Each Body	Number of Lines Between Bodies	Radius of Outer Boundary	Force Coefficient
Effect of η-line Attraction - 61 Points on Each Body						
1	0	100	61	10	20	0.8309
		250				0.7095
		500				0.6688
		1000				0.6565
		2000				0.6534
Effect of η-line Attraction - 31 Points on Each Body						
1	0	250	31	6	20	0.7399
		500				0.7037
		1000				0.7003
		2000				0.7129
Effect of Number of Lines Between Bodies - 61 Points on Each Body						
1	0	1000	61	6	20	0.6401
				10		0.6565
				14		0.6595
Effect of Number of Lines Between Bodies - 31 Points on Each Body						
1	0	1000	31	6	20	0.7003
				10		0.7646
				20		1.5149
		2000		6		0.7129
				10		0.7642
				20		1.0704

TABLE 12 (CONTINUED)

Configuration	Amplitude of ξ-line Attraction to Cut Intersections	Amplitude of η-line Attraction to Cut Intersections	Number of Points on Each Body	Number of Lines Between Bodies	Radius of Outer Boundary	Force Coefficient
Effect of ξ and η-line Attraction - Additional Points on Contour Near Cuts						
1	2000	1000	37	10	20	0.5577
	0	2000				0.6255
	1000					0.5513
	2000					0.5518
Effect of Addition of Points on Contour Near Cuts						
1	0	2000	31	10	20	0.7646
			37			0.6255
Effect of Outer Boundary Radius						
1	0	1000	31	10	10	0.7900
					20	0.7646
		2000	31		10	0.7834
					20	0.7642
		1000	61		10	0.6398
					20	0.6565
		2000	61		10	0.6394
					20	0.6534
Effect of Number of Lines Surrounding Bodies						
1	0	1000	61	10	20 (20 lines)	0.6441
					20 (40 lines)	0.6565

TABLE 12 (CONCLUDED)

Configuration	Amplitude of ξ-line Attraction to Cut Intersections	Amplitude of η-line Attraction to Cut Intersections	Number of Points on Each Body	Number of Lines Between Bodies	Radius of Outer Boundary	Force Coefficient
Miscellaneous .						
2	0	2000	31	--	10	0.7378
3	0	0	31	--	5	0.6843
					10	0.6821
3	0	0	61	--	10	0.6331

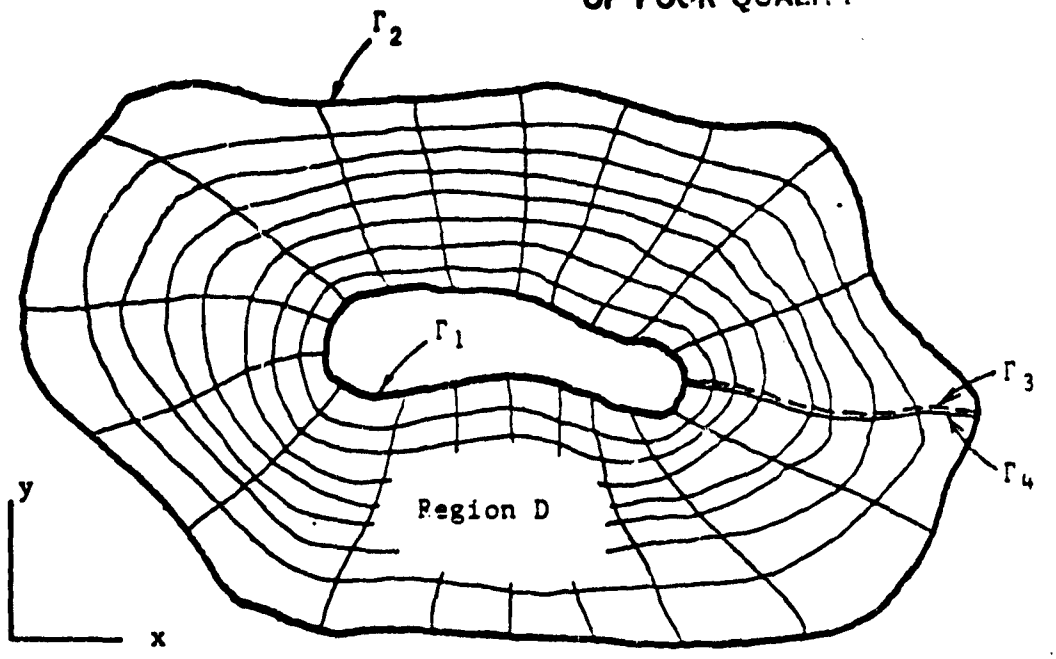

Physical Plane

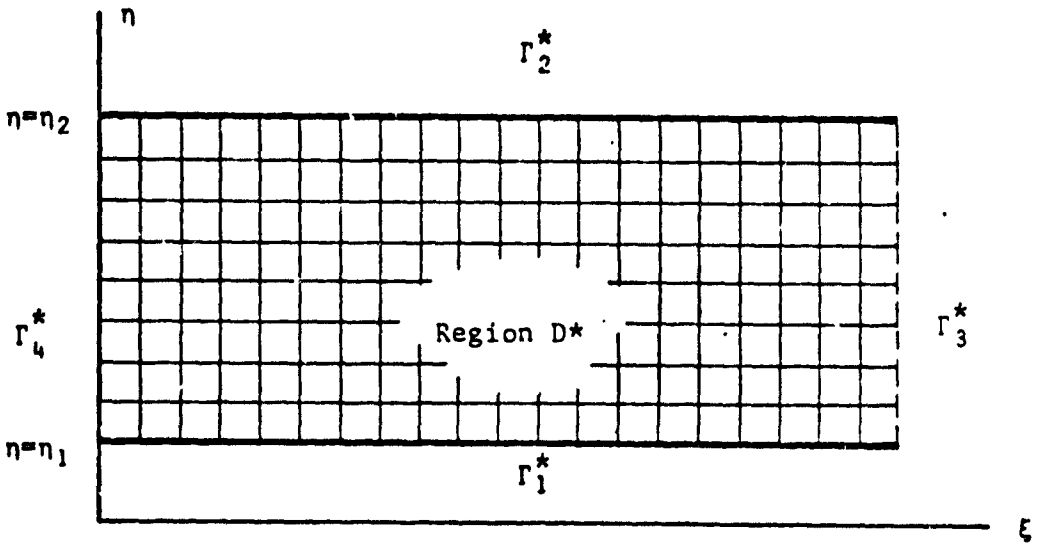

Transformed Plane

Figure 1. Field Transformation - Single Body

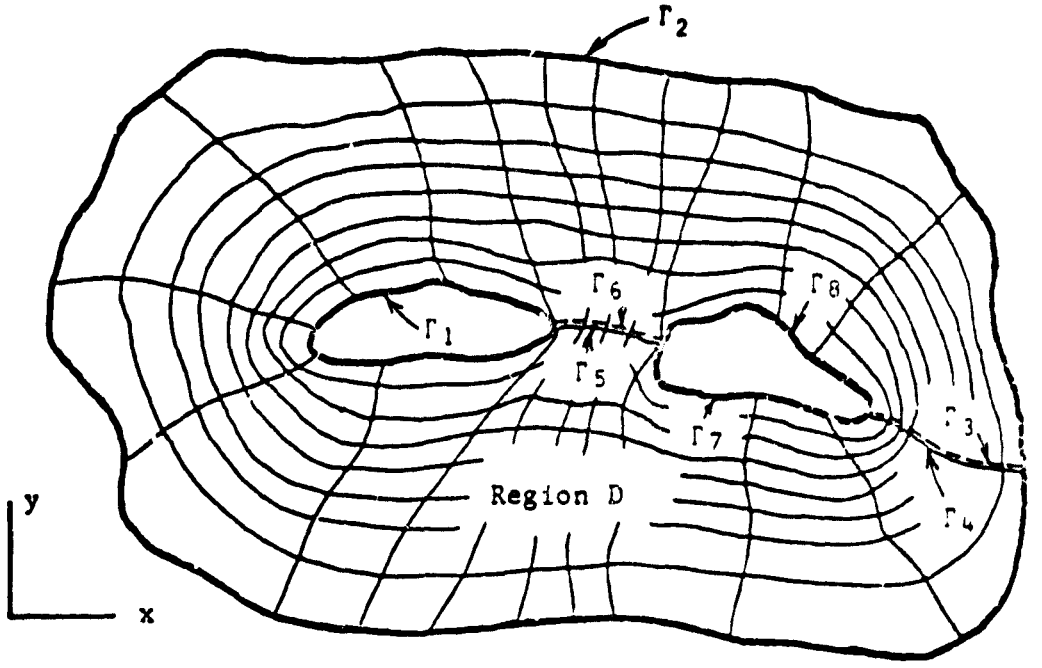

Physical Plane

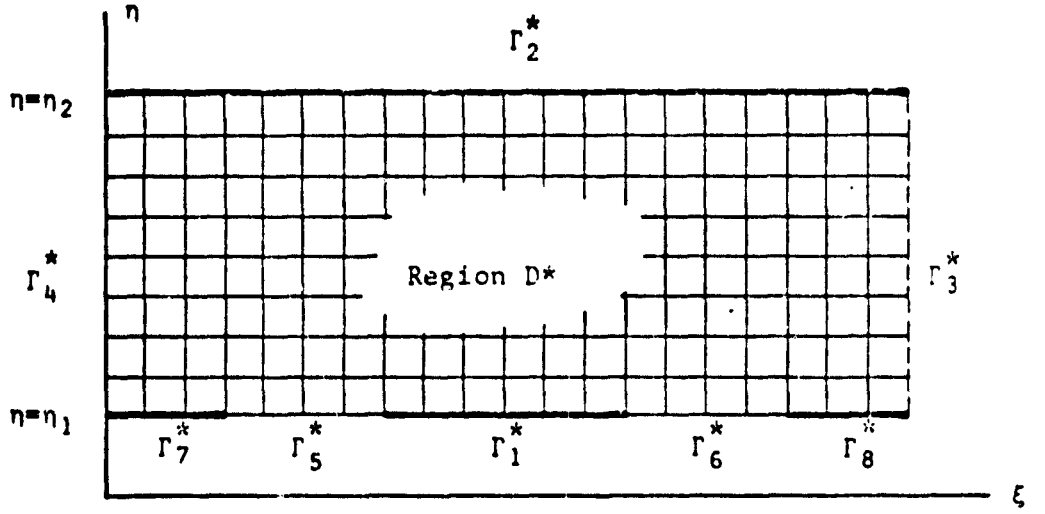

Transformed Plane

Figure 2. Field Transformation - Multiple Bodies

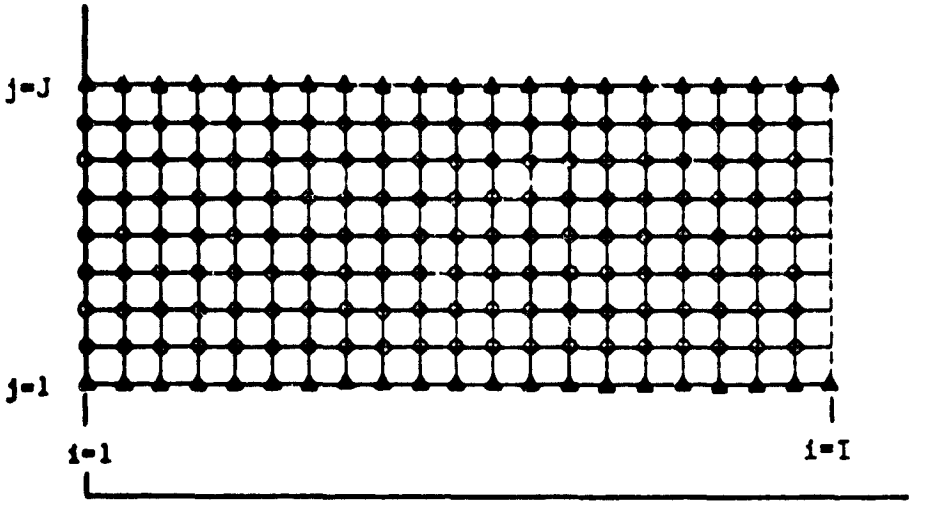

a) Single Body

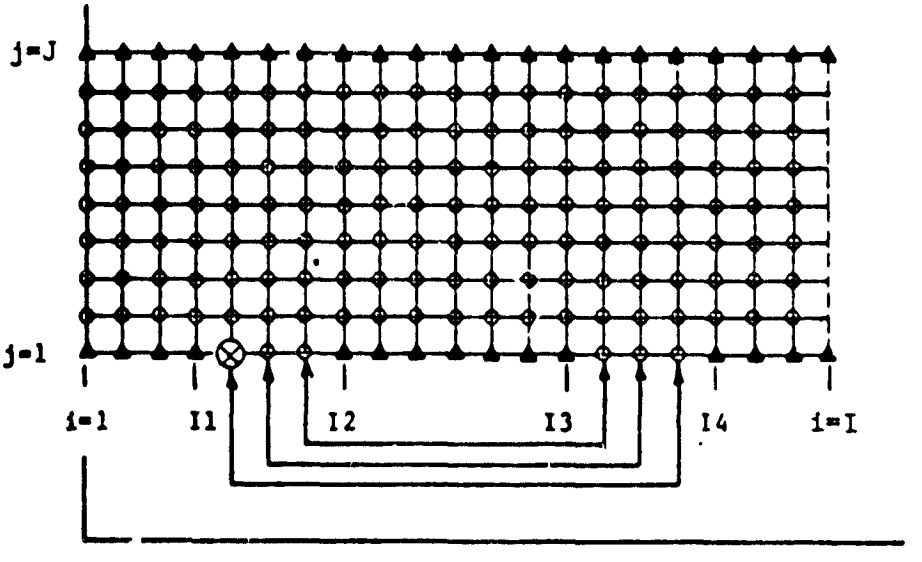

b) Two Body

Figure 3. Computational Grids - Single and Two Body Regions

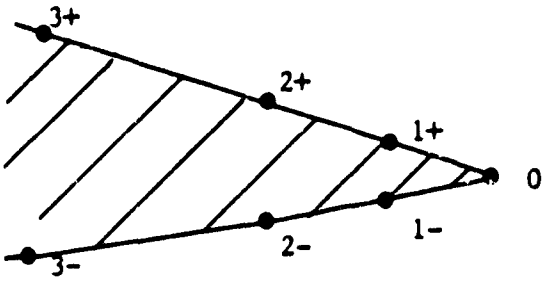

Figure 4

Extrapolation Points for Application of Kutta Condition

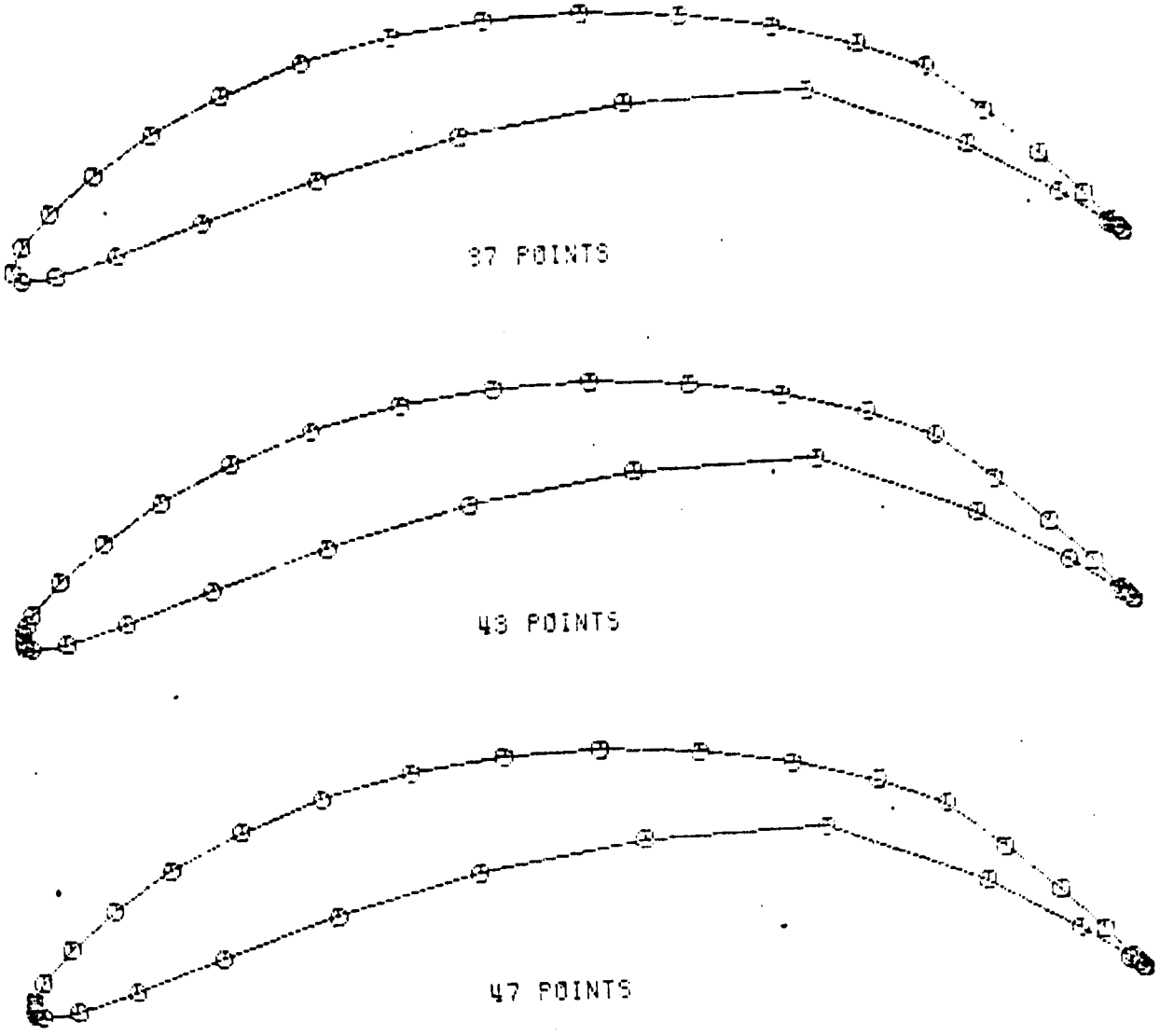

Figure 5. Karman-Trefftz Airfoil #1 Contours

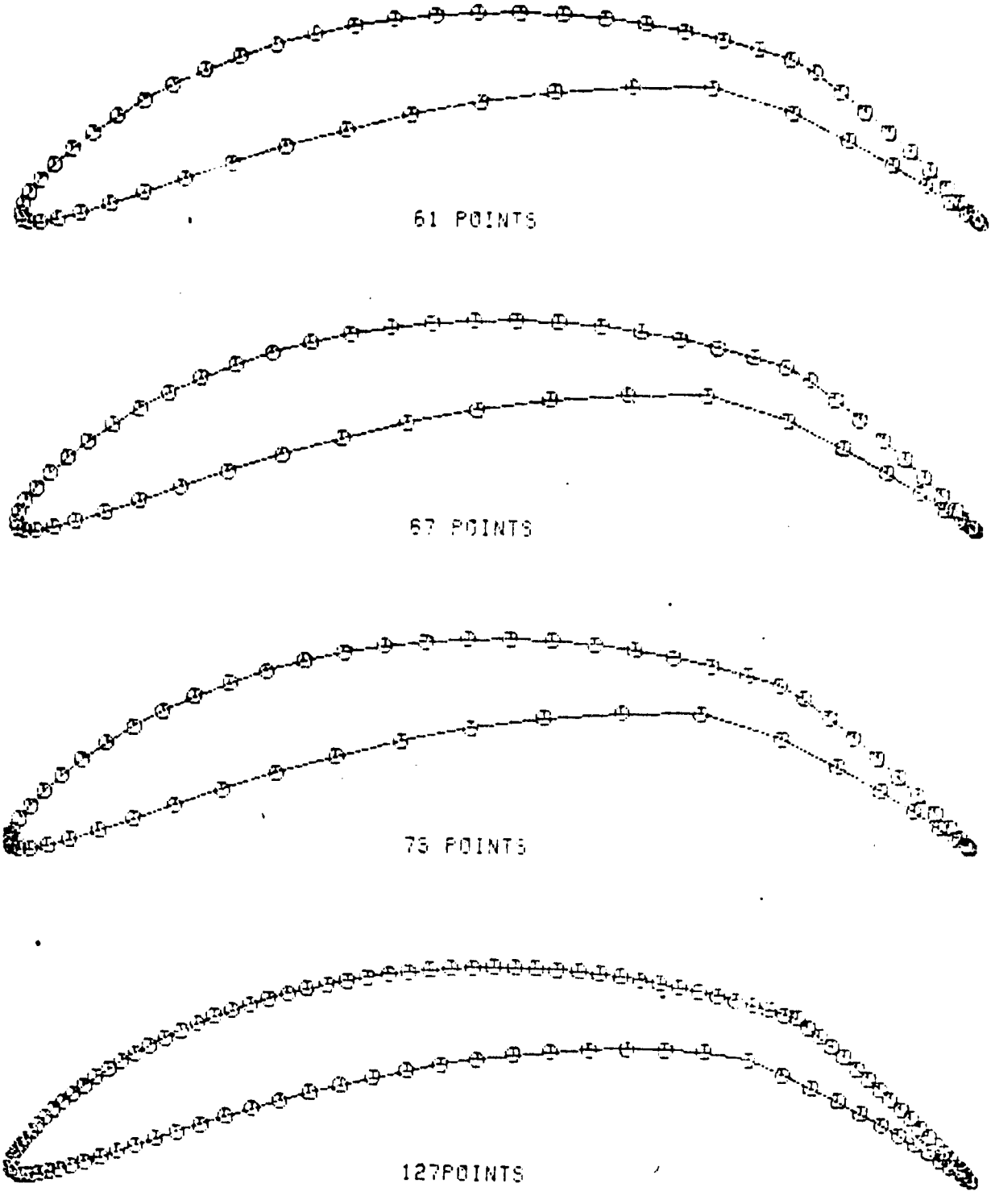

Figure 5. (Concluded)

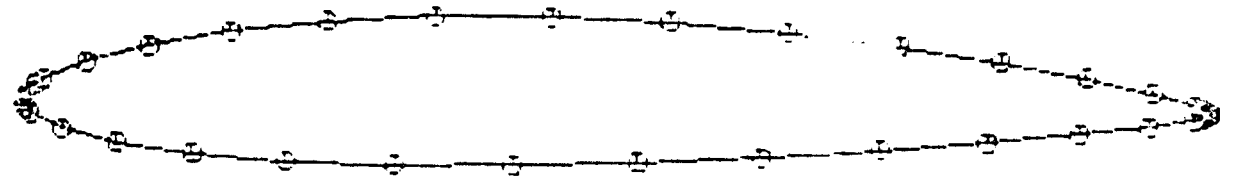

43 POINTS

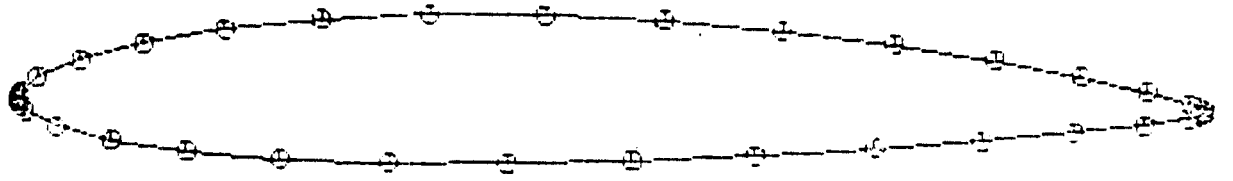

47 POINTS

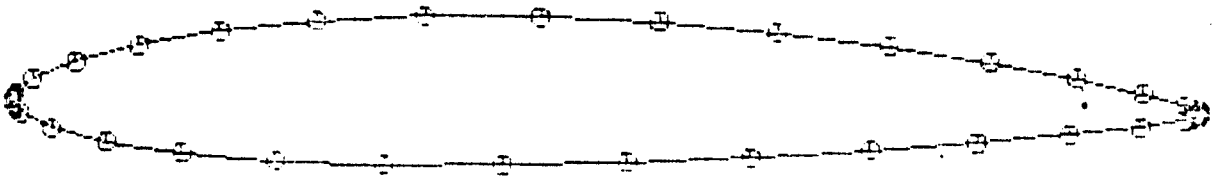

53 POINTS

Figure 6. Karman-Trefftz Airfoil #2 Contours

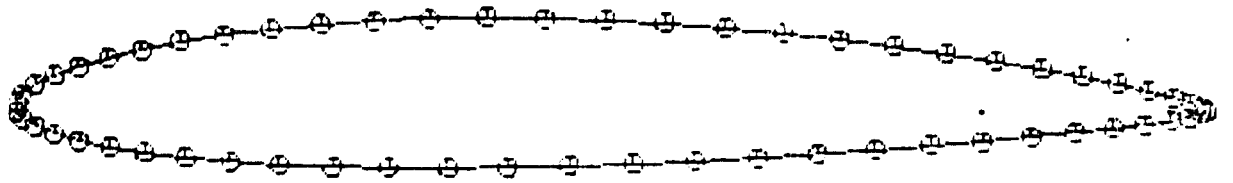

61 POINTS

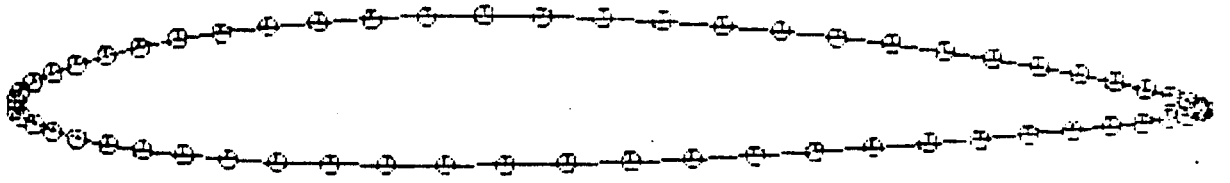

67 POINTS

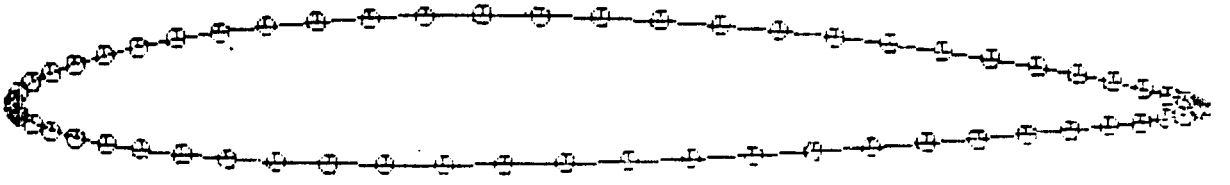

73 POINTS

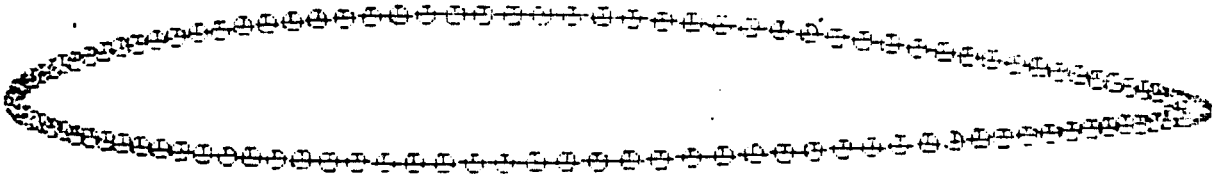

127POINTS

Figure 6. (Concluded)

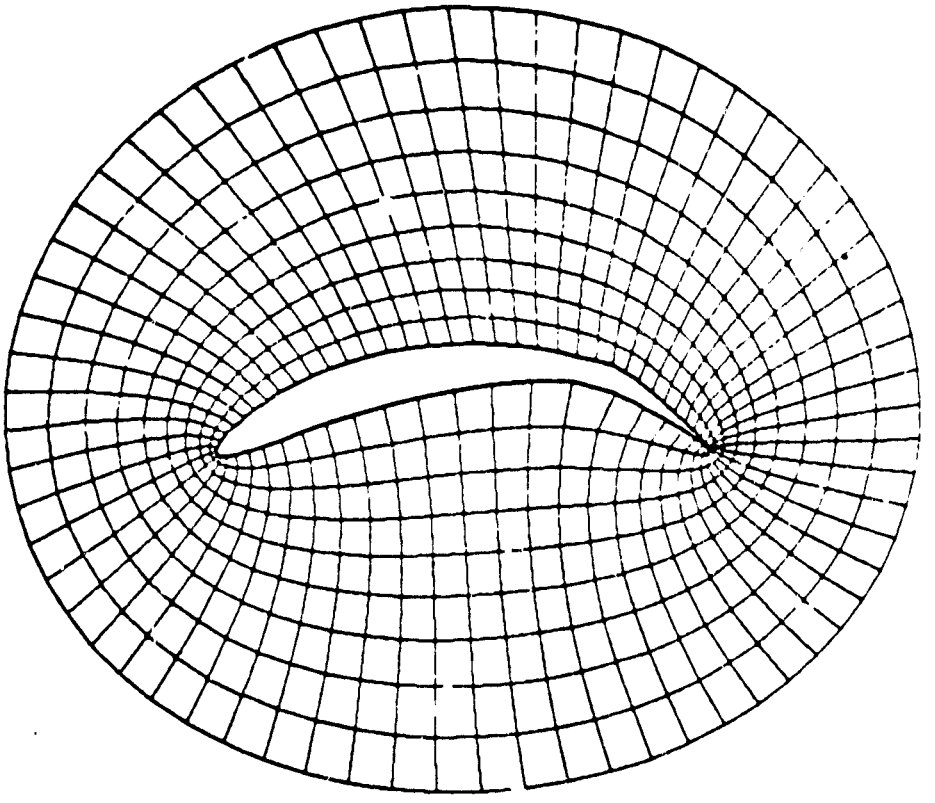

Airfoil #1

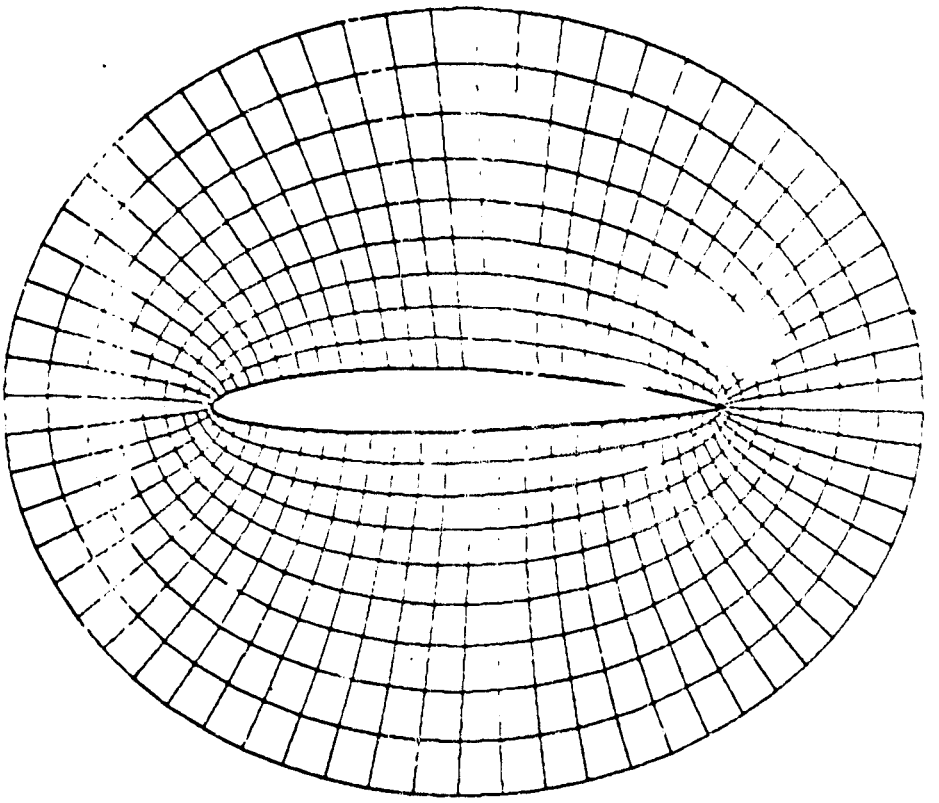

Airfoil #2

Figure 7. Typical Coordinate Systems

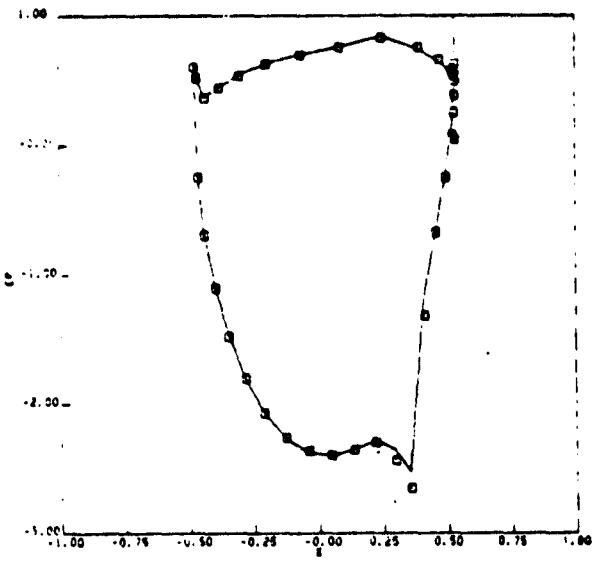

(a.) 27 Points (Case 16)

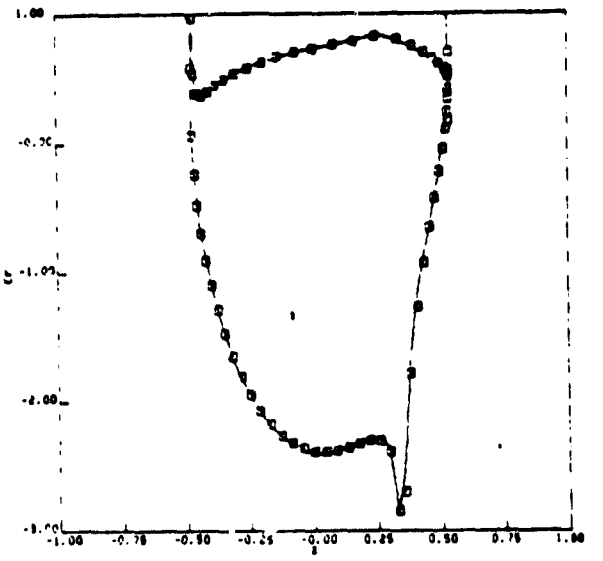

(b.) 67 Points (Case 19)

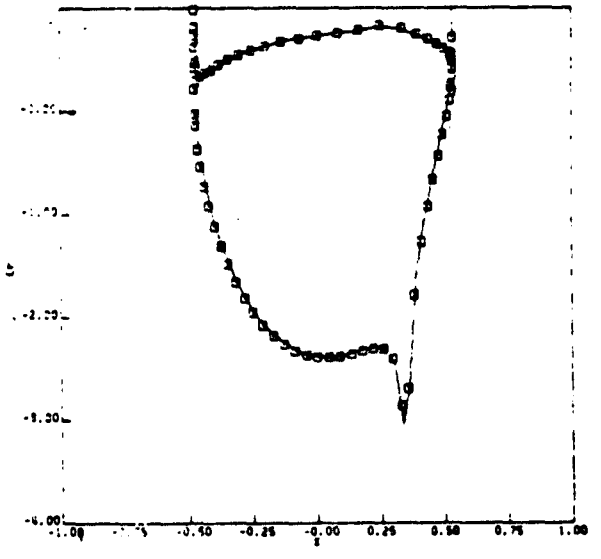

(c.) 73 Points (Case 5)

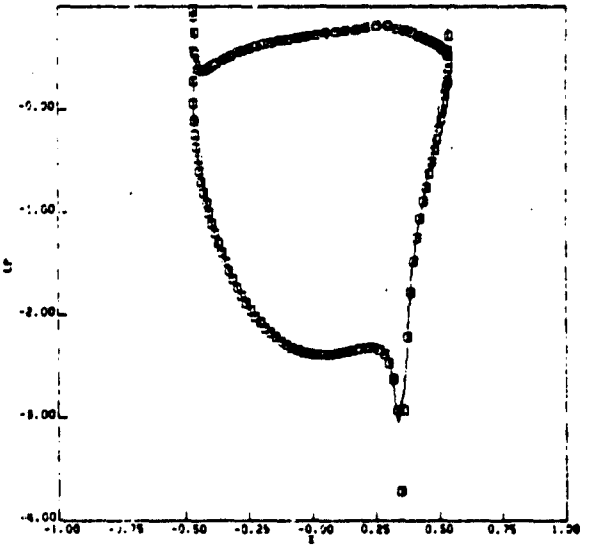

(d.) 127 Points (Case 1)

Figure 8. Effect of Contour Point Distribution on Pressure Distribution - Airfoil #1. (Solid line is analytical; symbols are numerical.)

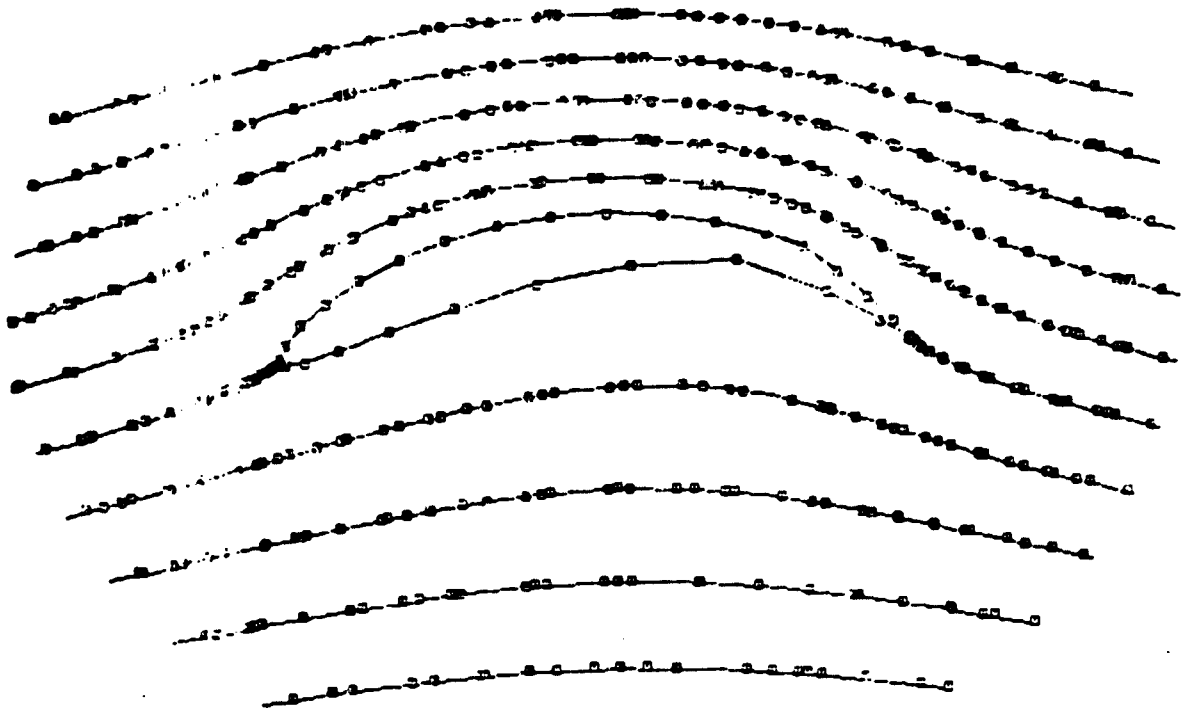

(a.) 37 Points (Case 16)

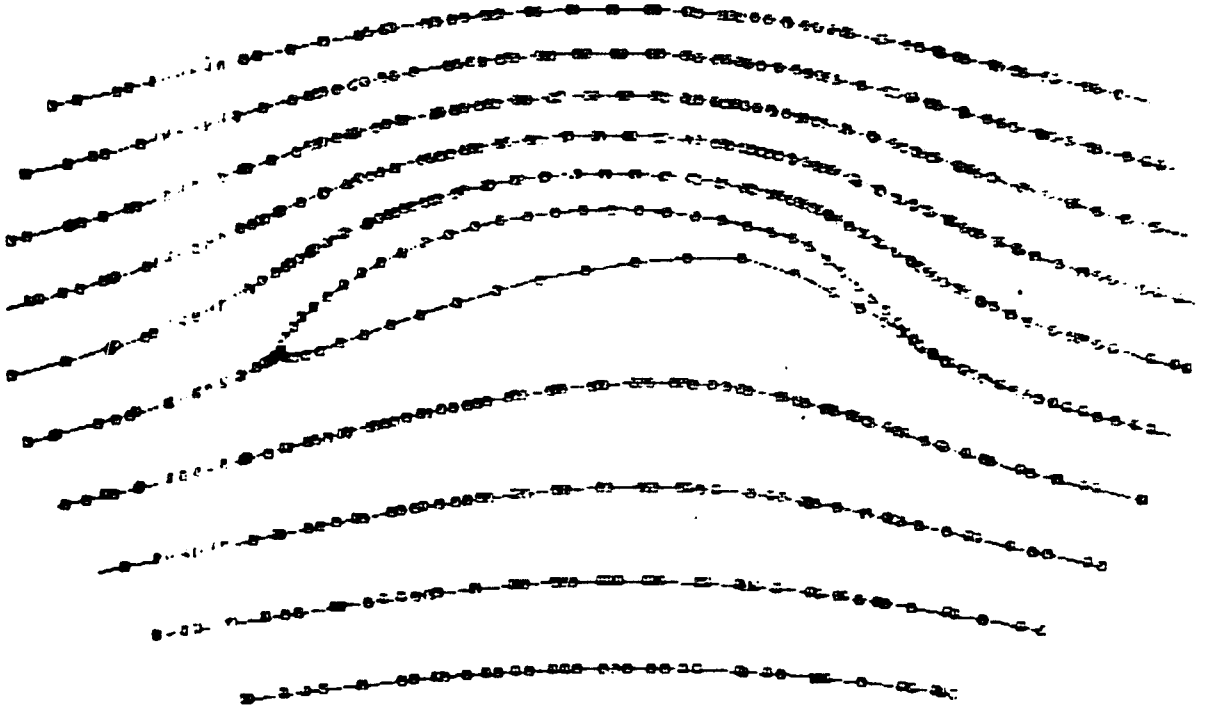

(b.) 67 Points (Case 19)

Figure 9. Effect of Contour Point Distribution on Streamlines - Airfoil #1. (Solid line is analytical; symbols are numerical.)

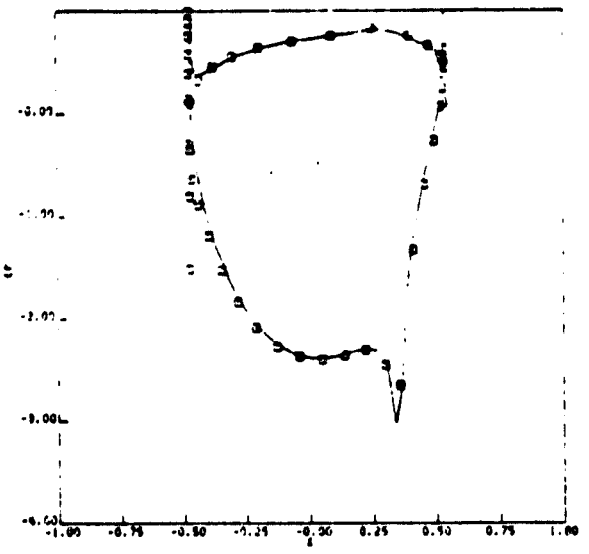

(a.) 6 Additional Points (Case 2)

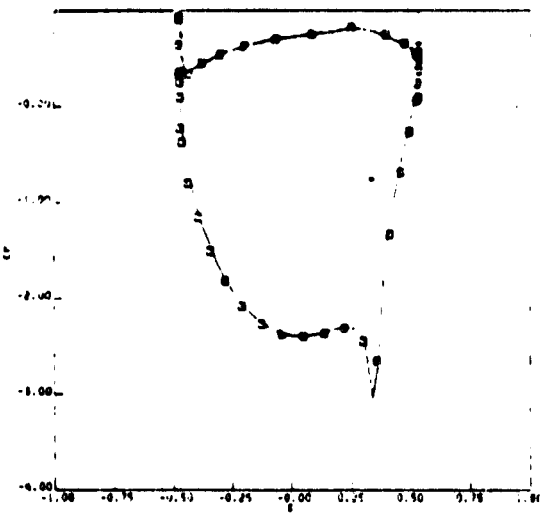

(b.) 12 Additional Points (Case 3)

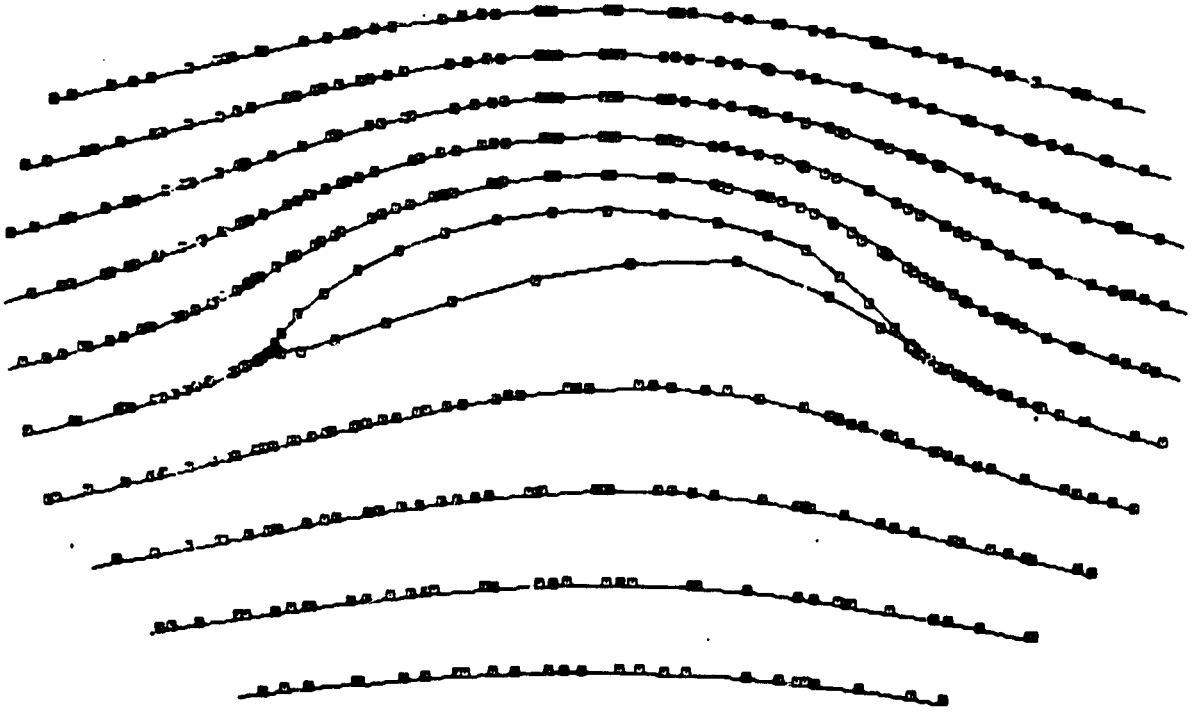

(c.) Streamlines, 6 Additional Points (Case 2)

Figure 10. Effect of Addition of Points Near Leading Edge - Airfoil #1. (Solid line is analytical; symbols are numerical.)

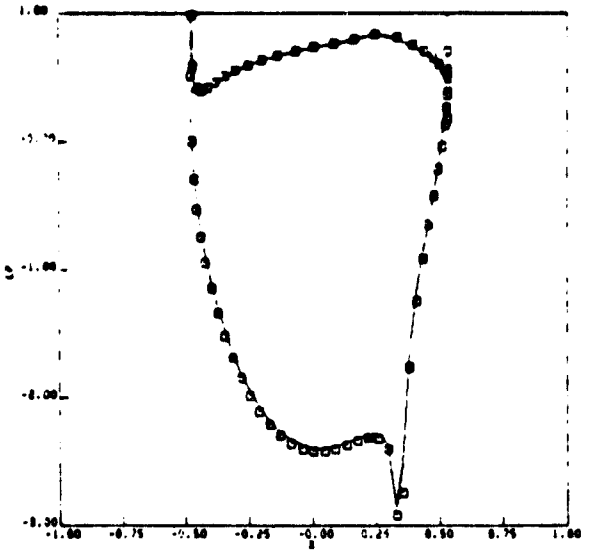

(a.) ∞ at 5, 30 Points (Case 11)

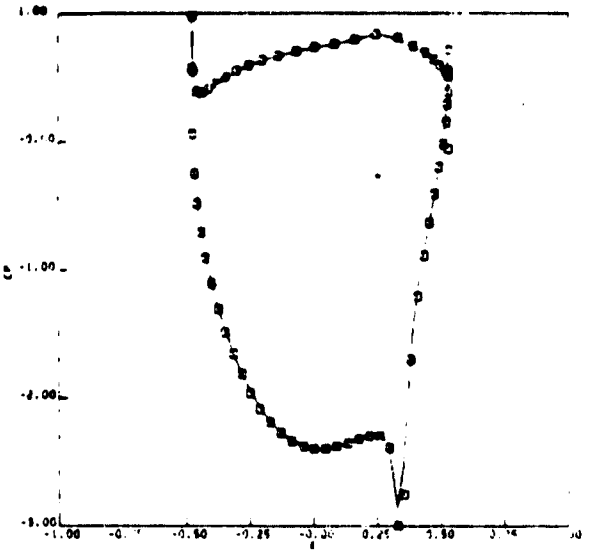

(b.) ∞ at 10, 60 Points (Case 7)

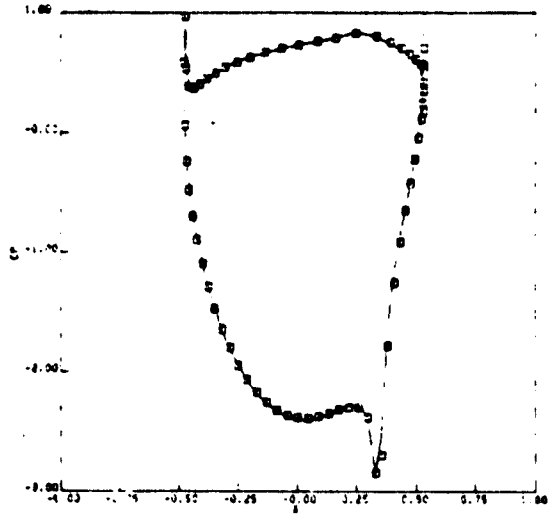

(c.) ∞ at 10, 30 Points (Case 32)

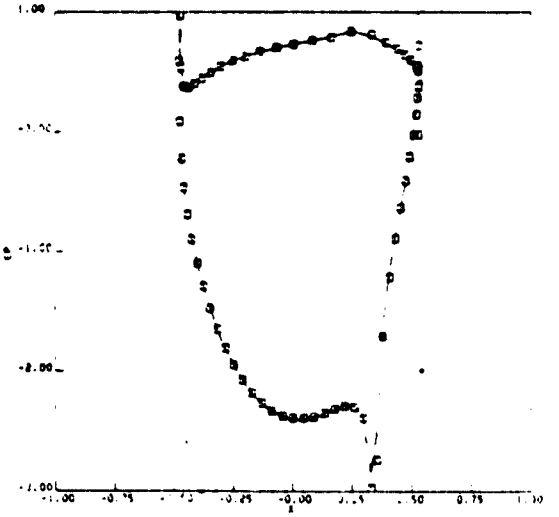

(d.) ∞ at 20, 60 Points (Case 8)

Figure 11. Effect of Distance to Outer Boundary - Airfoil #1.
(Solid line is analytical; symbols are numerical.)

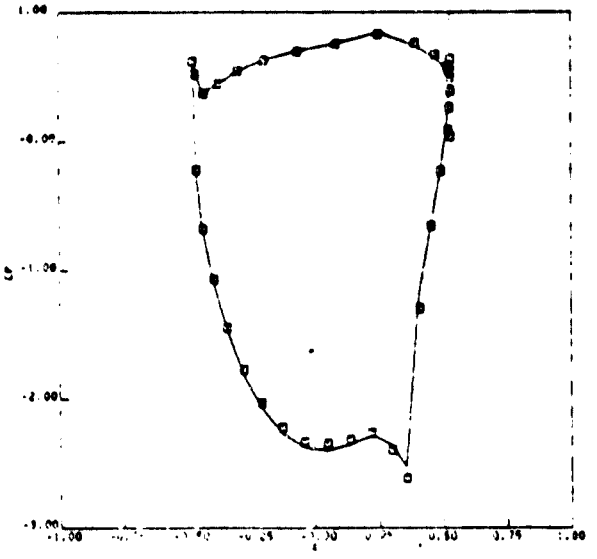

(a.) Coordinate System Convergence 10^{-4} (Case 14)

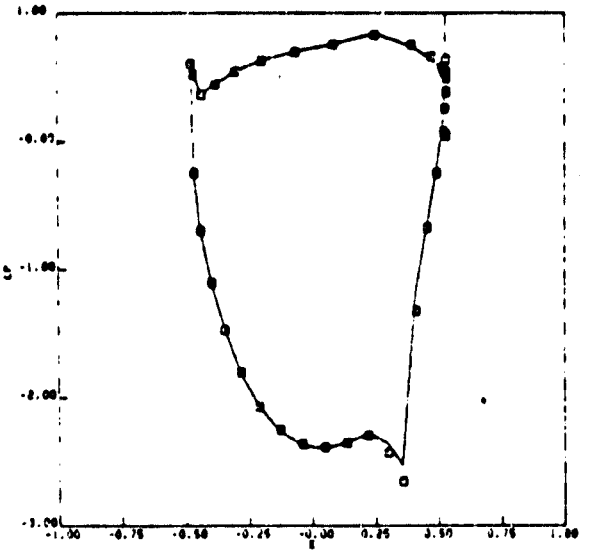

(b.) Coordinate System Convergence 10^{-4} (Case 15)

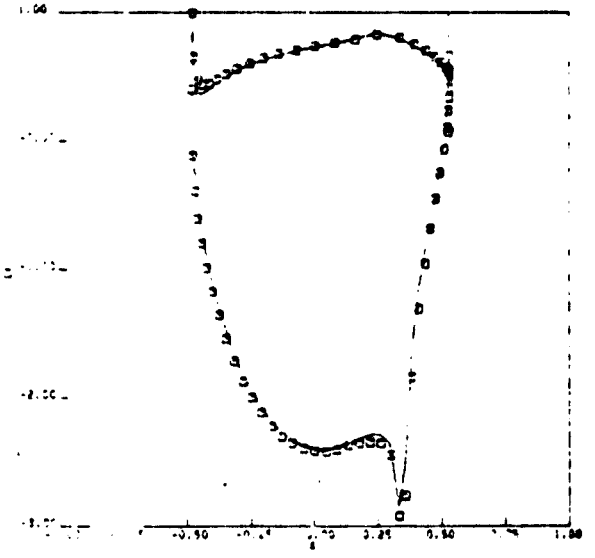

(c.) Stream Function Convergence 10^{-3} (Case 22)

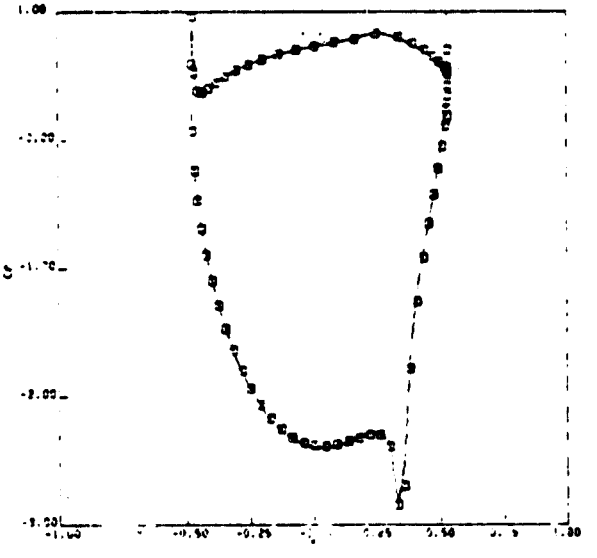

(d.) Stream Function Convergence 10^{-4} (Case 23)

Figure 12. Effect of Convergence Criteria - Airfoil #1. (Solid line is analytical; symbols are numerical.)

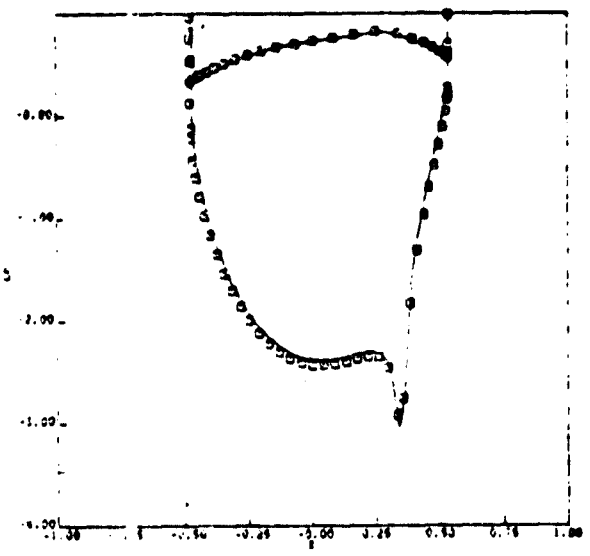

(a.) Stagnation Point at Trailing Edge (Case 26)

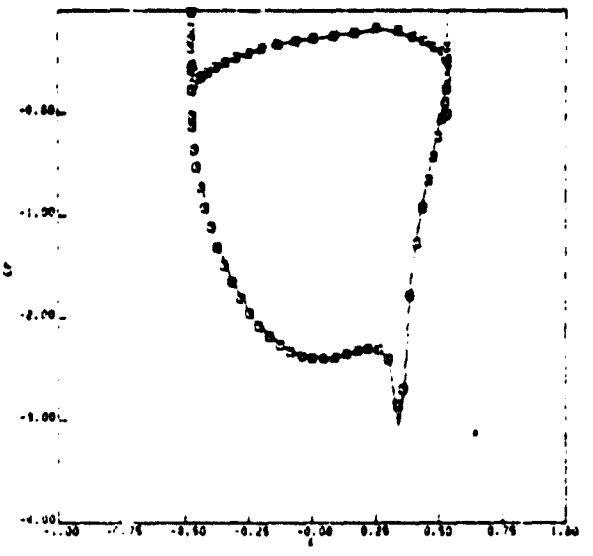

(b.) First-Order Extrapolation at Trailing Edge (Case 24)

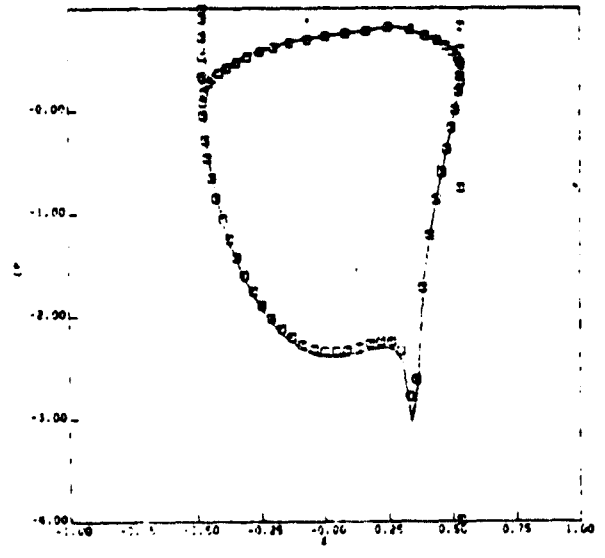

(c.) First-Order Velocity (Case 27)

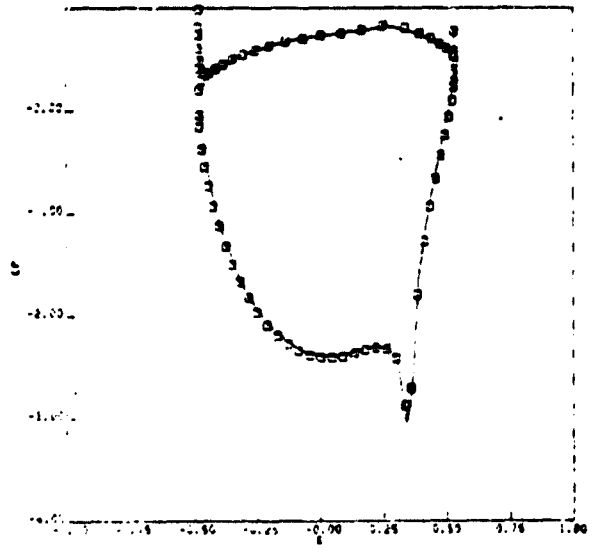

(d.) Third-Order Velocity (Case 28)

Figure 13. Effect of Extrapolation and Velocity Orders for Kutta Condition - Airfoil #1. (Solid line is analytical; symbols are numerical.)

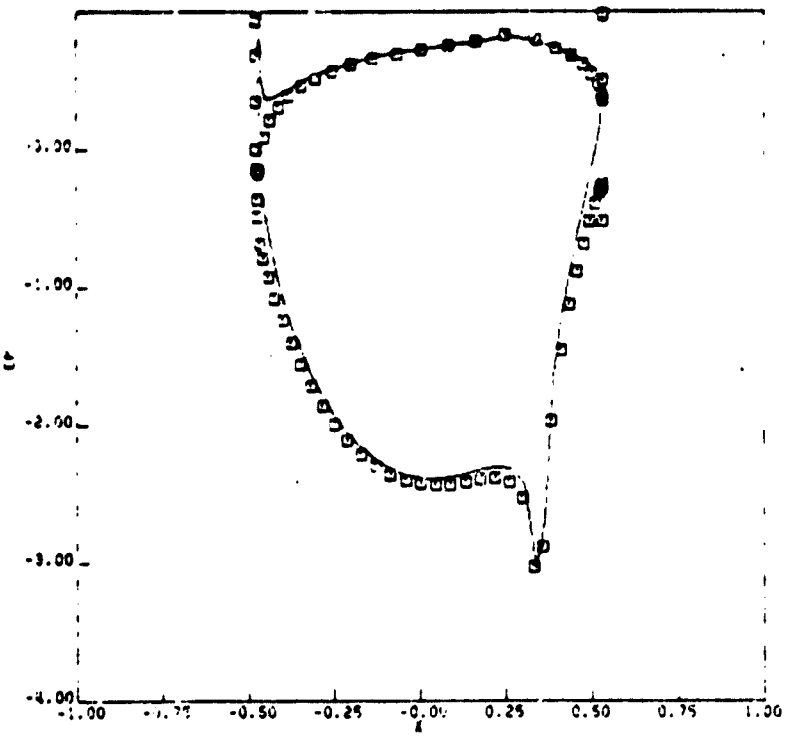

(a.) First Order (Case 29)

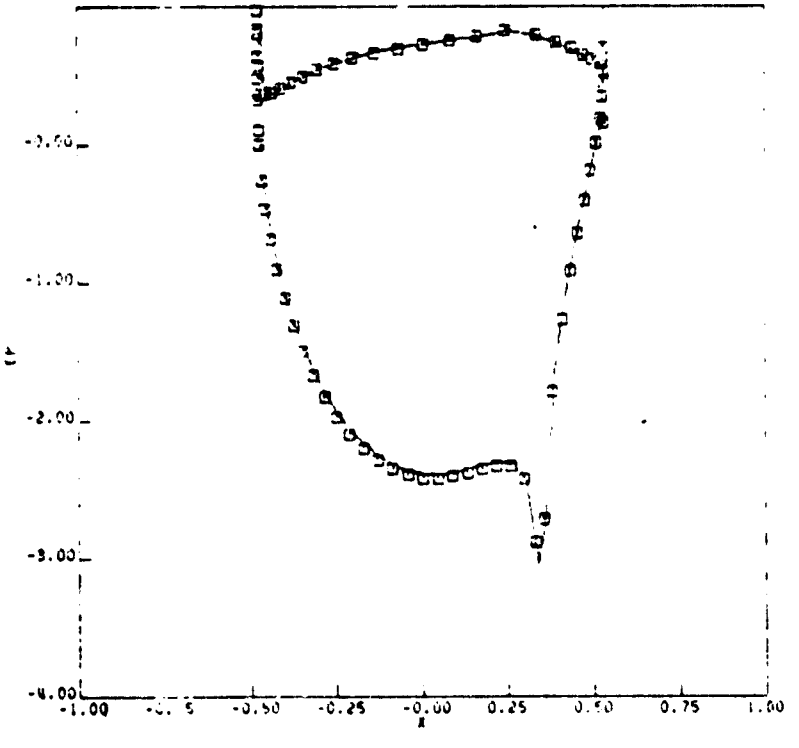

(b.) Third Order (Case 30)

Figure 14. Effect of Order of Velocity in Surface Pressure Calculation - Airfoil #1. (Solid line is analytical; symbols are numerical.)

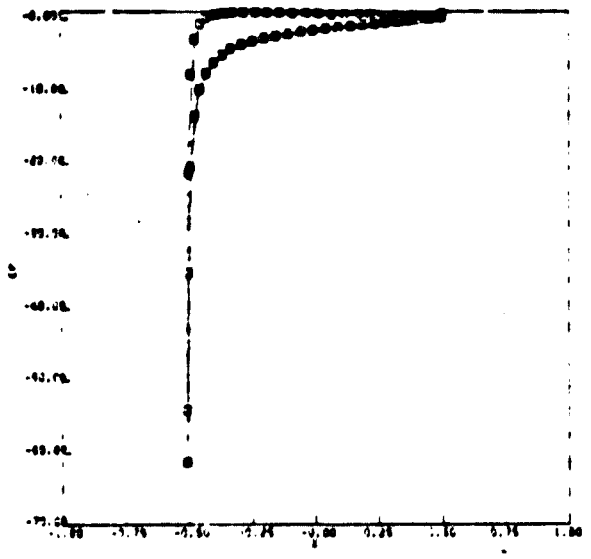

(a.) 61 Points (Case 6)

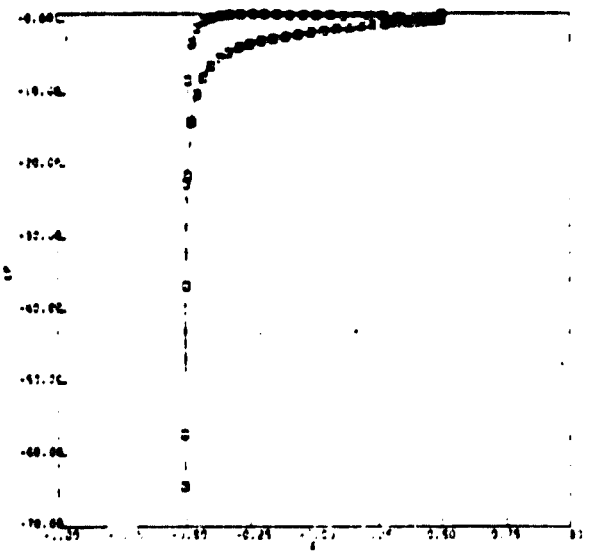

(b.) 67 Points (Case 20)

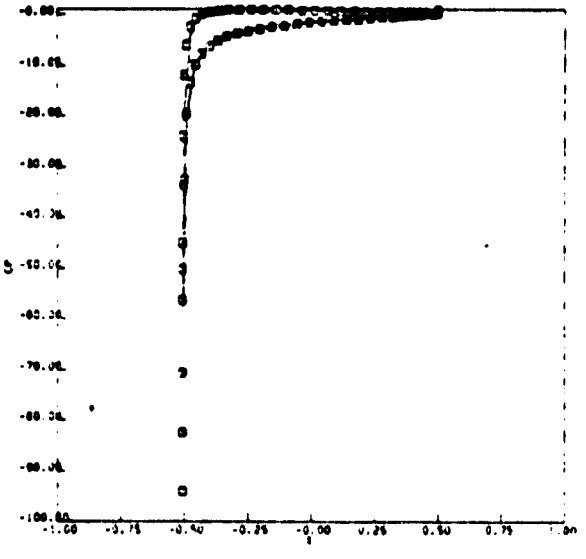

(c.) 73 Points (Case 5)

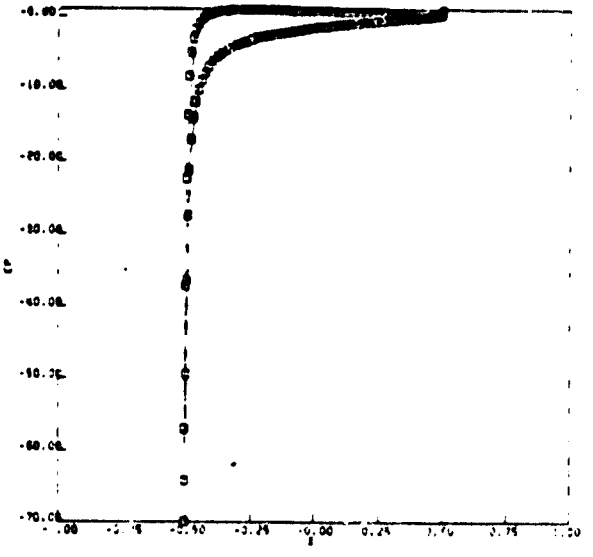

(d.) 127 Points (Case 1)

Figure 15. Effect of Contour Point Distribution on Pressure Distribution - Airfoil #2. (Solid line is analytical; symbols are numerical.)

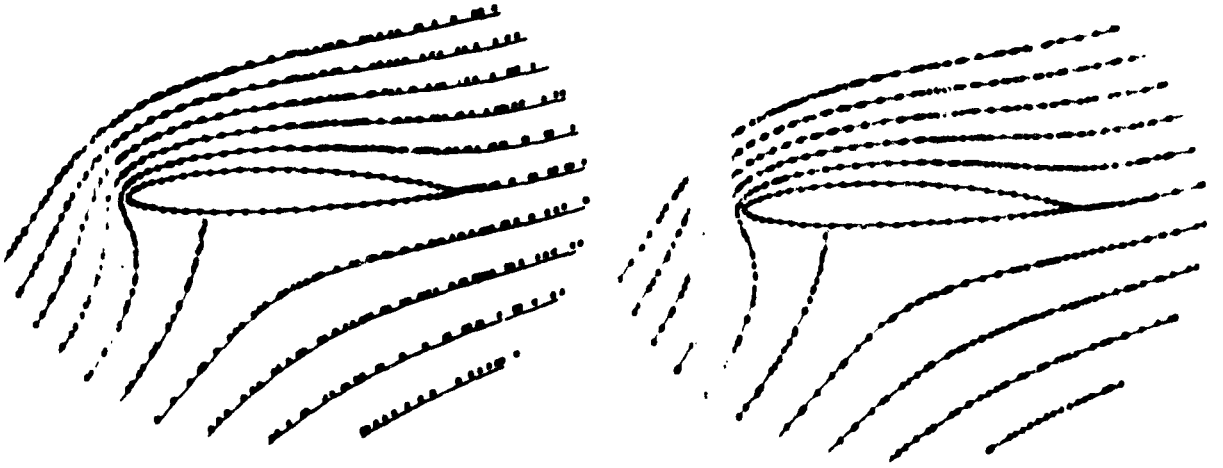

(a.) 37 Points (Case 6)

(b.) 67 Points (Case 20)

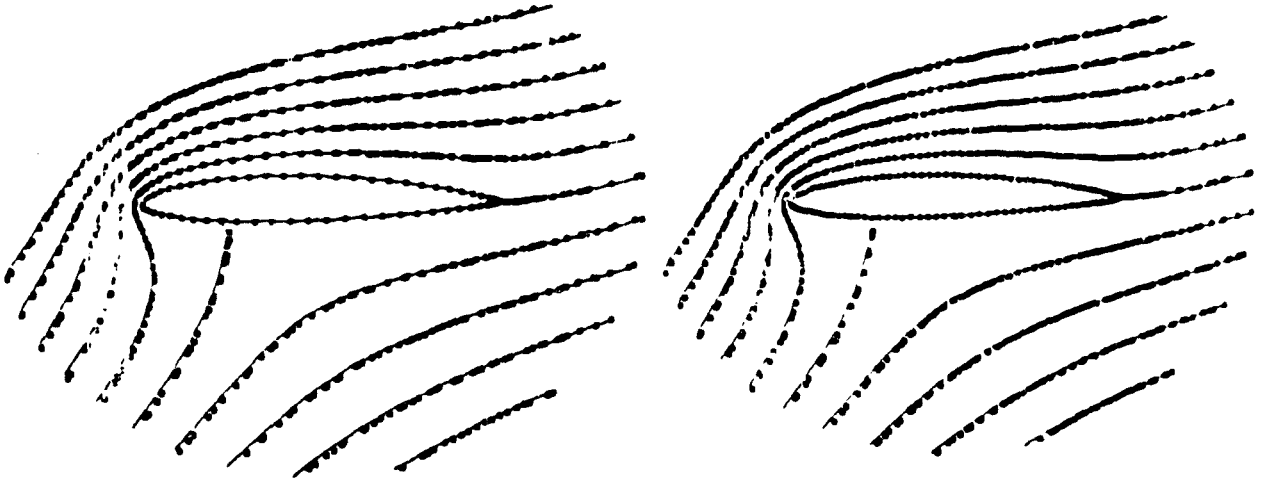

(c.) 73 Points (Case 5)

(d.) 127 Points (Case 1)

Figure 16. Effect of Contour Point Distribution on Streamlines - Airfoil #2. (Solid line is analytical; symbols are numerical.)

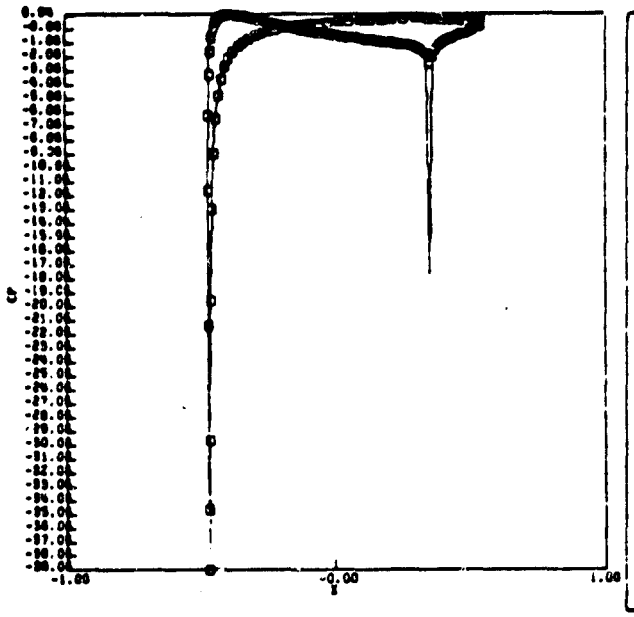

(a.) Pressure Distribution, Airfoil #1 (Case 33)

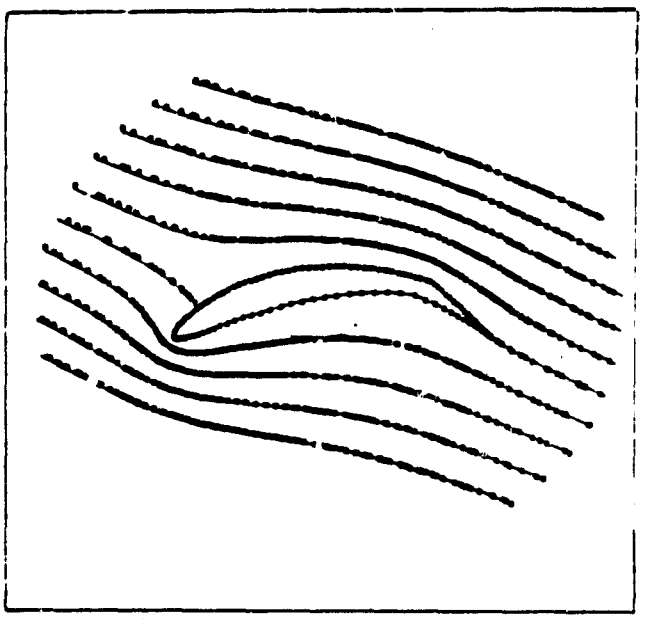

(b.) Streamlines, Airfoil #1 (Case 33)

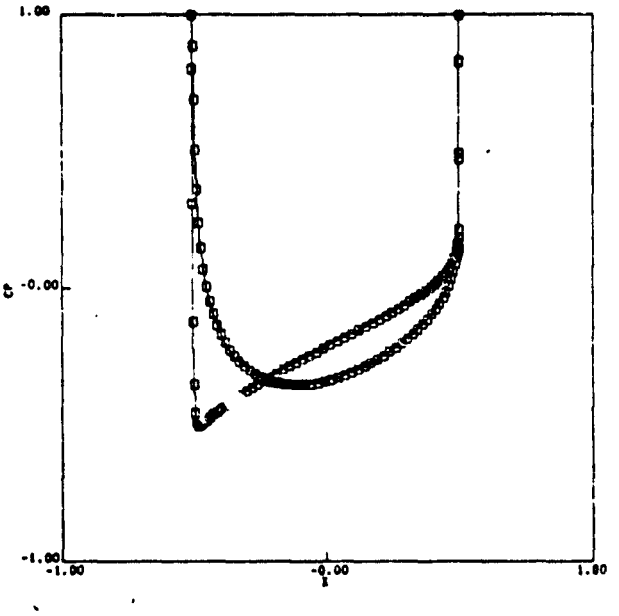

(c.) Pressure Distribution, Airfoil #2 (Case 34)

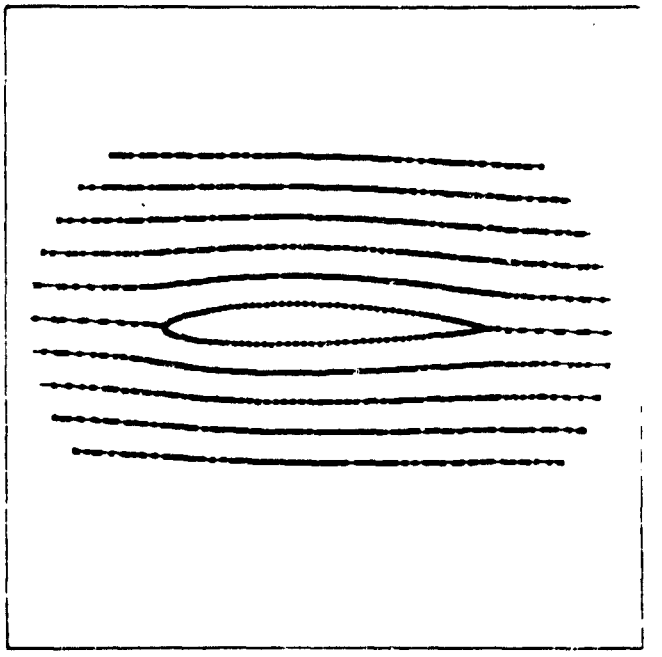

(d.) Streamlines, Airfoil #2 (Case 34)

Figure 17. Zero-Lift Angle Results - Airfoils #1 and #2.

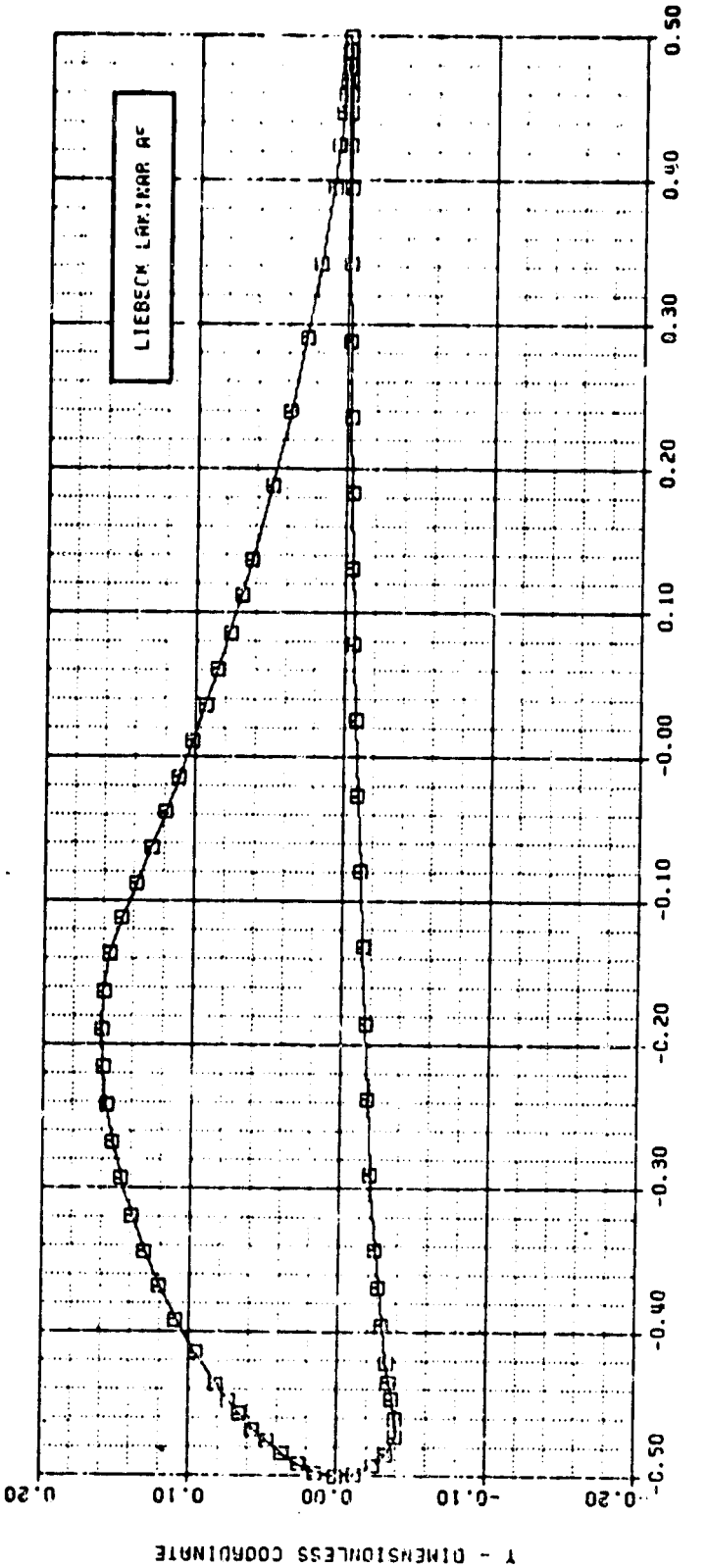

Figure 18. Liebeck Laminar Airfoil

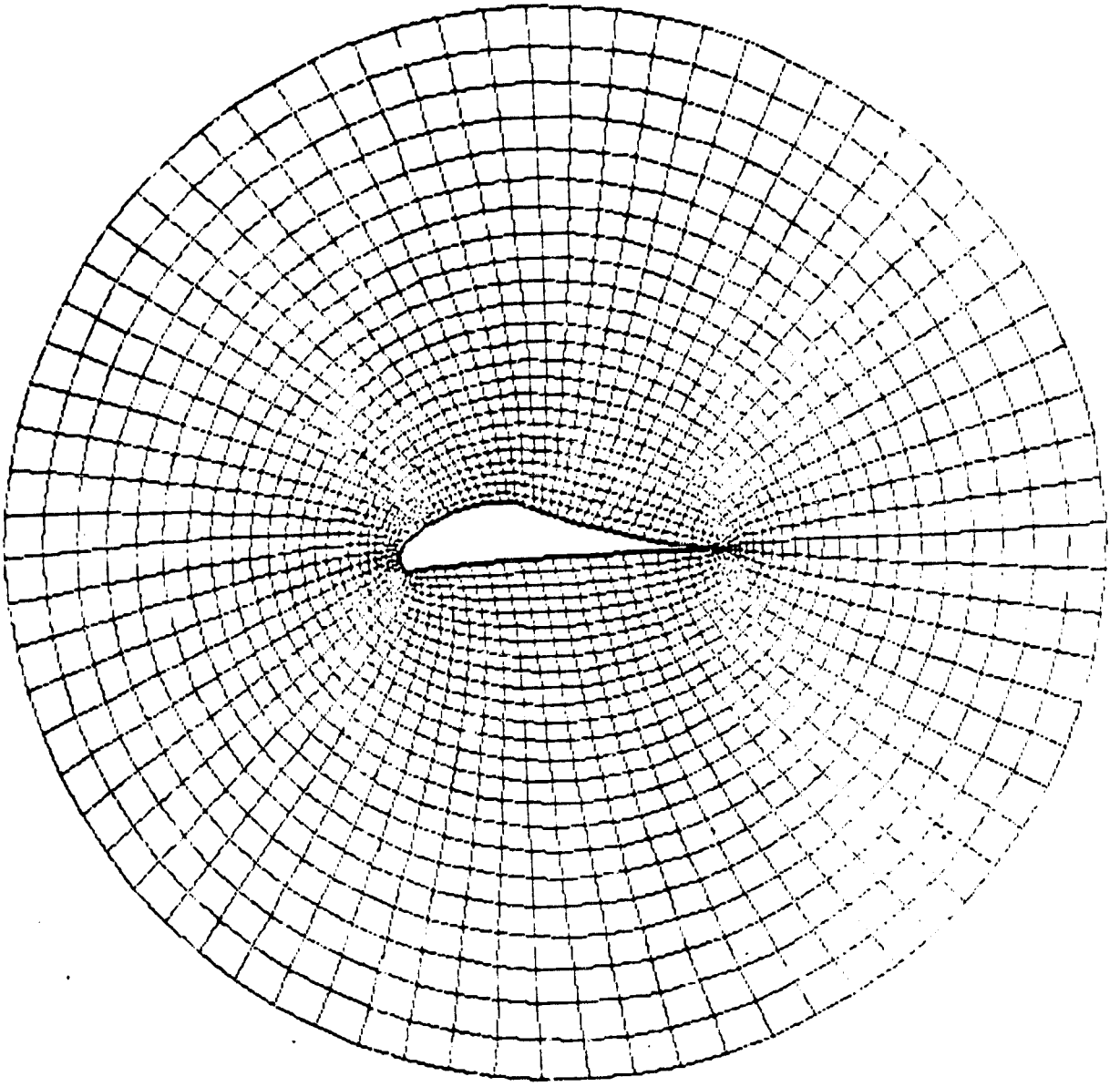

Figure 19. Coordinate System - Liebeck Laminar Airfoil

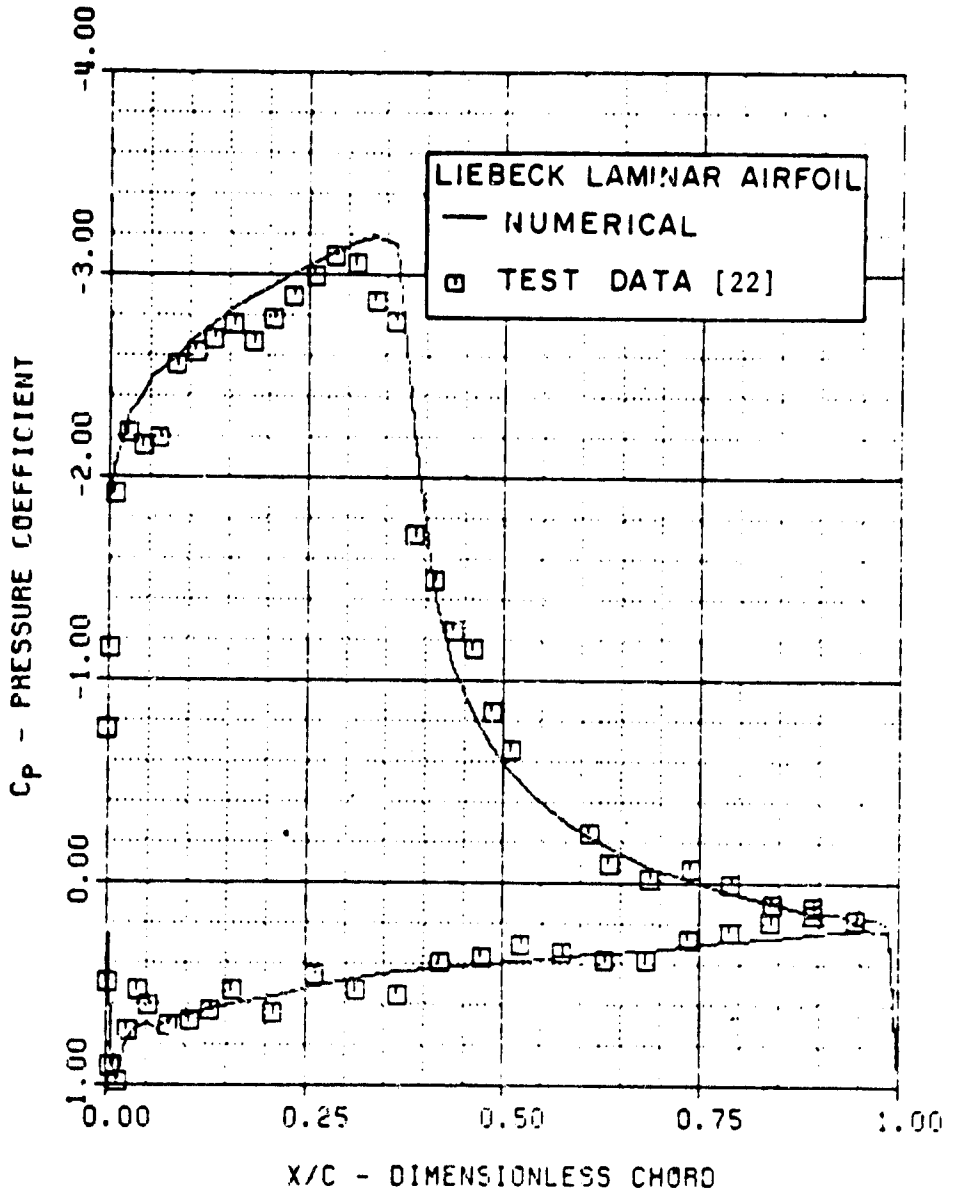

Figure 20. Comparison of Experimental and Numerical Pressure Distribution - Liebeck Laminar Airfoil

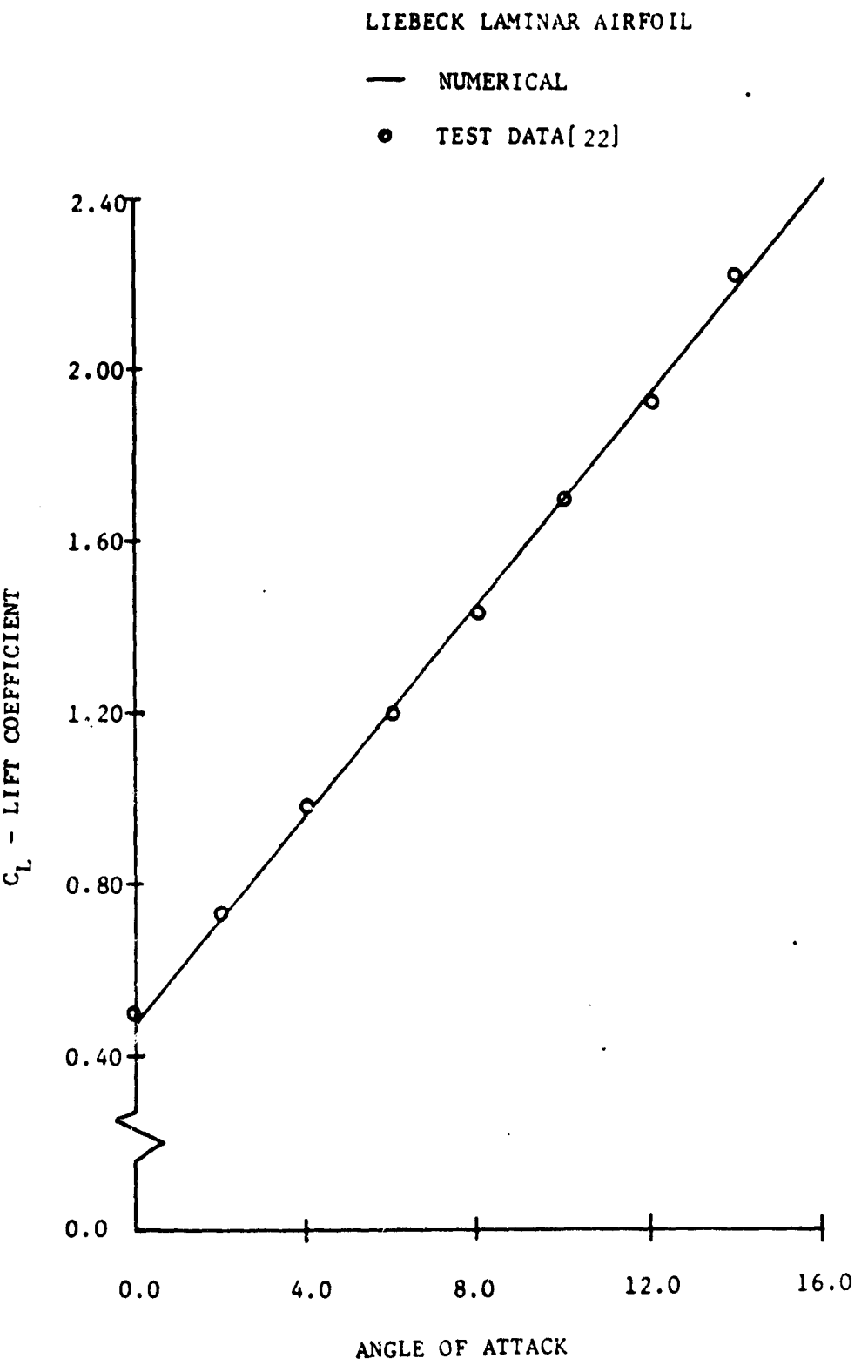

Figure 21. Comparison of Experimental and Numerical C_L Lift Curve - Liebeck Laminar Airfoil

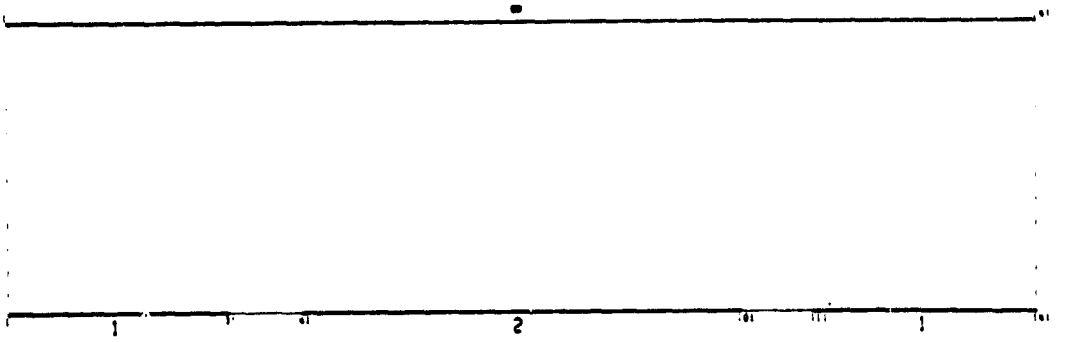

(a.) Configuration #1

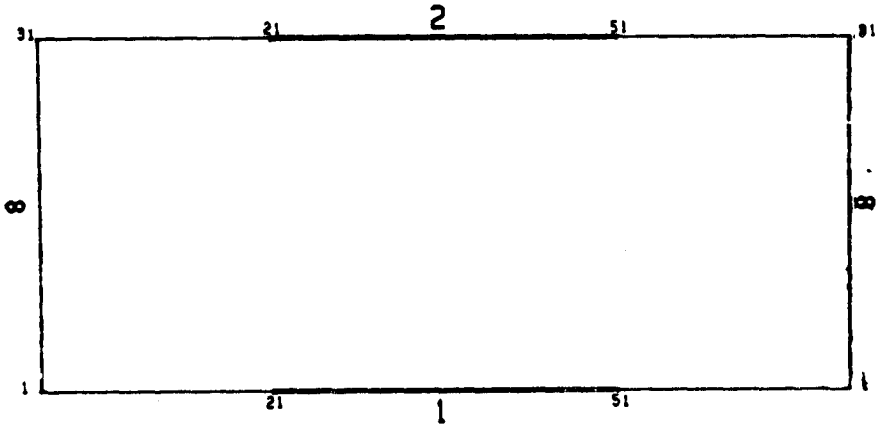

(b.) Configuration #2

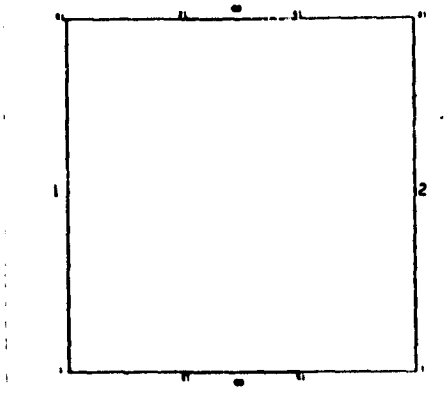

(c.) Configuration #3

Figure 22. Two-Body Coordinate System Configurations.

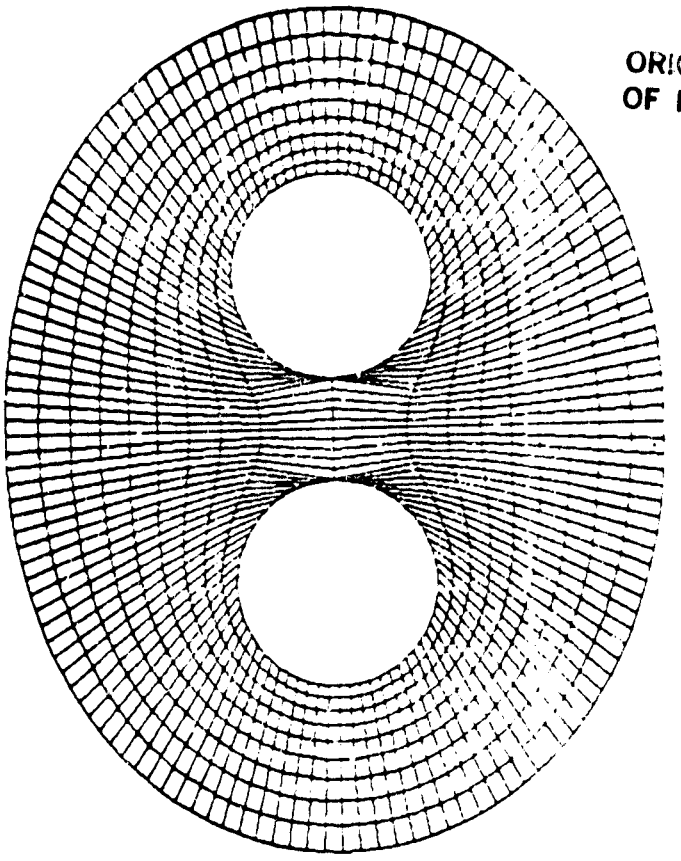

(a.) Coordinate System.

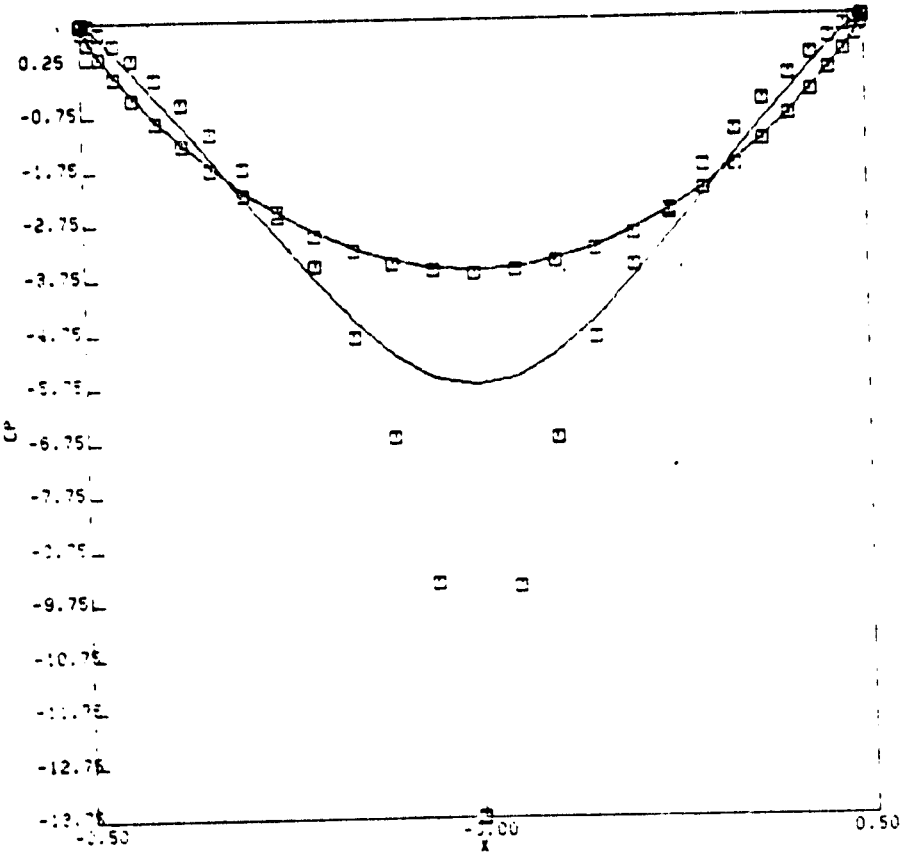

(b.) Pressure Distribution.

Figure 23. Coordinate System and Pressure Distribution for Two Circles - Configuration #1, 61 Points on Each Body.

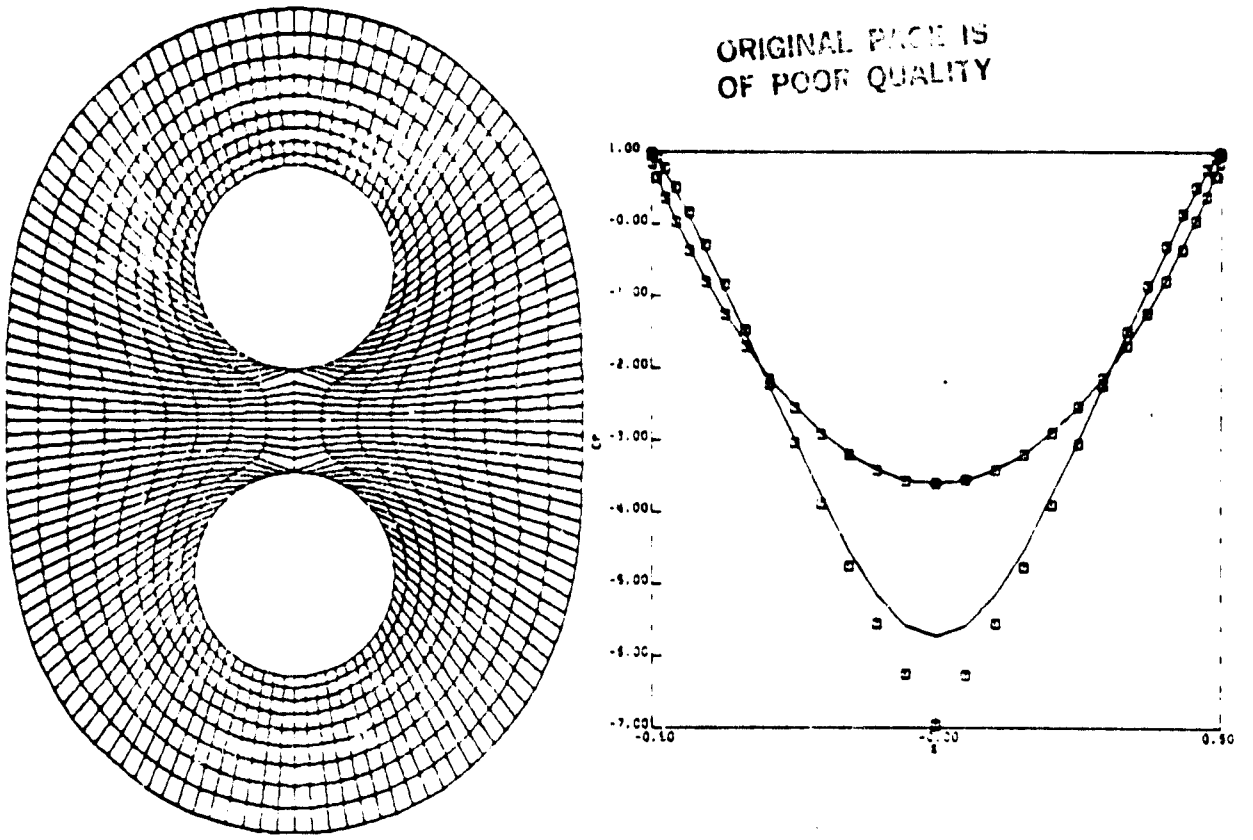

(a.) 100 Attraction to Cut Intersection

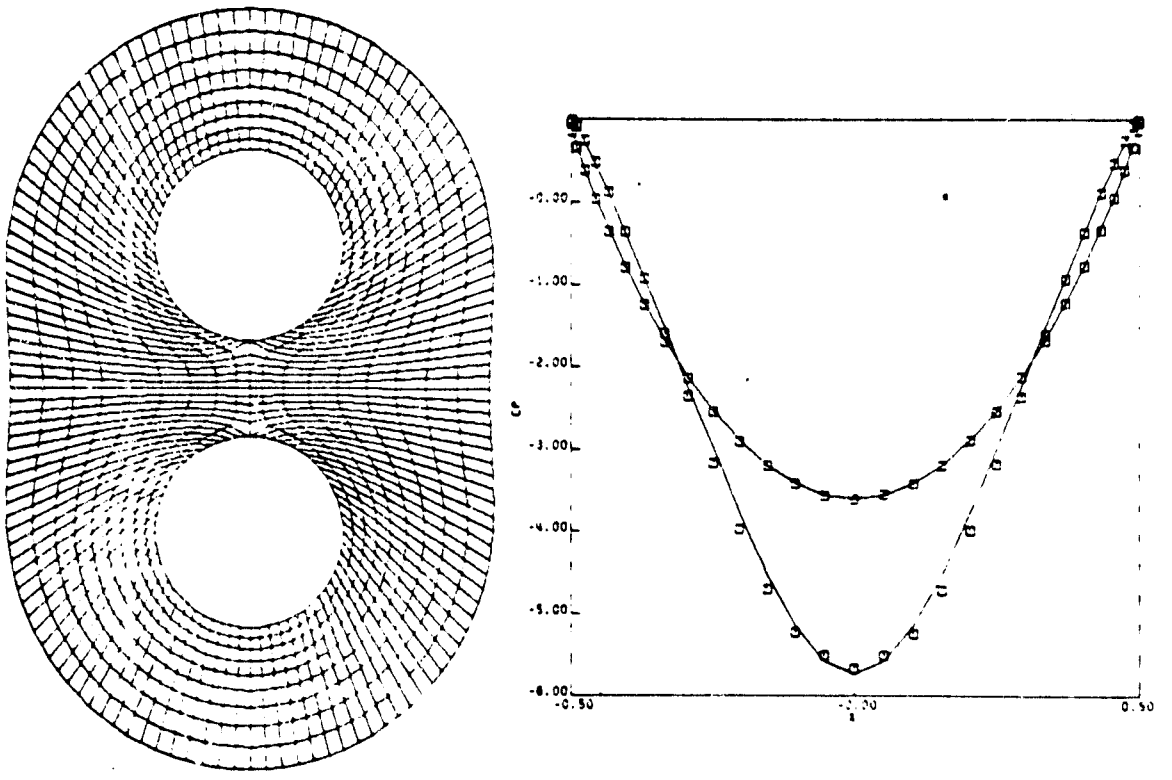

(b.) 250 Attraction to Cut Intersection

Figure 24. Controlled Coordinate System and Pressure Distribution for Two Circles - 61 Points on Each Body.

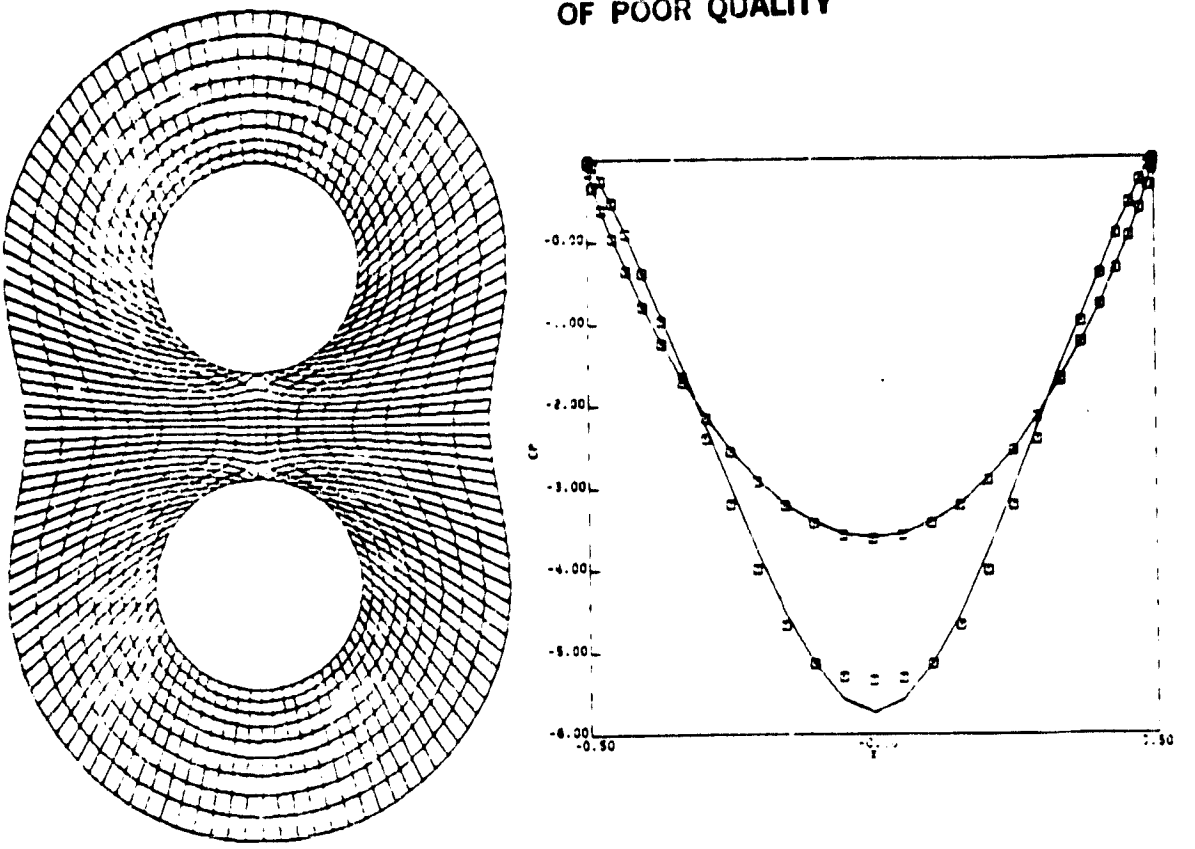

(c.) 500 Attraction to Cut Intersection

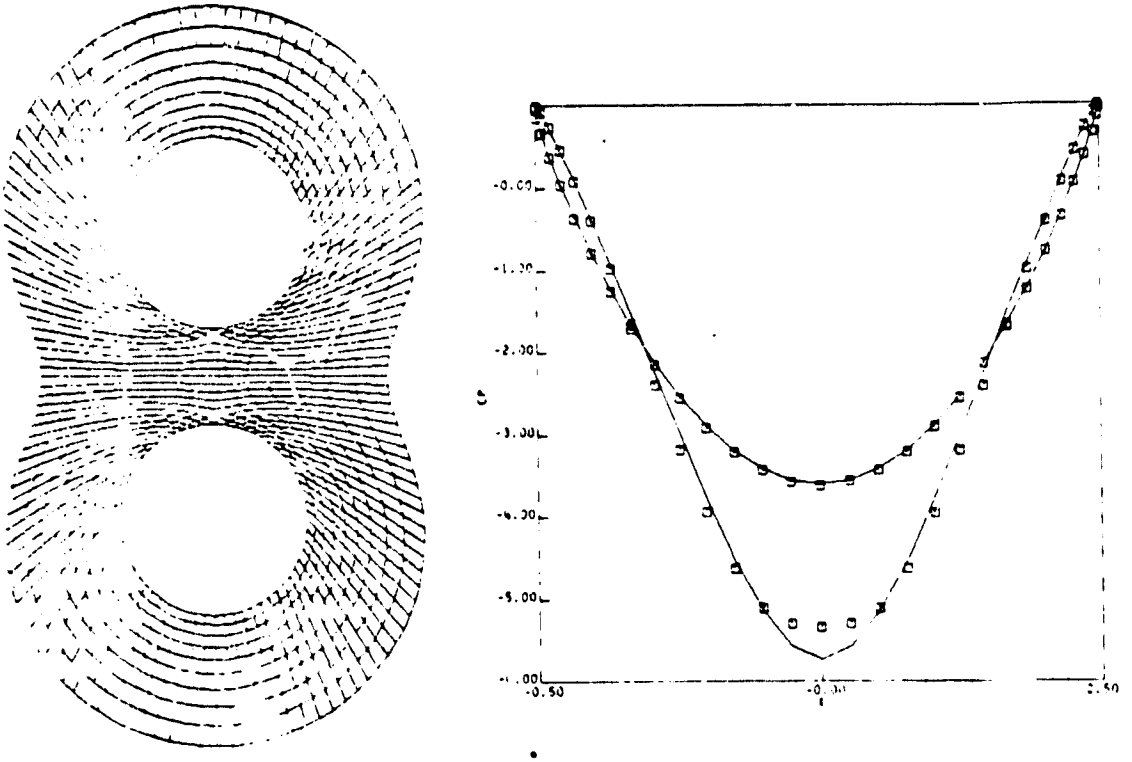

(d.) 1000 Attraction to Cut Intersection

Figure 24. (Continued)

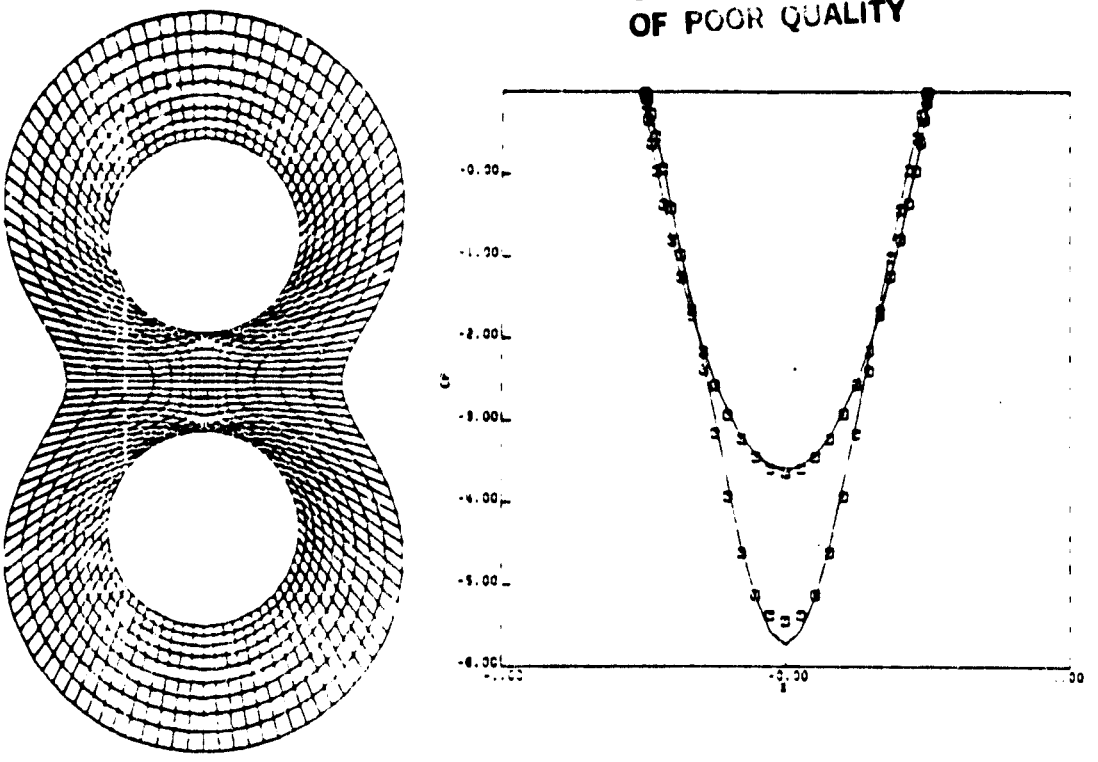

(e.) 2000 Attraction to Cut Intersection

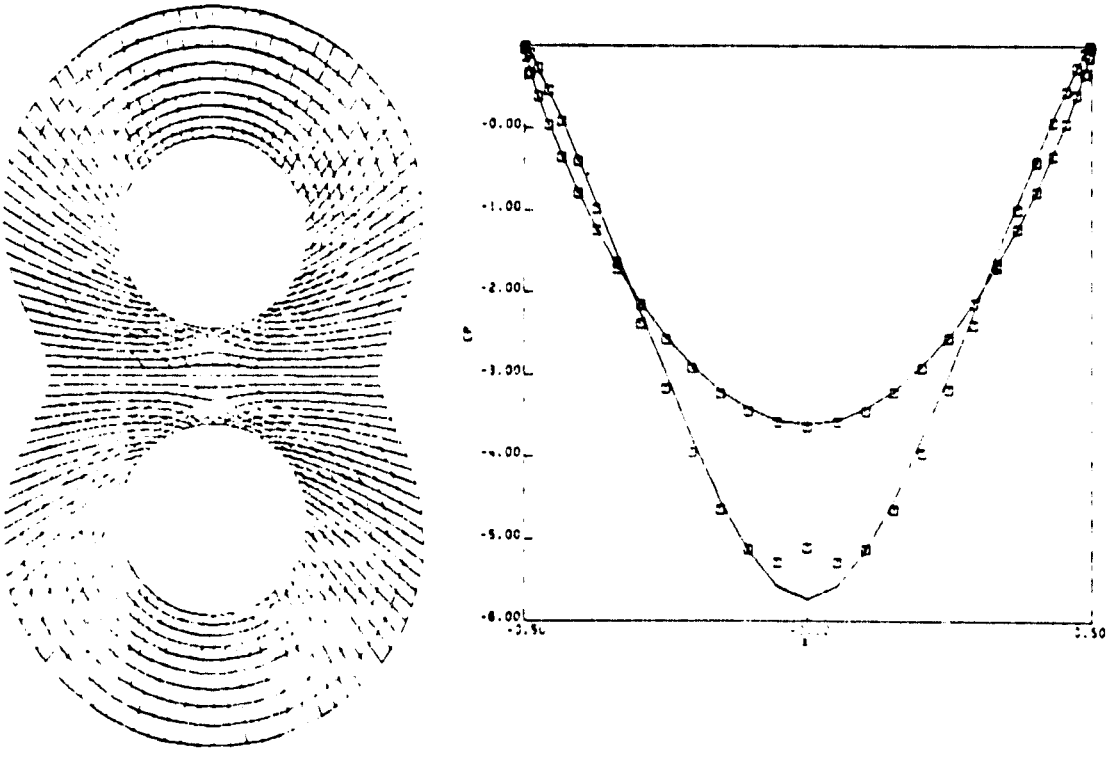

(f.) 1000 Attraction to Cut Intersection, Fewer Lines Between Bodies

Figure 24. (Concluded)

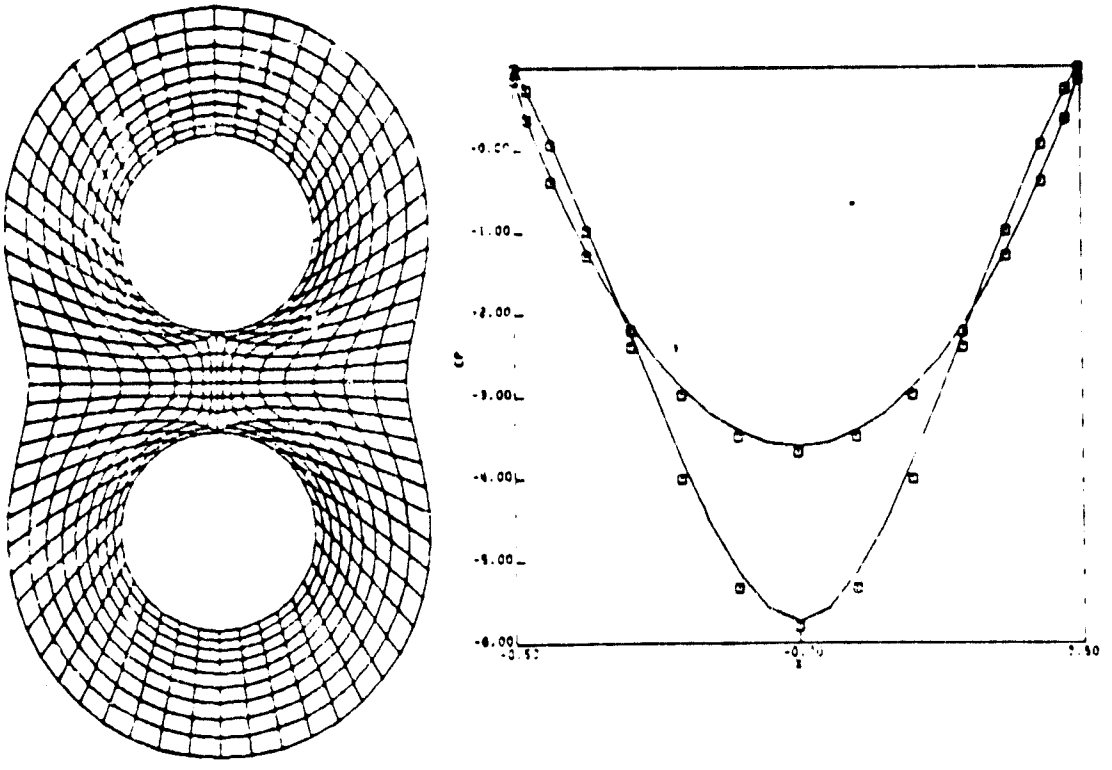

(a.) 500 Attraction to Cut Intersection

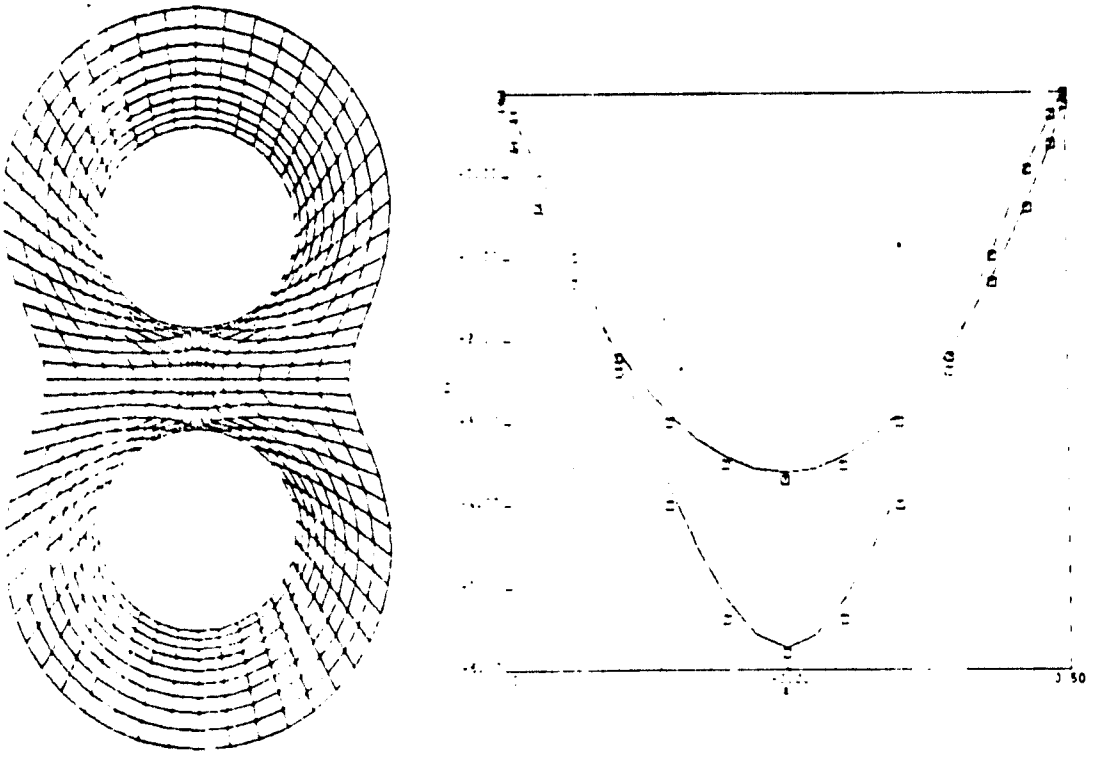

(b.) 1000 Attraction to Cut Intersection

Figure 25. Controlled Coordinate System and Pressure Distribution for Two Circles - 31 Points on Each Body.

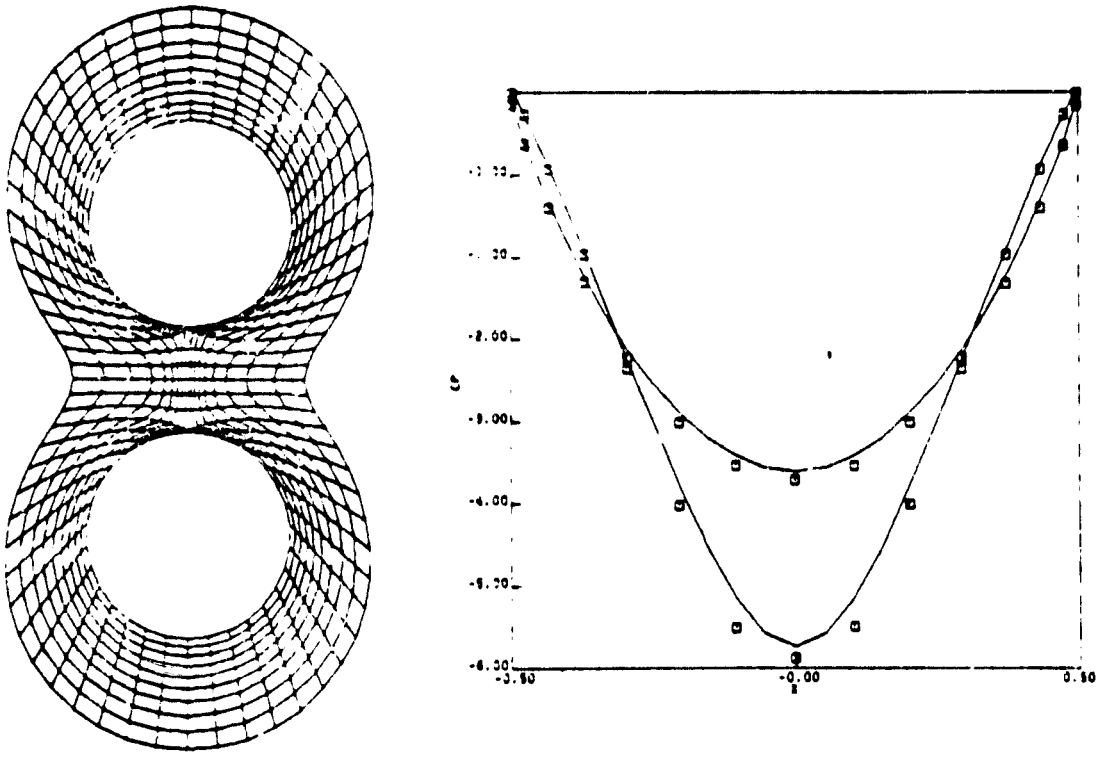

(c.) 2000 Attraction to Cut Intersection

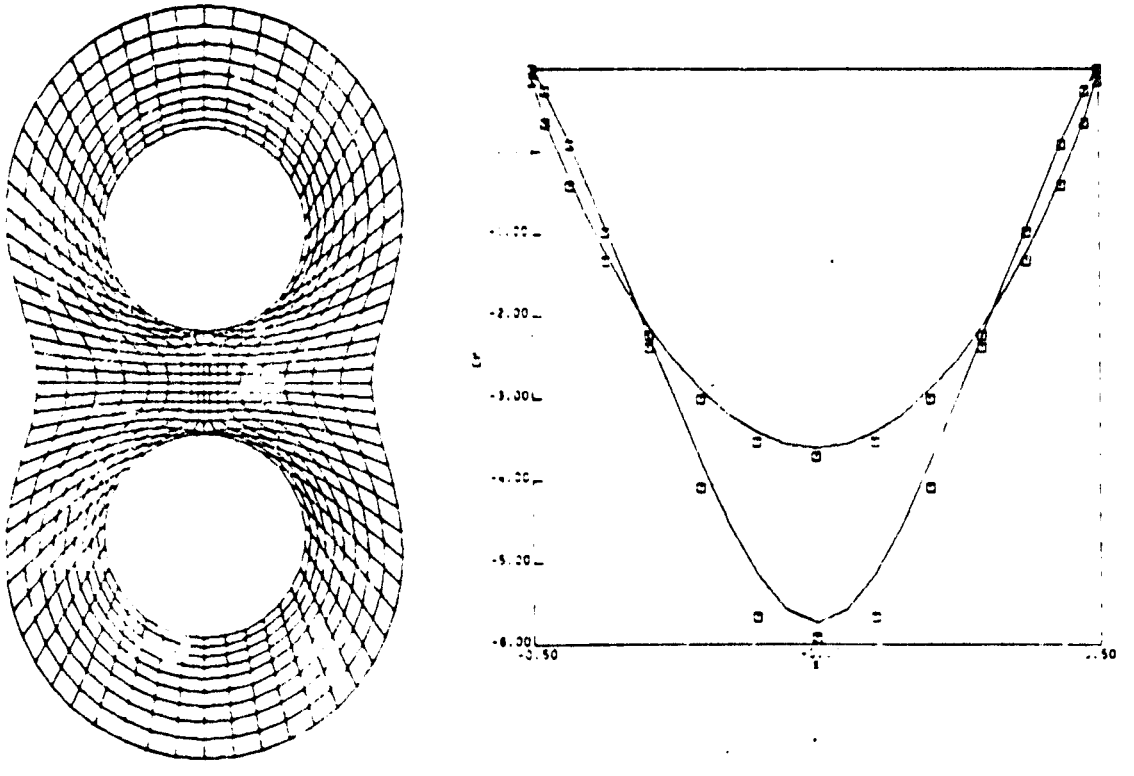

(d.) 1000 Attraction to Cut Intersection, More Lines Between Bodies

Figure 25, (Concluded)

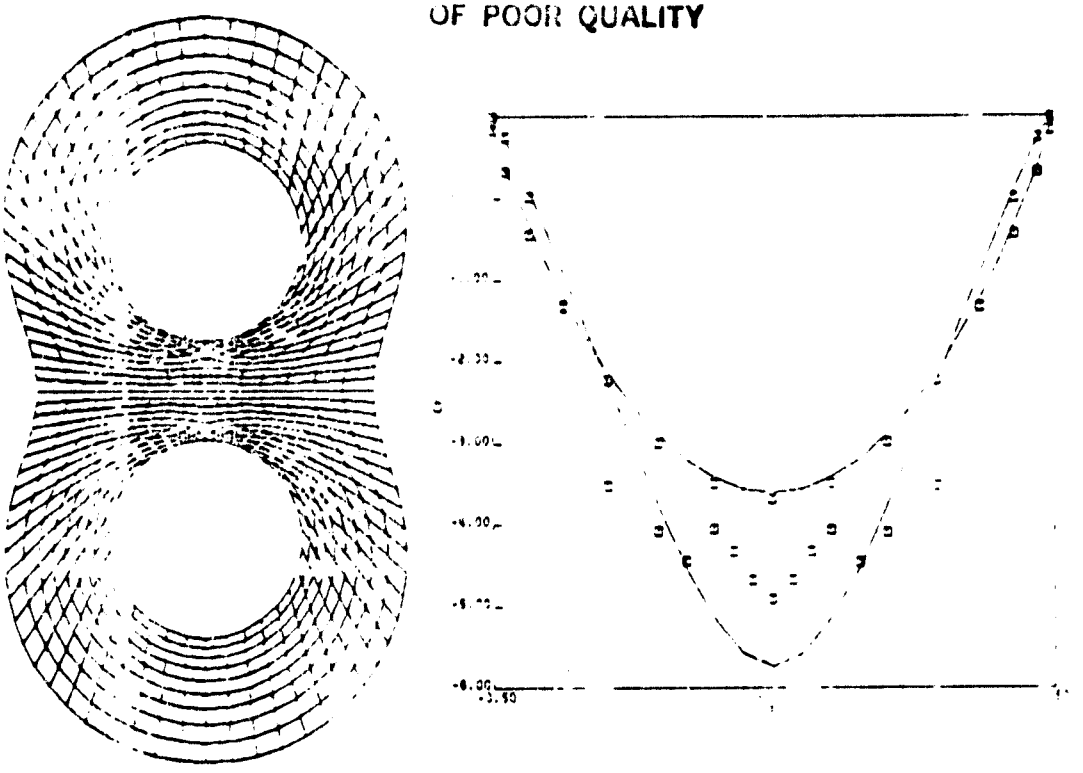

(a.) 2000 η-line Attraction to Cut Intersections

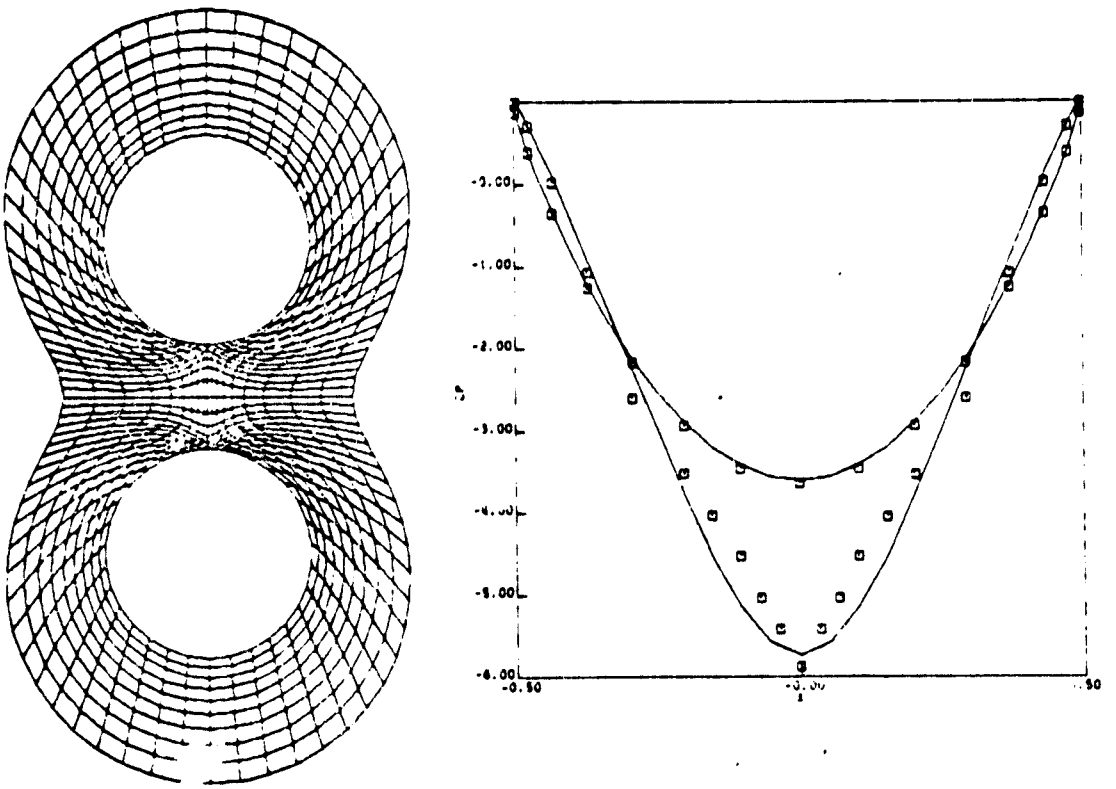

(b.) 2000 ξ and η-line Attraction to Cut Intersections

Figure 26. Controlled Coordinate System and Pressure Distribution for Two Circles - 37 Points on Each Body.

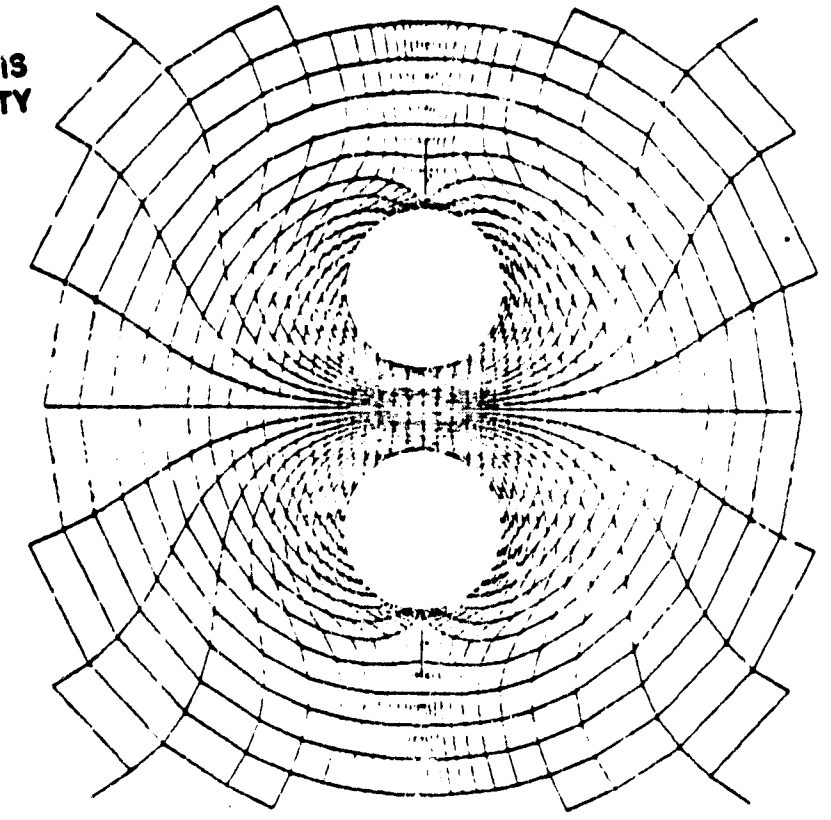

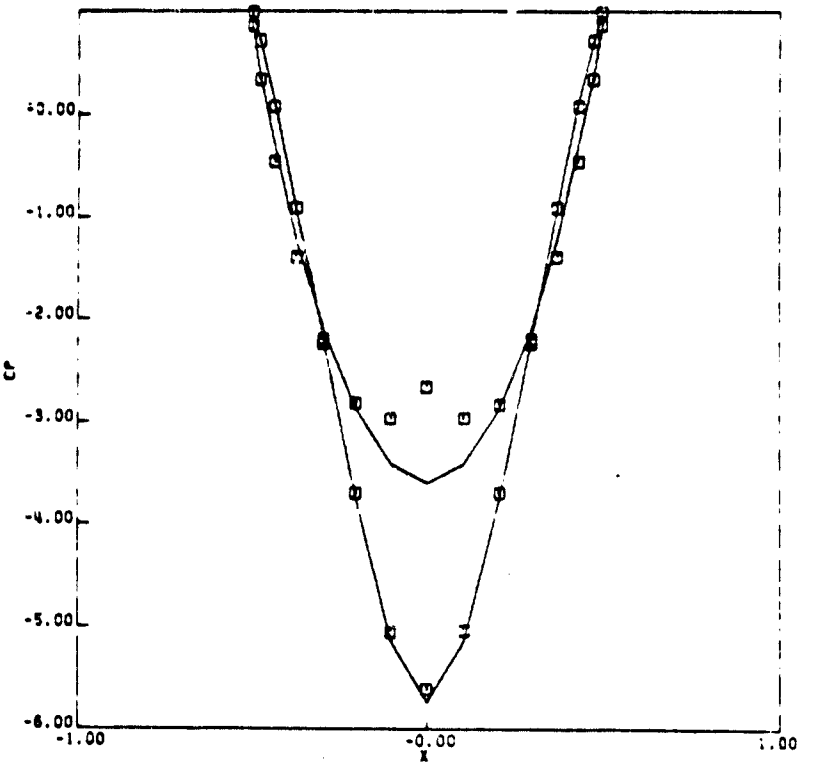

Figure 27. Controlled Coordinate System and Pressure Distribution for Two Circles, Configuration #2, 31 Points on Each Body.

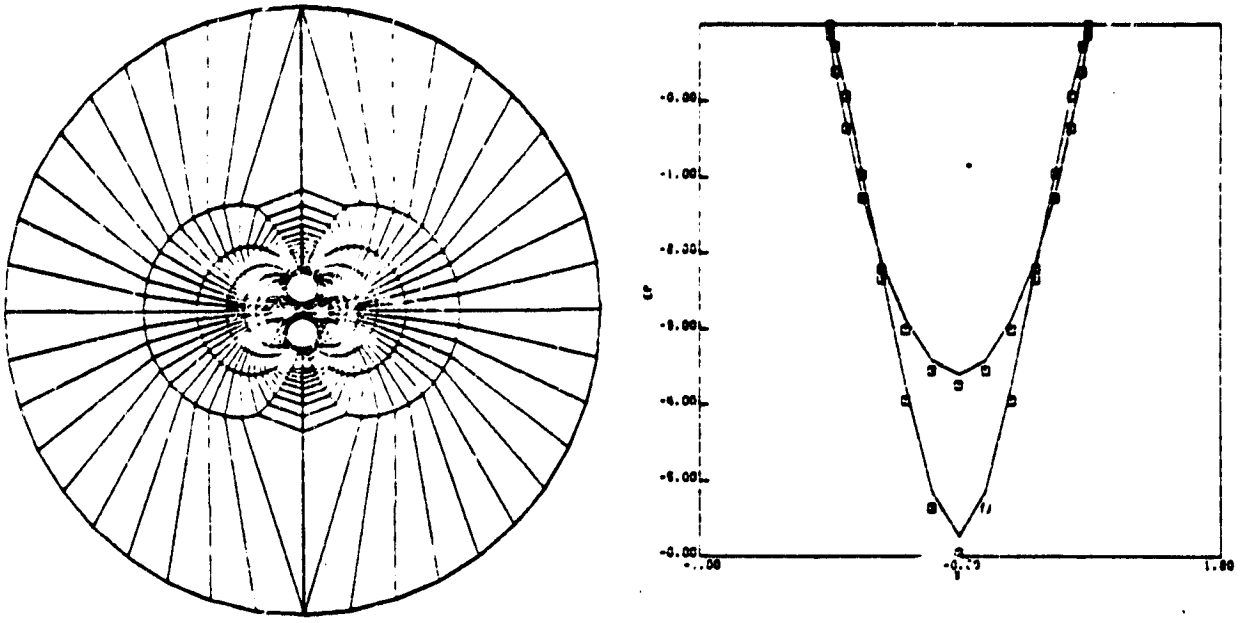

(a.) 31 Points on Each Body

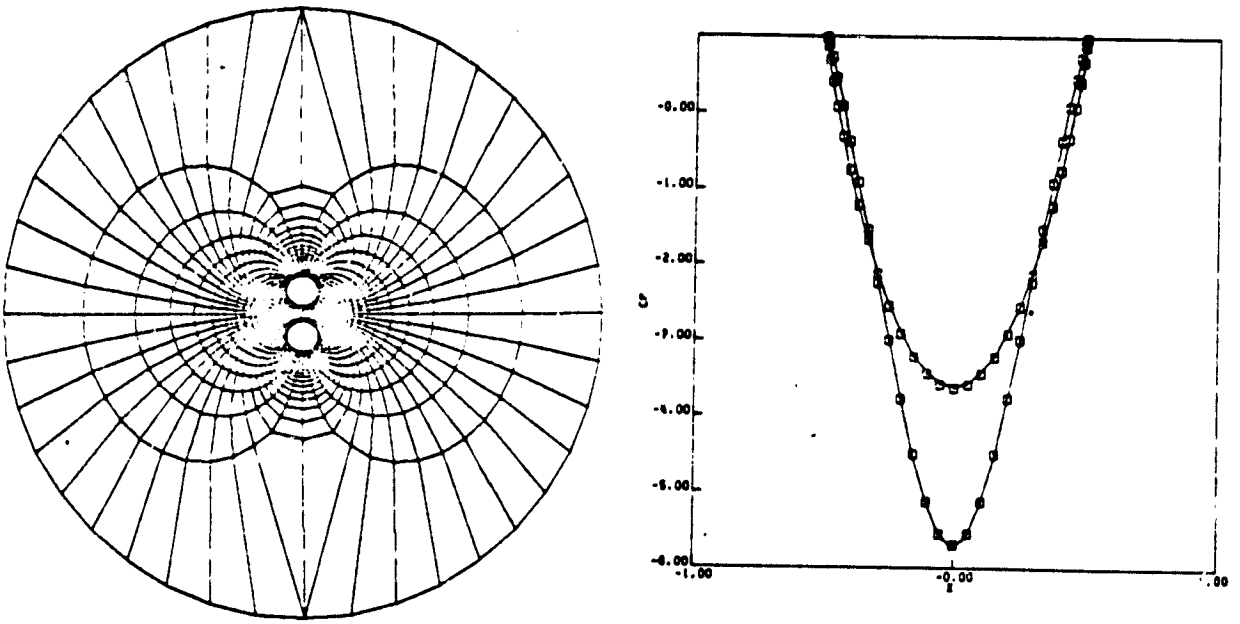

(b.) 61 Points on Each Body

Figure 28. Coordinate System and Pressure Distribution for Two Circles, Configuration #3.

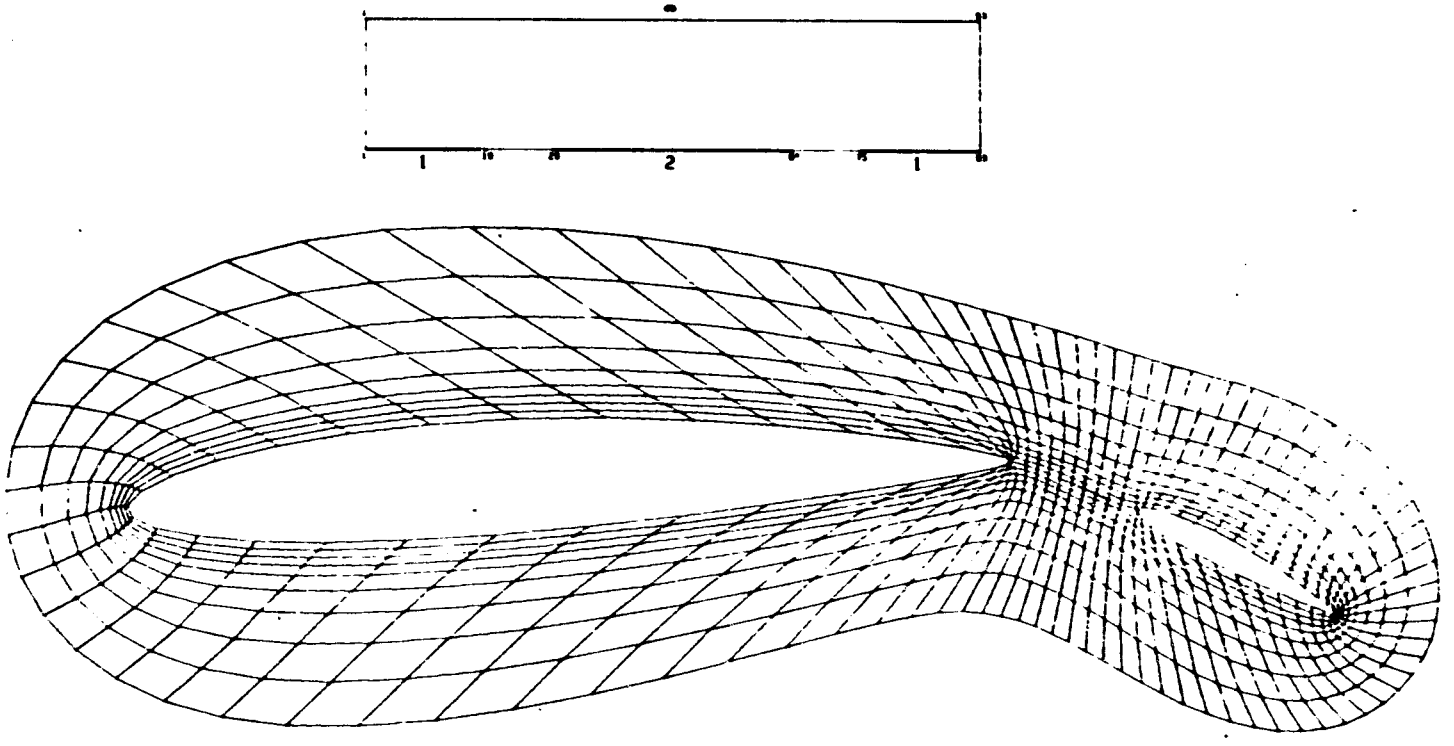

Figure 29. Coordinate System - Multiple Airfoil - Attraction to Body and Cut Intersections

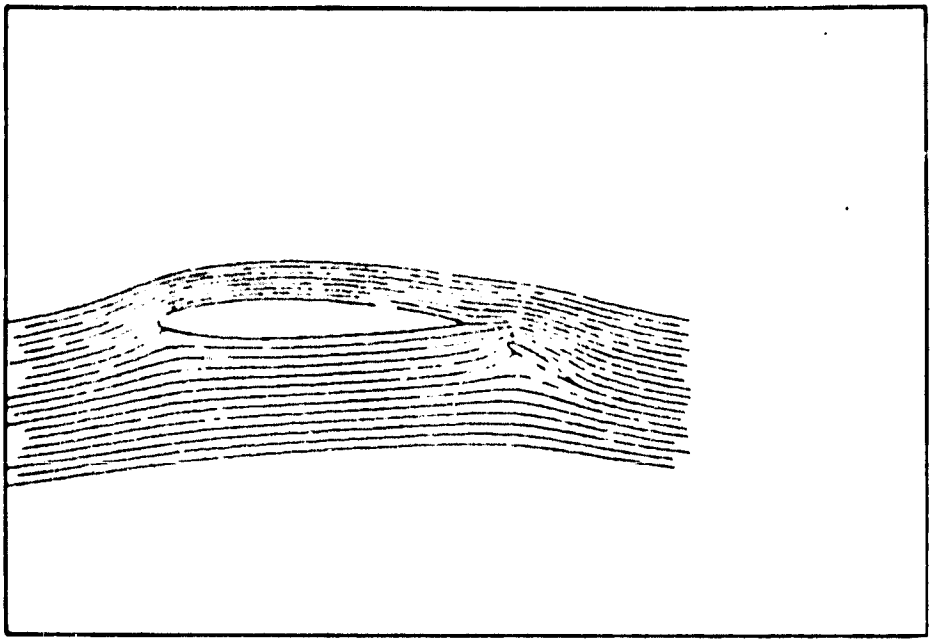

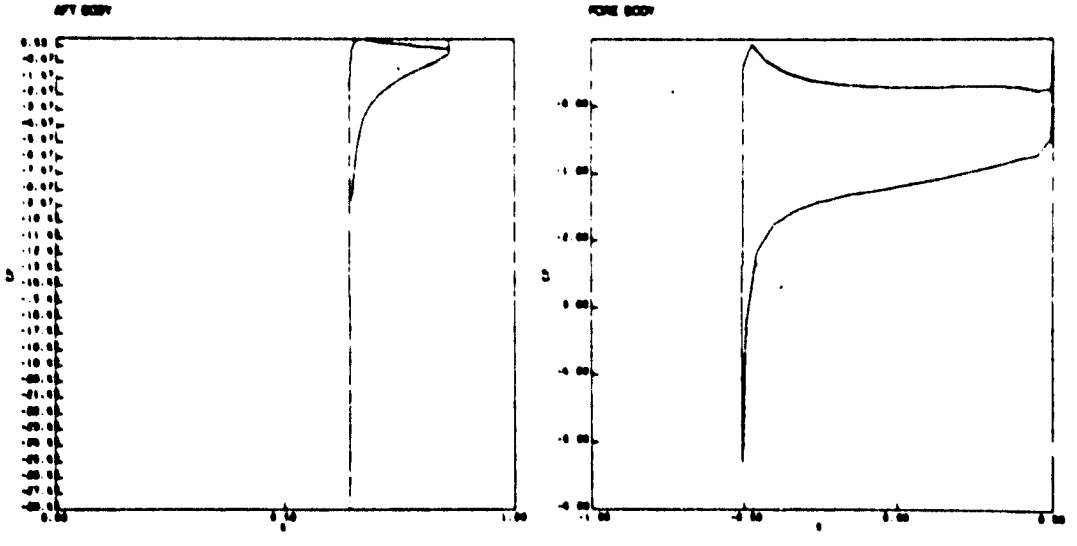

Figure 30. Potential Flow Streamlines and Pressure Distributions - Double Airfoil